JOURNAL OF CAVE AND KARST STUDIES

April 2010
Volume 72, Number 1
ISSN 1090-6924
A Publication of the National Speleological Society

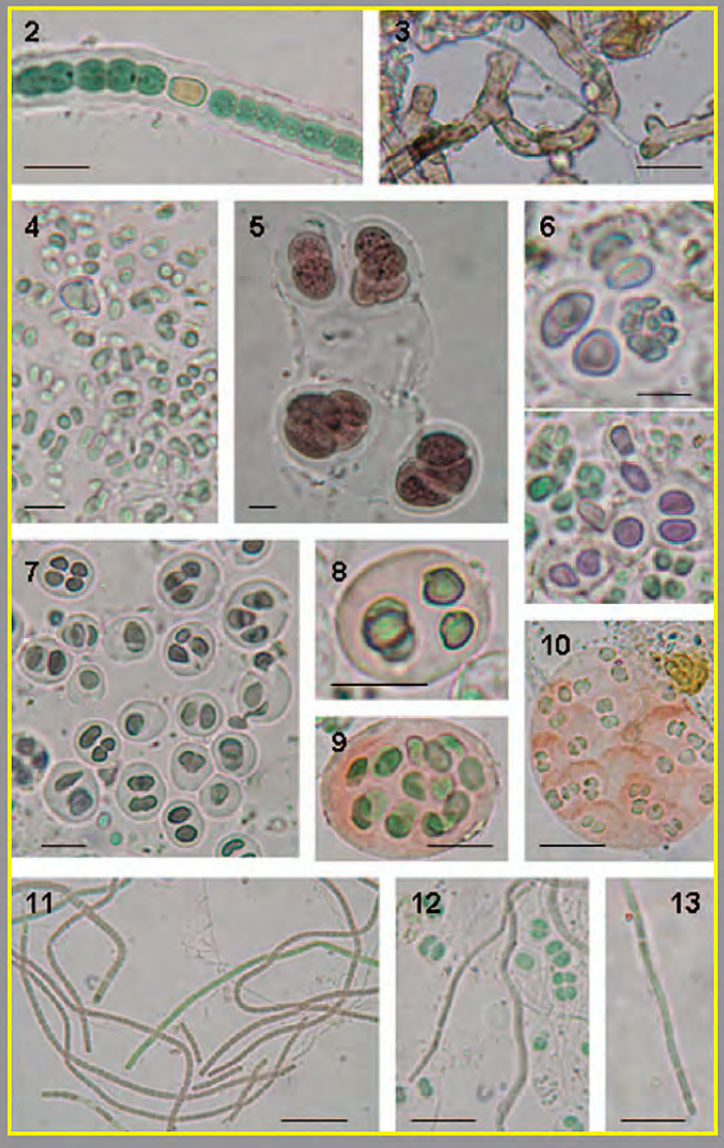

IN THIS ISSUE:

Published By
The National Speleological Society

The *Journal of Cave and Karst Studies* (ISSN 1090-6924, CPM Number #40065056) is a multi-disciplinary, refereed journal published three times a year by the National Speleological Society, 2813 Cave Avenue, Huntsville, Alabama 35810-4431 USA; Phone (256) 852-1300; Fax (256) 851-9241, email: nss@caves.org; World Wide Web: http://www.caves.org/pub/journal/.
Check the *Journal* website for subscripion rates. Back issues and cumulative indices are available from the NSS office.

POSTMASTER: send address changes to the *Journal of Cave and Karst Studies*, 2813 Cave Avenue, Huntsville, Alabama 35810-4431 USA.

The *Journal of Cave and Karst Studies* is covered by the following ISI Thomson Services Science Citation Index Expanded, ISI Alerting Services, and Current Contents/Physical, Chemical, and Earth Sciences.

Front cover: Plate 1 from Martinez and Asencio in this issue.

M.R. Ghanbarpour, K.C. Abbaspour, G. Jalalvand, and G.A. Moghaddam – Stochastic modeling of surface stream flow at different time scales: Sangsoorakh karst basin, Iran. *Journal of Cave and Karst Studies,* v. 72, no. 1, p. 1–10. DOI: 10.4311/jcks2007ES0017

STOCHASTIC MODELING OF SURFACE STREAM FLOW AT DIFFERENT TIME SCALES: SANGSOORAKH KARST BASIN, IRAN

M. Reza Ghanbarpour[1]*, Karim C. Abbaspour[2], Goudarz Jalalvand[3], and Ghodsieh Ashtiani Moghaddam[1]

Abstract: Karstic watersheds are one of the most important areas for water supply. Because the role of groundwater contribution to surface water flow in karst watersheds is not well understood, the commonly used hydrologic models in most regular basins do not provide satisfactory estimates of runoff in karstic regions. This paper uses time-series analysis to model karstic flow in the Sangsoorakh karst drainage basin in the Karkheh subbasin of southwest Iran. The comparison of model forecasting performance was conducted based upon graphical and numerical criteria. The results indicate that autoregressive integrated moving average (ARIMA) models perform better than deseasonalized autoregressive moving average (DARMA) models for weekly, monthly and bimonthly flow forecasting applications in the study area.

Introduction

Accurate simulation and forecasting of water availability is a key step in efficient planning, operation, and management of water resources. Developing reliable surface water flow forecasting methods for real-time operational water resources management becomes increasingly important. Various approaches, including physical and mathematical models, have been used for this purpose. The problem is more complicated in karstic basins due to the nature of the dynamic processes involved. Therefore, karstic basins should be considered distinct from other drainage areas (LeGrand, 1973). As Graupe et al. (1976) noted, karstic basins respond differently to rainfall than do non-karstic drainage areas in such a way that a part of the precipitation is often stored in underground storage spaces that discharges at springs after a delay and long after the rainfall has ceased. Hence, surface hydrology rules and relationships that are valid in non-karstic watersheds have a more complex situation in karstic basins.

Similarities of karstic aquifers to surface networks and their consistency throughout the whole of the karst drainage network are generally unknown (Glennon and Groves, 2002). Discrete recharge to a karst aquifer occurs through openings such as sinkholes. Karst aquifers recharged in this manner typically have numerous inputs of surface water to the subsurface with water draining along cracks, fissures, and zones of weakness in soluble bedrock (Lerch et al., 2005). Because karstic flow networks occur underground, karst drainage basins possess complex boundaries and inexact and sometimes unknown subsurface flow routes. Limestone basins behave differently from normal surface stream systems because of the nature of the underground drainage (Jakeman et al., 1984). Therefore, the commonly used surface hydrology models, such as curve number or rational method, which provides satisfactory estimates of runoff in most regular basins, may not provide accurate results in karstic regions.

Schomberg et al. (2005) analyzed 72 ungauged, agricultural watersheds in Minnesota and Michigan using the hydrologic model SWAT to determine the effects of land use and surficial geology on stream flow, sediment, and nutrients. Some streams in those watersheds are influenced by karst topography. They found seasonal and annual differences in flow and nutrient and sediment loading across different land forms and land use types. Jourde et al. (2007) analyzed the contribution of karst groundwater to surface water flow using a hydrologic model. They found that the model was unable to replicate recorded flood hydrographs at both the upstream (non-karstic watershed) and downstream (karstic watershed) gauging stations.

Time-series analysis (Box and Jenkins, 1976) has been widely used in the field of hydrology and water resources for simulation and forecasting (Hipel and McLeod, 1994). Time-series analysis provides effective tools for selecting a model that describes the historical time series behavior. Selected models could be used to forecast future events. Studies have shown that stochastic time-series models are very useful within the field of complex karstic flow systems, when detailed information are not available (Graupe et al., 1976; Jakeman et al., 1984; Dimitrov et al., 1997). The behavior and the response function of the karstic system can be characterized by autoregressive models, spectral and cross correlation analyses, and transfer function noise. Autoregressive stochastic methods have been used by Ozis

* Corresponding Author
[1] Faculty of Natural Resources, Sari Agricultural Sciences and Natural Resources University, P.O.Box: 737, Sari, Iran, m_ghanbarpour@yahoo.com
[2] Swiss Federal Institute for Aquatic Science and Technology, EAWAG, Ueberlandstr, 133, P.O. Box 611, 8600 Duebendorf, Switzerland
[3] Lar consulting company, Sharifi Street, No. 23, Tehran, Iran

and Keloglu (1976) for flow simulation in karstic basins in Turkey. In these basins, karstified limestone formations are predominant. In most basins, daily and monthly first order autoregressive models were the most appropriate stochastic models. Graupe et al. (1976) used an autoregressive model and moving average for simulating and forecasting flow in karstic basins. In their research, Graupe et al. found that the first order autoregressive model for partial karstic basins and second order autoregressive model for complete karstic basins were identified as the best models. A mathematical overview of single and cross correlation and spectral analyses was presented by Mangin (1984). Dimitrov et al. (1997) also used time series stochastic models including autoregression on the dependent variable as well as on the residuals and multiple regression using different time lags in a karstic basin in Bulgaria. In this basin, the limestone thickness varied within the range 20–250 m. The average elevation of the basin was about 800–1000 m. The Upper Cretaceous limestone is highly karstified and both surface and underground karst forms exist. They concluded that the stochastic linear differential equation with independent error process was the best approach for flow estimation when detailed information on the rainfall-runoff processes is not available. Mathevet et al. (2004) analyzed the hydrological functioning of a karst system using some time-series analysis methods including correlation and spectral analyses and noise and wavelet analyses. The non-stationary and timescale-dependent behavior of the system was studied.

The objective of this research was to develop and compare two stochastic models for flow forecasting in the Sangsoorakh karst basin located in the Karkheh sub-basin in southwest Iran. The models are based on a seasonal autoregressive integrated moving average (ARIMA) and a deseasonalized autoregressive moving average (DARMA). For this study, stochastic approaches were used to develop weekly, monthly, and bi-monthly flow simulation and forecasting models.

METHODS AND MATERIALS

STUDY AREA

The Sangsoorakh karst drainage basin covers an area of 53.4 km^2 in the Karkheh subbasin in southwest Iran (Fig. 1). The highest elevation of the basin is 3498 m in southeastern portion and the lowest is 1760 m in the northeastern portion. The average rainfall is 636 mm yr^{-1} (Jalalvand, 1999). The average annual discharge of the basin at the hydrometric station is 4.2 m^3 s^{-1}. The estimated runoff coefficient is about 0.32 (Jalalvand, 1999). The average monthly temperature is 6.1 °C with a minimum of −7.5 °C in December and a maximum of 19.0 °C in August. The soil in the area is mountainous with shallow depth and light texture (sandy) and with plenty of stones and gravels. This area is covered by natural rangeland especially near Sarab-Gamasyab Spring (Fig. 2). Most parts of the basin are karstic

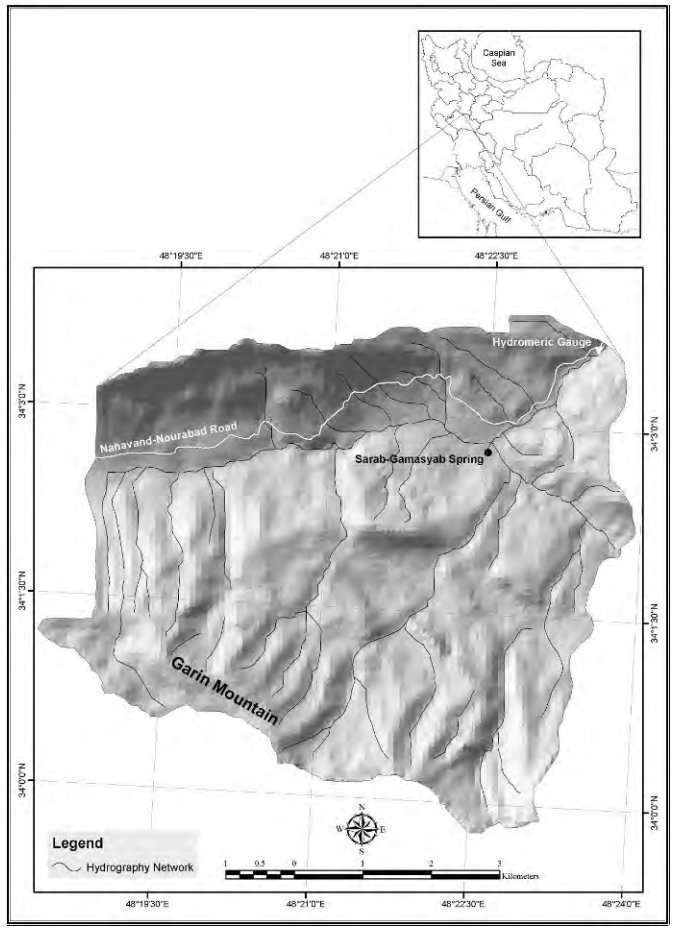

Figure 1. Location of Sangsoorakh Basin in the Karkheh Basin in western Iran.

(Jalalvand, 1999). Flow simulation and forecasting is very important in the study area for management of water resources, estimation and prediction of spring floods, and for water supply planning. Furthermore, increasing the relative accuracy for flow forecasting in high- and low-flow seasons for efficient water resources management has special economic values.

DATA

The data collected in this study consisted of weekly, monthly, and bimonthly flow rates, which were measured using a hydrometric gauge at the outlet of the basin. The data period for this study was for the water years of 1979–80 to 2003–04. A split sample procedure was used for calibration and validation. In each of the weekly, monthly, and bi-monthly databases, flow data from 1979–80 to 1997–98 were used for calibration and data from 1998–99 to 2003–04 for validation.

GEOLOGY OF THE BASIN

This area is located in the overthrusted Zagros zone. It is an intensely fractured and faulted narrow band found between Sanandaj-Syrjan and the folded Zagros zones

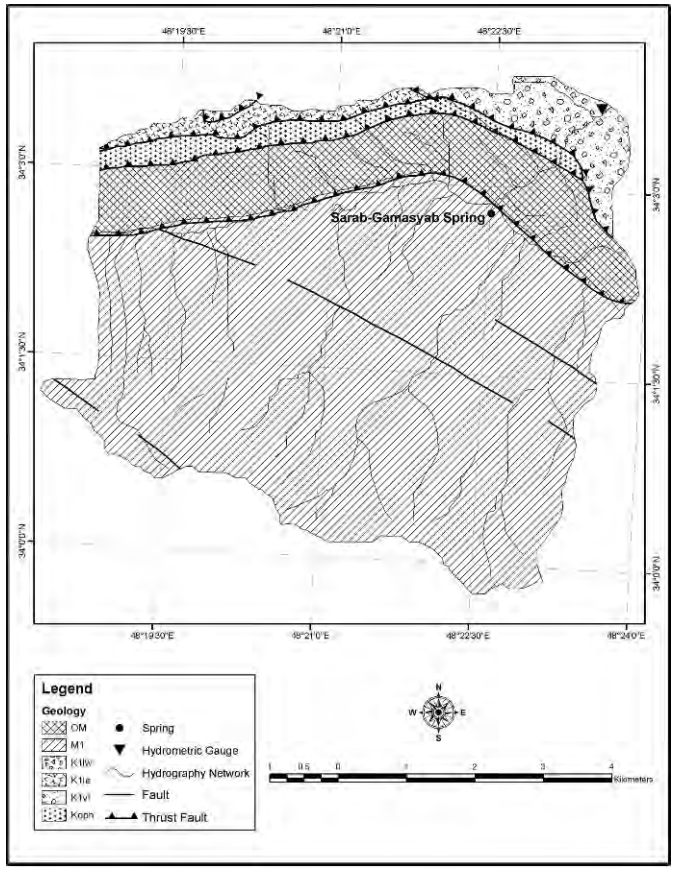

Figure 2. Sangsoorakh geology map and its karstic formations (Jalalvand, 1999).

(Fig. 2). The top part of region is mainly covered by sedimentary and metamorphic rocks. Sedimentary rocks consist of karstic limestone and conglomerates. Metamorphic formations mostly consist of crystallized limestone and low-grade metamorphic shale that are white-gray to dark-gray in color, and in some cases, there are lime-marl to marl layers. Geomorphic activities have created many clay and calcite filled pores.

In Figure 2, the first geologic unit, Cretaceous rocks from oldest to youngest are indicated as K1vl, K1le, K1lw. K1lv is a pyroclastic member that consists of crystallized limestone and volcanic rocks. As shown in Figure 2, these rocks cover most of the northern region around the basin outlet. The second member, K1le, consists of carbonate rocks such as weathered microsparite and dolomicrite in various shades of gray color in the north and northwestern part of the region. Therefore, it can be said that these are an indicator facie among other facies. K1lw is a thick to massive member that is crystallized white limestone and is located in northwestern part of the region. According to the Nahavand geological map (1:100,000), all these members belong to the lower Cretaceous period (Jalalvand, 1999).

The second unit is ophiolite that is exposed along Garin Mountain in Nahavand-Nourabad road. It is about 10-km-long and more than 200-m-wide. It is the main outcrop in the basin and consists of red plugic limestone and radiolarian cherts within basaltic volcanic rocks. This unit has been covered by Oligo-Miocene deposits.

Tertiary deposits of Oligo-Miocene age cover 80 percent of the basin, and consist of OM and M1 members. OM is a kind of tectonic thrusted member that is composed of sand, shale, and siltstone with thin layers of gray limestone. As a result of faulting, bedding slopes in varying directions, and in some places, are near vertical. The limestone has many microfossil traces. The thickness of micro-conglomerates is about 10 m and consists of shale, crystallized limestone, and old sandstone. The microfossils were studied in a thin carbonate layer and were found to belong to upper-Oligocene and lower-Miocene units (Jalalvand, 1999).

M1, which is located in the southern part of Garin Mountain, is 360–400-m-thick and composed of biomicrite carbonate rocks with many microfossil traces. There are many macropores in this unit caused by infiltrating surface water and dissolution of limestone, which led to the creation of a karstic environment. In addition, canyons, clints, and avens are some other forms of karst morphology that exist in this unit.

Time Series Analysis

Time-series models can be used to describe the stochastic structure of a hydrologic data series. In this study, the ARIMA (Box and Jenkins, 1976) and the DARMA (Hipel and McLeod, 1994) models were used to model weekly, monthly, and bimonthly flow time series.

The ARIMA model is constructed using a combination of moving average (MA) and autoregressive (AR) processes, after differencing the data to remove nonstationarity. For the nonseasonal component of a seasonal ARIMA model, the MA operator is written as

$$\theta(B) = 1 - \theta_1 B - \theta_2 B^2 - \ldots - \theta_q B^q \qquad (1)$$

where q is the order of the nonseasonal MA operator, θ_j, $j = 1, 2, \ldots, q$, are the MA parameters, and B is the backward shift operator such that $BZ_t = Z_{t-1}$. The AR operator is written as

$$\phi(B) = 1 - \phi_1 B - \phi_2 B^2 - \ldots - \phi_p B^p \qquad (2)$$

where p is the order of the nonseasonal AR operator, and ϕ_i, $i = 1, 2, \ldots, p$, are the nonseasonal AR parameters. The nonseasonal ARIMA model for a set of equispaced measurements, $Z = \{Z_1, Z_2, \ldots, Z_n\}$, can be written as

$$\phi(B)(1-B)^d(Z_t) = \theta(B)a_t \qquad (3)$$

where d is the number of differences, t is discrete time, and a_t is the white noise series which has a finite variance and a mean of zero. Differencing removes nonstationarity in a time series. When differencing is not required, the model is referred to as an ARMA model. Construction of ARIMA models is conducted based on the three stages of model

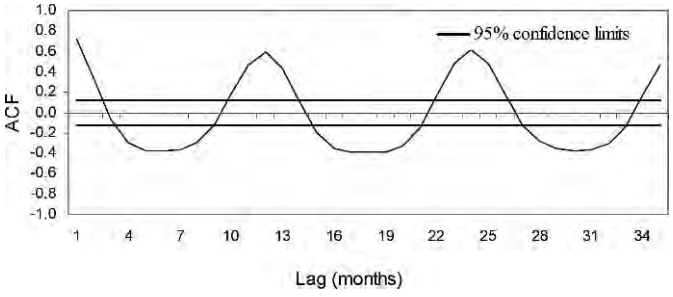

Figure 3. ACF for the monthly flow data series for the Sangsoorakh Hydrometric Station.

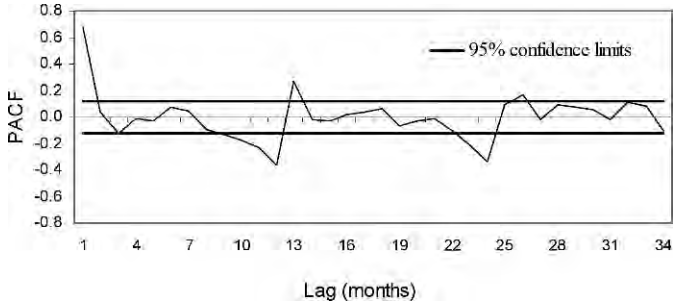

Figure 5. PACF for the seasonally differenced monthly flow data series for the Sangsoorakh Hydrometric Station.

building: identification, estimation, and diagnostic checking, which is discussed in detail by Hipel et al. (1977). The 95% confidence limits are calculated using

$$Var[p_k] \cong \frac{1}{N}\left(1+2\sum_{i=1}^{q} p_i^2\right) \qquad \text{for } (k>q) \qquad (4)$$

under the assumption that p_k is zero for all nonzero lag and N is length of the data series

The nonseasonal ARIMA model in Equation (3) can be expanded to the seasonal case by adding seasonal differencing, as well as seasonal MA and AR operators to produce the seasonal ARIMA model defined as

$$\phi(B)\Phi(B^s)(1-B)^d\,(1-B^s)^D\,(Z_t-\mu)=\theta(B)\Theta(B^s)a_t \qquad (5)$$

for which

1. the seasonal length is s (s = 12 for monthly data),
2. $(1-B^s)^D$ is the seasonal differencing operator of order D,
3. $\Theta(B^s)=1-\Theta_1 B^s-\Theta_2 B^{2s}-\ldots-\Theta_Q B^{Qs}$ is the seasonal MA operator of order Q,
4. Θ_i is the ith seasonal MA parameter,
5. and $\Phi(B^s)=1-\Phi_1 B^s-\Phi_2 B^{2s}-\ldots-\Phi_p B^{Ps}$ is the seasonal AR operator of order P where Φ_i is the ith seasonal AR parameter.

The notation $(p,d,q)(P,D,Q)_s$ is used to represent the seasonal ARIMA model in Equation (5). The three entries within the first set of parentheses stand for the orders of the nonseasonal AR, differencing, and MA operators, respectively, while the three numbers contained inside the second set of parentheses give the orders of the seasonal AR, differencing, and MA operators, respectively. Finally, prior to fitting the seasonal ARIMA model in Equation (6) to the Z_t time series, the series may first be transformed by a Box-Cox transformation, for which a logarithmic transformation is a special case, to eliminate problems with nonnormality and heteroscedasticity in the estimated model residuals (Hipel and McLeod, 1994).

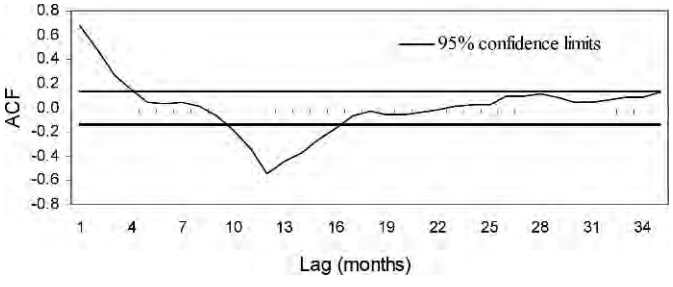

Figure 4. ACF for the seasonally differenced monthly flow data series for the Sangsoorakh Hydrometric Station.

The second stochastic method, DARMA is a widely used approach to model seasonal data series. In this method, first the series should be deseasonalized and then an appropriate nonseasonal stochastic model fit to the deseasonalized data. Two standard deseasonalization techniques that have been widely used are

$$w_{i,j}=Z_{i,j}^{\lambda}-\bar{\mu}_j \qquad (6)$$

and

$$w_{i,j}=\frac{\left(Z_{i,j}^{\lambda}-\bar{\mu}_j\right)}{\bar{\sigma}_j} \qquad (7)$$

where $Z_{i,j}$ is the transformed observation for the ith year, jth month, μ_j is the fitted mean for season j, σ_j is the fitted standard deviation for season j, and the superscript λ is the exponent of an appropriate Box-Cox transformation (Hipel and McLeod, 1994). After the series are deseasonalized, nonseasonal ARMA models are fitted to the data. Finally, the notation DARMA (p,q) is employed to represent this type of deseasonalized model where p and q stand for the orders of the nonseasonal and seasonal AR and MA operators presented in Equations (2) and (1), respectively.

Calibration of time-series models is conducted based on the three stages of model building: identification, estimation, and diagnostic checking (Box and Jenkins, 1976; Hipel et al., 1977; Hipel and McLeod, 1994). The purpose of the identification stage is to determine the differencing required to produce stationarity and the persistence structure in the series using interpretation of the autocorrelation function

Table 1. Selected ARIMA models and the model parameters.

Time Interval	Model	Model Parameters					
		p_1	p_2	p_3	q_1	P_1	Q_1
Weekly	$ARIMA(3,0,0)(0,1,1)_{52}$	0.885	⋯	⋯	0.089	0.062	0.687
	$ARIMA(3,0,1)(0,1,1)_{52}$	0.885	⋯	0.662	−0.009	−0.384	1.345
	$ARIMA(2,0,0)(0,1,1)_{52}$	0.888	⋯	⋯	⋯	0.124	0.698
	$ARIMA(1,0,0)(0,1,1)_{52}$	0.890	⋯	⋯	⋯	⋯	0.798
Monthly	$ARIMA(1,0,0)(0,1,1)_{12}$	0.889	⋯	⋯	⋯	⋯	0.594
	$ARIMA(1,0,1)(0,1,1)_{12}$	0.890	⋯	0.138	⋯	⋯	0.684
	$ARIMA(2,0,1)(0,1,1)_{12}$	0.890	⋯	−0.772	⋯	0.552	−0.220
	$ARIMA(3,0,1)(0,1,1)_{12}$	0.885	⋯	−0.733	−0.005	0.537	−0.182
Bimonthly	$ARIMA(1,0,1)(1,1,1)_6$	0.876	−0.185	−0.193	⋯	⋯	0.387
	$ARIMA(1,0,0)(1,1,1)_6$	0.875	−0.201	⋯	⋯	⋯	0.526
	$ARIMA(2,0,1)(1,1,1)_6$	0.877	−0.185	−0.523	⋯	0.185	0.057
	$ARIMA(2,0,0)(1,1,1)_6$	0.875	−0.191	⋯	⋯	−0.056	0.557

The notation $(p,d,q)(P,D,Q)_s$ is used to represent the seasonal ARIMA model in which p, d and q are order of the nonseasonal AR, differencing and MA operators respectively. P, D and Q are the order of the seasonal AR, differencing and MA operators and s is number of season per year.

(ACF) and the partial autocorrelation function (PACF). In the estimation stage, the approximate maximum likelihood estimates (MLEs) for the model parameters is obtained by employing the unconditional sum of squares method, as suggested by Box and Jenkins (1976). The third stage of time-series analysis consists of diagnostic checking of the estimated model residuals and is used to evaluate the ARIMA and DARMA models performance. To determine whether the residual are white noise and normally independently distributed, residual autocorrelation function (RACF) tests (Hipel et al., 1977) are employed. The Akaike information criteria (*AIC*) (Akaike, 1974) and Schwars' approximation of the Bayes Information Criterion (*BIC*) (Schwars, 1978) were utilized to select the most appropriate model from the candidate set of calibrated models

$$AIC = -2Ln(ML) + 2K \tag{8}$$

$$BIC = -2Ln(ML) + KLn(n) \tag{9}$$

where ML is maximum likelihood, K is the number of adjustable parameters, and n is the length of the time series. The optimal model is chosen to minimize the *AIC* or *BIC* criterion, depending on which criterion is selected.

Table 2. Selected DARMA models and the model parameters.

Time Interval	Model	Model Parameters			
		$p1$	$p2$	$p3$	$q1$
Weekly	$DARMA(3,0)$	0.686	0.065	0.077	⋯
	$DARMA(2,1)$	1.256	−0.324	⋯	0.571
	$DARMA(1,1)$	0.854	⋯	⋯	0.178
	$DARMA(1,0)$	0.789	⋯	⋯	⋯
Monthly	$DARMA(1,1)$	0.671	⋯	⋯	0.161
	$DARMA(1,0)$	0.562	⋯	⋯	⋯
	$DARMA(2,1)$	−0.131	0.543	⋯	−0.846
	$DARMA(2,0)$	0.498	0.112	⋯	⋯
Bimonthly	$DARMA(1,1)$	0.335	⋯	⋯	−0.224
	$DARMA(1,0)$	0.503	⋯	⋯	⋯
	$DARMA(2,1)$	−0.066	0.22	⋯	−0.624
	$DARMA(2,0)$	0.538	−0.068	⋯	⋯

The notation (p,q) is used to represent the deseasonalized ARMA model in which p *and* q are order of the nonseasonal AR and MA operators respectively.

For validation of the models, one-step-ahead forecasts for the test portion of the time series were generated using the selected set of calibrated models. Plotting the observed and estimated data series for each model could be used as an indication of reliability of the models at the validation stages. The forecasting performance of all the models at the validation stage was compared based on the mean absolute error (MAE), root mean square error (RMSE), and Nash-Sutcliffe efficiency (NSE) (Nash and Sutcliffe, 1970), as defined in Equations 10, 11 and 12. The procedure having lower MAE and RMSE values can be assumed to be the most accurate model for flow forecasting in the study area. NSE values equal to 1 indicate a perfect fit between simulated and observed data. An NSE value of 0 indicates that the model predictions are not acceptable (Motovilov et al., 1999). To investigate the models' overall forecasting performance at the verification stage, the coefficients of determination (R^2) were considered. R^2 indicates the strength of fit between observed and forecasted stream flow and it has the range of values between 0 and 1.

$$MAE = \frac{1}{n}\sum_{i=1}^{n}[X_{Oi} - X_{Ei}] \tag{10}$$

Table 3. Comparison of the selected ARIMA models.

Time Interval	Model	Comparison Criteria		
		AIC	*BIC*	RACF
Weekly	$ARIMA(3,0,0)(0,1,1)_{52}$	153.6	429.6	Residuals are normally distributed
	$ARIMA(3,0,1)(0,1,1)_{52}$	154.1	435.1	Residuals are normally distributed
	$ARIMA(2,0,0)(0,1,1)_{52}$	159.03	430.4	…
	$ARIMA(1,0,0)(0,1,1)_{52}$	171.5	438.03	…
Monthly	$ARIMA(1,0,0)(0,1,1)_{12}$	−22.3	35.9	…
	$ARIMA(1,0,1)(0,1,1)_{12}$	−22.3	39.3	Residuals are normally distributed
	$ARIMA(2,0,1)(0,1,1)_{12}$	−24.5	40.6	Residuals are normally distributed
	$ARIMA(3,0,1)(0,1,1)_{12}$	−22.3	46.2	Residuals are normally distributed
Bimonthly	$ARIMA(1,0,1)(1,1,1)_{6}$	−2.02	32.83	Residuals are normally distributed
	$ARIMA(1,0,0)(0,1,1)_{6}$	−2.59	26.9	Residuals are normally distributed
	$ARIMA(1,0,1)(0,1,1)_{6}$	−1.64	30.53	…
	$ARIMA(2,0,1)(0,1,1)_{6}$	−3.24	34.54	…

$$RMSE = \sqrt{\frac{1}{n}\sum_{i=1}^{n}[X_{Oi} - X_{Ei}]^2} \tag{11}$$

$$NSE = \left(1 - \frac{\sum\left(X_{Oi} - X_{Ei}\right)^2}{\sum\left(X_{Oi} - \overline{X_{Oi}}\right)^2}\right) \tag{12}$$

where n is number of data observations, X_{Oi} is observed value, X_{Ei} is estimated value, and $\overline{X_{Oi}}$ is the average of observed values.

RESULTS AND DISCUSSION

Weekly, monthly, and bimonthly stochastic ARIMA and DARMA models were developed using a time-series analysis procedure for the basin under study. To determine the autocorrelation structure in the series, we plotted the ACF and PACF that reflect linear dependence among observations separated by different time lags. As an example, the ACF for the monthly flow is illustrated in Figure 3. The ACF follows an attenuating sine wave pattern. Examination of this function revealed that the data have seasonality, which requires removal using one order of seasonal differencing.

Figures 4 and 5 show the ACF and PACF, respectively, for the seasonally differenced monthly flow-time series. As

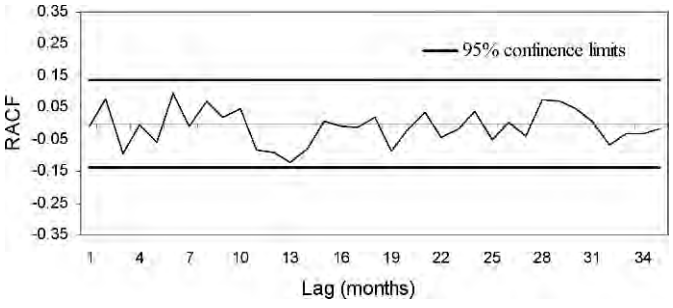

Figure 6. RACF for the selected $ARIMA(1,0,1)(0,1,1)_{12}$ monthly model for the Sangesourakh Hydrometric Station.

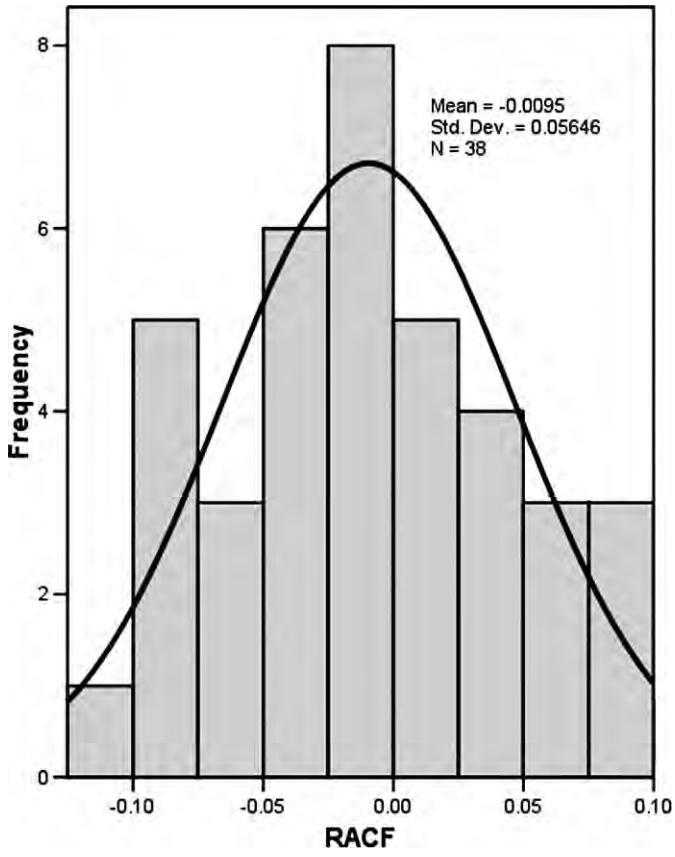

Figure 7. Plot of the residuals (RACF) of $ARIMA(1,0,1)(0,1,1)_{12}$ monthly model with normal curve.

Table 4. Comparison of the selected DARMA models.

Time Interval	Model	Comparison Criteria		
		AIC	*BIC*	RACF
Weekly	*DARMA*(3,0)	−120.05	−100.66	Residuals are normally distributed
	DARMA(2,1)	−120.29	−100.91	…
	DARMA(1,1)	−119.07	−104.5	Residuals are normally distributed
	DARMA(1,0)	−104.94	−95.25	…
Monthly	*DARMA*(1,1)	−83.25	−72.96	Residuals are normally distributed
	DARMA(1,0)	−82.89	−76.03	…
	DARMA(2,1)	−83.5	−69.84	…
	DARMA(2,0)	−83.8	−73.53	Residuals are normally distributed
Bimonthly	*DARMA*(1,1)	−316.39	−308.34	Residuals are normally distributed
	DARMA(1,0)	−317.48	−312.12	…
	DARMA(2,1)	−314.94	−304.21	…
	DARMA(2,0)	−315.96	−307.91	…

evident in Figure 4, the ACF did not truncate but rather damps out, suggesting that a nonseasonal AR parameter was needed in the model. Because the PACF truncated after lag 1 (Fig. 5), one nonseasonal AR parameter should be included in the model. There was a significant value at lag 12 that indicated the presence of a seasonal MA term in the model. In a similar way, all possible models were identified for data series at the other time scales. Table 1 presents the four selected ARIMA models for the weekly, monthly, and bimonthly flow in the study area.

For the case of DARMA models, all flow-time series were deseasonalized. For weekly data, flows were deseasonalized using the estimated means of the series (Equation (6)). For monthly data, it was necessary to use both Equations (6) and (7), but for bimonthly data, flows were first transformed using natural logarithms and then deseasonalized using Equation (6). Then, the three mentioned modeling stages of time-series analysis were followed to calibrate the DARMA forecasting models. Deseasonalized models are useful for describing time series in which the mean and variance within each season are stationary across the year. Table 2 presents four selected DARMA models which might be suitable for simulating flow time series at different time scales.

Table 5. Summary of the performance analysis of forecasting models.

Time Interval	Model	*MAE*	*RMSE*	*NSE*	R^2
Weekly	ARIMA	1.41	1.82	0.49	0.52
	DARMA	1.46	1.89	0.43	0.50
Monthly	ARIMA	1.25	1.57	0.61	0.54
	DARMA	1.29	1.68	0.56	0.60
Bimonthly	ARIMA	1.24	1.5	0.62	0.56
	DARMA	1.23	1.56	0.59	0.59

The approximate maximum likelihood (MLE) estimates for the model parameters were obtained by employing the unconditional sum of squares method suggested by Box and Jenkins (1976). Model parameters for ARIMA and DARMA models are shown in Table 1 and 2, respectively. For checking the adequacy of the models fitted to the time series, residual autocorrelation function (RACF) tests were employed. The *AIC* and *BIC* were used to select the best fit model out of the various competing models.

Table 3 shows the comparison between all ARIMA models based on RACF, *AIC*, and *BIC*. With respect to these criteria, the $ARIMA(3,0,0)(0,1,1)_{52}$ model performs better than the other three weekly models. For the monthly and bimonthly flow series, $ARIMA(1,0,1)(0,1,1)_{12}$ and $ARIMA(1,0,1)(1,1,1)_6$ are more accurate. A plot of the RACF for the selected $ARIMA(1,0,1)(0,1,1)_{12}$ model is shown in Figure 6. From Figure 6, it can be noted that the estimated values fall within the 5% significance interval. The residuals were white noise and normally distributed (Figure 7).

A comparison of all DARMA models is shown in Table 4. Based on the mentioned diagnostic criteria, *DARMA*(1,1) were selected as the most reliable weekly, monthly, and bimonthly DARMA models, respectively.

One-step-ahead forecasts for the verification part of the weekly, monthly, and bimonthly flow (1998–99 to 2003–04)

Table 6. Statistical comparison of the forecasting models using paired-sample *t*-test analysis.

Model Time Interval	*t*	Degrees of Freedom	Significance
Weekly	−1.732	259	0.084
Monthly	−10.188	59	0.00
Bimonthly	6.457	29	0.00

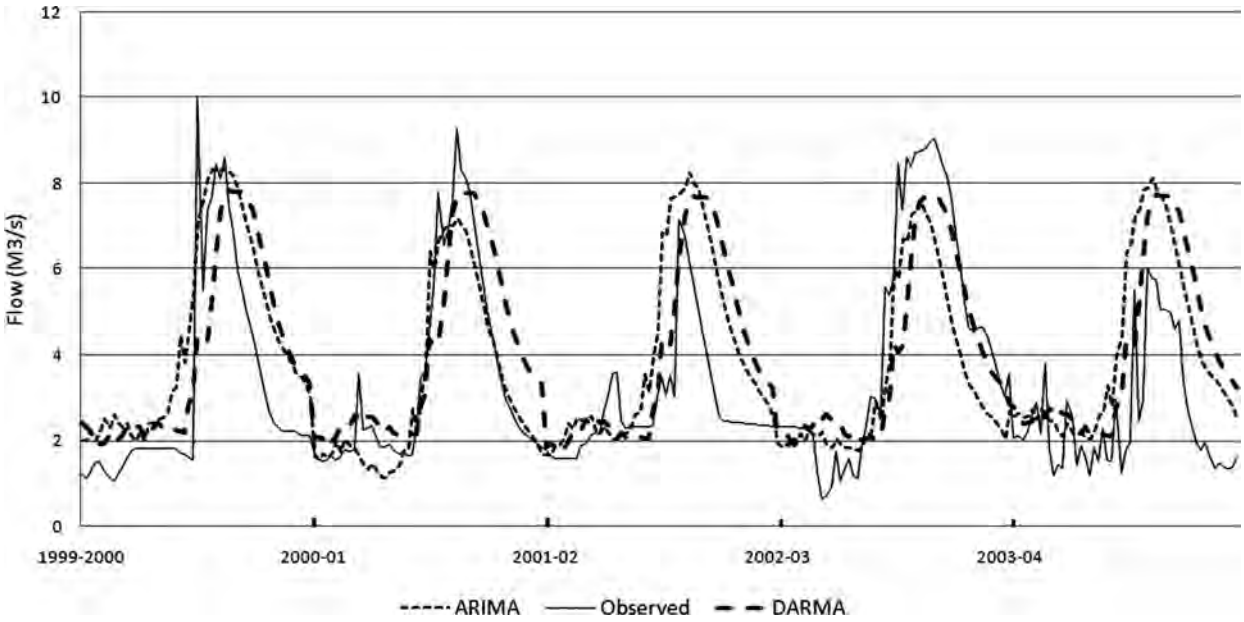

Figure 8. Comparison of observed and forecasted weekly flow using ARIMA and DARMA models for validation period (1999–00 to 2003–04).

were generated using the selected set of the ARIMA and DARMA models. The resulting calibrated models were then examined for use in predicting flow data series at the three different time scales.

We used the validation data sets to compare the forecasting ability of the ARIMA and DARMA models. Table 5 gives the indices used to compare the goodness of model simulation for weekly, monthly, and bimonthly time scales.

For the case of the weekly flow forecasting, the seasonal ARIMA model provides slightly better results than DARMA in terms of MAE and RMSE. As can be seen in Table 6, the differences are significant at the 0.05 level based on a paired sample *t*-test analysis. However, the results of the monthly and bimonthly ARIMA and DARMA models were slightly similar and the differences are not significant at the 0.05 level (Table 6). The NSE was used to evaluate the simulation accuracies of the two models. The NSE of the ARIMA in comparison to the DARMA models is more satisfactory (Motovilov et al., 1999). The NSF for weekly, monthly, and bimonthly flow is 0.49, 0.61 and 0.62, respectively (Table 5).

To show the validation results of the models for weekly, monthly, and bimonthly flows, in Figures 8, 9, and 10, respectively, we plot both the observations and the predictions. As seen in Figure 8 for the weekly simulation, DARMA slightly overestimates the flow during the recession periods. Overestimation of the flow by the DARMA model during recession periods also could be seen in Figures 9 and 10. However, it could be concluded that the weekly, monthly, and bimonthly ARIMA models are more suitable than DARMA in the study area, especially for dry periods.

CONCLUSIONS

Two time-series analysis models, ARIMA and DARMA, have been used to simulate the surface water discharges in a karst basin by the identification, estimation, and diagnostic check stages of stochastic model construction (Hipel and McLeod, 1994). The main objective of this work was to provide a set of numerical comparisons between stochastic-flow simulation and forecasting models for a small karstic watershed.

As demonstrated by the simulation experiments outlined in the paper, selected ARIMA and DARMA models statistically preserve specified historical statistics. Also, diagnostic checks reveal that the normality assumptions for the residuals are fulfilled and model parsimony is preserved. Therefore, the calibrated ARIMA and DARMA models adequately simulate weekly, monthly, and bimonthly flows in the study area.

A comparison of model predictions with historical data for the period of 1979–80 to 2003–04 water years demonstrated the accuracy of the models. As indicated in this research, forecasts of flows are reasonably accurate for both of the modeling techniques. The NSE for both models at three time scales are more than 0.43 and it shows that simulation results are all satisfactory (Motovilov et al., 1999). However, it has been found that the weekly, monthly, and bimonthly ARIMA models perform better than DARMA models based on the results of the

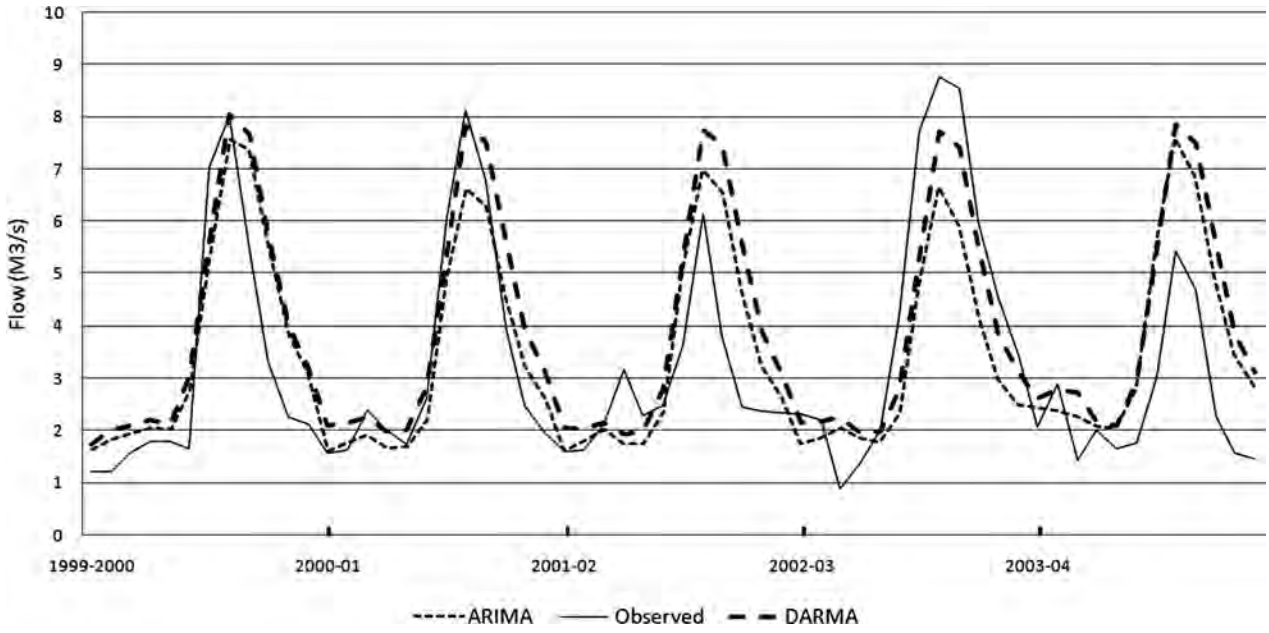

Figure 9. Comparison of observed and forecasted monthly flow using ARIMA and DARMA models for validation period (1999–00 to 2003–04).

numerical and graphical comparison of forecasting performance of the models.

The process of rainfall-runoff is more complicated in karst than non-karst basins because it has been shown in some previous studies. Schomberg et al. (2005) found that two gauges with a predicted coefficient of variation (CV) of flow greater than the actual CV of flow were in predominantly loess areas with karst influence. Predictability, constancy and CV of flow were all predicted as overly flashy by their SWAT model, which is heavily influenced by karst geology. They concluded that karst watersheds are more complex and more poorly understood

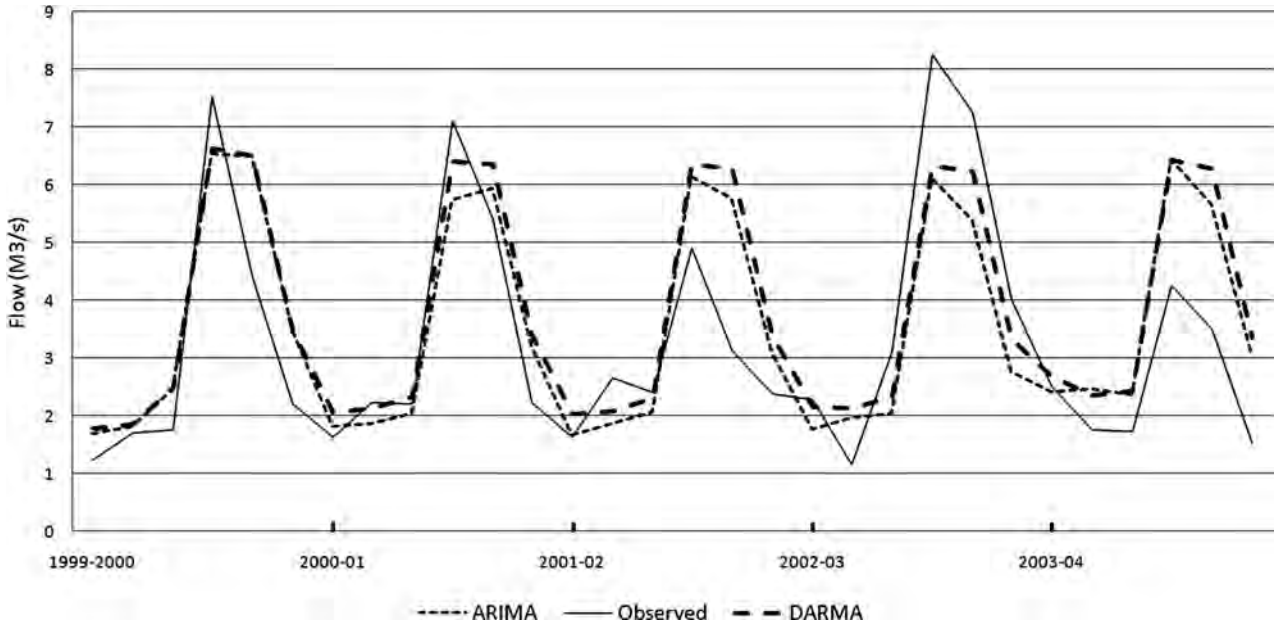

Figure 10. Comparison of observed and forecasted bimonthly flow using ARIMA and DARMA models for validation period (1999–00 to 2003–04).

than non-karst systems (Felton, 1994) and have been shown to require more specialized calibration to obtain accurate results (Spruill et al., 2000). Jourde et al. (2007) have shown that surface runoff hydrologic models cannot simulate the flow in the karstic part of the watershed under study because there is an additional contribution to surface flow from the karstic area and it is probably related to a delayed contribution of karst groundwater to surface flow. They suggest a fully coupled surface–subsurface hydrologic model to characterize the dynamics of the karst groundwater contribution to the surface drainage network.

In a karstic system, surface water flow is an observed output of the basin, which is available usually with better accuracy. As noted by Graupe et al. (1976) and Dimitrov et al. (1997), the application of stochastic models, such as the ones used in this study, offers an inexpensive solution to the operational input data, especially when insufficient spatial and temporal hydrodynamic information is available. However, more research is necessary to prove that stochastic time-series models could have better capabilities than physical models within the field of complex karstic flow systems.

ACKNOWLEDGEMENT

The authors would like to thank the referees for their very helpful comments on the manuscript.

REFERENCES

Akaike, H., 1974, A new look at the statistical model identification: IEEE Transactions on Automatic Control, v. 19, p. 716–723.

Box, G.E.P., and Jenkins, G.M., 1976, Time series analysis: Forecasting and control, revised edition, San Francisco, Holden-Day.

Dimitrov, D., Machkova, M., and Damyanov, G., 1997, On the karst spring discharge forecasting by means of stochastic modeling, *in* Gunay, G., and Johnson, A.I., eds., Karst waters & environmental impacts, Rotterdam, Balkema, p. 353–359.

Felton, G.K., 1994, Hydrologic responses of a karst watershed: Transactions of the ASAE, v. 37, p. 143–150.

Glennon, A., and Groves, C., 2002, An examination of perennial stream drainage patterns within the Mammoth Cave Watershed, Kentucky: Journal of Cave and Karst Studies, v. 64, no. 1, p. 82–91.

Graupe, D., Isailovic, D., and Yevjevich, V., 1976, Prediction model for runoff from karstified catchments, *in* Proceedings of the U.S.-Yugoslavian Symposium on Karst Hydrology and Water Resources, Dubrovnik, June 2–7, 1975, p. 277–300.

Hipel, K.W., McLeod, A.I., and Lennox, W.C., 1977, Advances in Box-Jenkins modeling, Part one, Model construction: Water Resources Research, v. 13, p. 567–575.

Hipel, K.W., and McLeod, A.I., 1994, Time series modeling of water resources and environmental systems, Amsterdam, Elsevier, 1013 p.

Jakeman, A.J., Greenway, M.A., and Jenings, J.N., 1984, Time-series models for the prediction of stream flow in a karst drainage system: Journal of Hydrology, v. 23, no. 1, p. 21–33.

Jalalvand, G., 1999, Investigation of hydro-geomorphology of Gamasiyab river basin [Ms.c. thesis], Tehran, University of Tehran, 154 p. (in Persian).

Jourde, H., Roesch, A., Guinot, V., and Bailly-Comte, V., 2007, Dynamics and contribution of karst groundwater to surface flow during Mediterranean flood: Environmental Geology, v. 51, p. 725–730.

LeGrand, H.E., 1973, Hydrological and ecological problems of karst regions: Science, v. 179, no. 4076, p. 859–864.

Lerch, R.N., Wicks, C.M., and Moss, P.L., 2005, Hydrologic characterization of two karst recharge areas in Boone County, Missouri: Journal of Cave and Karst Studies, v. 67, no. 3, p. 158–173.

Mangin, A., 1984, Pour une meilleure connaissance des systemes hydrologiques a partir des analyses correlatoires et spectrales: Journal of Hydrology, v. 67, p. 25–43.

Mathevet, T., Lepiller, M., and Mangin, A., 2004, Application of time-series analyses to the hydrological functioning of an Alpine karstic system: the case of Bange-L'Eau-Morte: Hydrology and Earth System Sciences, v. 8, no. 6, p. 1051–1064.

Motovilov, Y.G., Gottschalk, L., Engeland, K., and Rohde, A., 1999, Validation of a distributed hydrological model against spatial observations: Agriculture and Forest Meteorology, v. 98–99, p. 257–277.

Nash, J.E., and Sutcliffe, J.V., 1970, River flow forecasting through conceptual models, Part 1: A discussion of principles: Journal of Hydrology, v. 10, p. 282–290.

Ozis, U., and Keloglu, N., 1976, Some features of mathematical analysis of karst, *in* Proceedings of the U.S.-Yugoslavian Symposium on Karst Hydrology and Water Resources, Dubrovnik, June 2–7, 1975, p. 221–235.

Schomberg, J.D., Host, G., Johnson, L.B., and Richard, C., 2005, Evaluating the influence of landform, surficial geology, and land use on streams using hydrologic simulation modeling: Aquatic Sciences, v. 67, p. 528–540.

Schwars, G., 1978, Estimating the dimension of a model: Annals of Statistics, v. 6, p. 461–464.

Spruill, C.A., Workman, S.R., and Taraba, J.L., 2000, Simulation of daily and monthly stream discharge from small watersheds using the SWAT model: Transactions of the ASAE, v. 43, p. 1431–1439.

A. Martínez and A.D. Asencio – Distribution of cyanobacteria at the Gelada Cave (Spain) by physical parameters. *Journal of Cave and Karst Studies,* v. 72, no. 1, p. 11–20. DOI: 10.4311/jcks2009lsc0082

DISTRIBUTION OF CYANOBACTERIA AT THE GELADA CAVE (SPAIN) BY PHYSICAL PARAMETERS

Antonia Martínez and Antonia Dolores Asencio
Div. Botánica. Dpto. de Biología Aplicada. Universidad Miguel Hernández. Avda. Universidad, s/n. 03202 Elche, Alicante, Spain, aasencio@umh.es

Abstract: As part of an extensive study of the caves in the Province of Alicante (SE Spain), the distribution of cyanobacteria and physical data for the Gelada Cave are presented. This cave is 9.4 m deep, 0.9 to 5.0 m high, 1.2 m wide, and is located in a karst region. Photon flux density, relative humidity, and temperature were measured, and the environmental ranges of conditions where growth occurred fluctuated between 0.0008–0.06 $\mu E.m^{-2}s^{-1}$, 55.0–95.0% and 5.4–18.0 °C, respectively. All the microorganisms determined from the Gelada Cave were cyanobacteria. Other frequently observed groups in caves, such as Bacillariophyta and Chlorophyta, were not detected because the cave was too weakly illuminated and dry. Cyanobacteria were found to be grouped as blue, brown, green, or gray patina according to the sampling sites and their constituent organisms. The primary common stress factor on the distribution of algal communities in the Gelada Cave is light shortage, followed by humidity, lack of nutrients, and temperature. Twenty-two epilithic cyanobacteria were identified, ten of which have not been previously reported in caves. The species studied are included in the Chroococcales order (77.30%), followed by the Oscillatoriales order (13.60%) and by the Nostocales (4.55%) and Stigonematales (4.55%) orders. The extreme values of the environmental parameters are presented for each taxon in this cave.

Introduction

Caves present a microclimate that is characterized not only by temperature and relative humidity values that remain nearly constant all year round, but also by a luminous intensity that varies from the entrance to the back of the cave.

There are data sets on algal flora in caves from many countries and most continents. However, little information is available about algal communities in Spanish caves, and even less about the environmental conditions they require (Aboal et al., 1994; Asencio and Aboal, 1996, 2000 a,b; Asencio et al., 1996; Beltrán and Asencio, in press, Cañaveras et al., 2001; Gracia-Alonso, 1974; Hernández-Mariné and Canals, 1994; Hernández-Mariné et al., 1999; Ruíz-Sánchez et al., 1991).

The purpose of this study conducted at the Gelada Cave was to characterize the cyanobacterial communities and to document their distribution within the cave in accordance with environmental conditions as part of an extensive study of caves in the Province of Alicante (SE Spain).

Study Area

The Gelada Cave is located in the Font Roja Nature Reserve (38°38′51″N, 0°32′46″W) at an altitude of 1050 m in the municipality of Alcoy (Alicante, Spain). The climate of this region is Mediterranean, with continental and mountain influences depending on the altitude. Summers are dry with not excessively high temperatures, while winters are harsh with some snowfalls. Rainfall is relatively high and variable depending on exposure and altitude, with maximum precipitations in autumn (46 mm), winter (39 mm) and spring (44 mm), and minimum precipitations in summer (10 mm). The mean annual temperature is between 12 °C and 15 °C. There are limestone rocks in the area dating back to the Tertiary.

The entrance to the cave (Fig. 1) faces north and is 9.4 m deep, 0.9 to 5.0 m high and 1.2 m wide.

Material and Methods

Prior to collecting from the surface of walls at nineteen points at the Gelada Cave where colonization was evident, photon flux density (Photosynthetically Active Radiation - PAR), air temperature, and relative humidity measurements were taken in winter and summer. An LI-1400 datalogger model (LICOR) with an LI-192 sensor and a Delta Ohm HD 8501 H thermohygrometer, were used. Electrodes were placed on the rock surface.

Samples were taken using a scalpel and were placed into labeled plastic bags. Scraped material was used directly for observation under a light microscope or as inoculate for cultures in BG11 medium (Rippka et al. 1979). The cultures were maintained at 25 °C, 70 $\mu E.m^{-2}s^{-1}$, with a photoperiod of 16 h light and 8 h darkness. Species were determined by studying the material collected from the field and the cultured material.

Results and Discussion

The mean relative humidity in the Gelada Cave was 81.0% in both summer and winter. Values ranging between

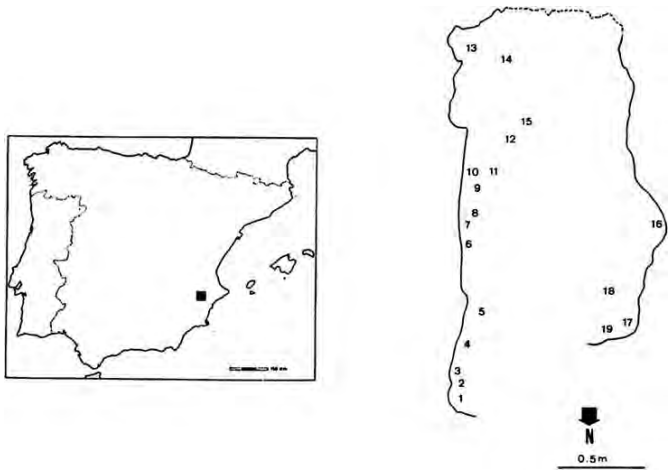

Figure 1. Geographical situation of Gelada Cave in Font Roja Nature Reserve in Alcoy, Alicante (SE Spain). Numbers show sampling sites.

a maximum of 95.0% inside the cave and a minimum of 55.0% at the entrance of the cave were recorded. These values coincide with the Quinçay Cave (Leclerc et al., 1983) and the Vapor Cave (Hernández-Mariné et al., 1999), however, they differ from those recorded at other areas in SE Spain, such as the Andragulla Shelter (Asencio and Aboal, 1996), the La Serreta Cave (Asencio and Aboal, 2000a) and the L'Aigua Cave (Beltrán and Asencio, in press), given the poor exposure of the area to the exterior, which modifies its environmental parameters.

The mean temperature in the Gelada Cave reaches 13.6 °C in summer and 6.2 °C in winter. Values ranging between a maximum temperature of 18.0 °C in summer and a minimum temperature of 5.4 °C in winter were recorded at points close to the entrance. The differences in temperature registered during the day varied between 1.7 °C in summer and 1.2 °C in winter, which are similar to those recorded at Quinçay: 1 °C (Leclerc et al., 1983). These values differ from those recorded during the most extreme seasons at other areas in SE Spain, such as the Andragulla Shelter with a range of 20.6 °C to 6.0 °C (Asencio and Aboal, 1996), the La Serreta Cave with between 6.4 °C in summer and 3.8 °C in winter (Asencio and Aboal, 2000a), and the L'Aigua Cave with a range of 12.1 °C to 4.3 °C (Beltrán and Asencio, in press).

The mean PAR values recorded in the Gelada Cave reached 0.01 $\mu E.m^{-2}.s^{-1}$ in summer and 0.006 $\mu E.m^{-2}.s^{-1}$ in winter. Values ranging between a maximum of 0.06 $\mu E.m^{-2}.s^{-1}$ in summer in the entrance and a minimum of 0.0008 $\mu E.m^{-2}.s^{-1}$ in winter inside the cave were recorded. These values were lower than those recorded at the Quinçay Cave where the maximum value reached was 0.2 $\mu E.m^{-2}.s^{-1}$ (Leclerc et al., 1983). These values differ from those recorded during the most extreme seasons at other areas in SE Spain, such as the Andragulla Shelter: 1504.0 $\mu E.m^{-2}.s^{-1}$ in summer and 1.4 $\mu E.m^{-2}.s^{-1}$ in winter (Asencio and Aboal, 1996), the La Serreta Cave: 1241.0 $\mu E.m^{-2}.s^{-1}$ in summer and 0.1 $\mu E.m^{-2}.s^{-1}$ in winter (Asencio and Aboal, 2000a), and the L'Aigua Cave: 1142 $\mu E.m^{-2}.s^{-1}$ in summer and 0.3 $\mu E.m^{-2}.s^{-1}$ in winter (Beltrán and Asencio, in press).

The fact that the relative humidity, temperature, and PAR values recorded inside the Gelada Cave remained more or less constant throughout the year indicates that this is, strictly speaking, a cave in accordance with Hoffmann (1989). This is in contrast to other caves and shelters in SE Spain, which present a less constant microclimate given their more direct exposure to the exterior (Asencio and Aboal, 1996; Asencio and Aboal, 2000a and Beltrán and Asencio, in press).

A total of twenty-two species have been identified and characterized along with the environmental parameters in the Gelada Cave (Appendix 1 and Table 1).

The cyanobacteria studied are included in the *Chroococcales* order, where the most diversity has been verified (77.30%), followed by the *Oscillatoriales* order (13.60%), then by the *Nostocales* (4.55%) and *Stigonematales* (4.55%) orders. The abundance of the *Chroococcales* species in the Gelada Cave, along with the predominance of *Oscillatoriales*, as opposed to *Nostocales*, coincides with some caves in Belgium (Garbacki et al., 1999) with similar temperature and humidity values.

Of the twenty-two species found, seventeen were coccoid and five were filamentous species. At sampling points 1, 8, 14, 15, 16 and 17, coccoid species were found exclusively. Coccoid species, as opposed to filamentous species, predominated at points 2, 3, 4, 5, 6, 7, 10 and 11. Filamentous species, as opposed to coccoid species, predominated at points 9, 13 and 18. A number of coccoid and filamentous species coincided at points 12 and 19. The predominance of coccoid species, as opposed to filamentous species, at the Gelada Cave coincides with the findings in the La Serreta Cave (Asencio and Aboal, 2000a), unlike caves and shelters that are not so deep and where filamentous species predominate (Asencio and Aboal, 1996). Coccoid forms are more abundant in dark areas, whereas filamentous forms tend to be more diverse in illuminated locations, unlike the findings of Vinogradova et al., (1998) who considered the opposite scenario.

The collected species are characterised by the presence of mucilaginous sheaths whose volume may vary considerably. Sheaths act as water reservoirs to avoid drying and prolong activity under drought conditions (Friedmann, 1972; Caiola et al., 1996; Nienow, 1996; Potts, 1999 and Potts and Friedmann, 1981). Occasionally, sheaths appear coloured because of pigments acting as filters to diminish the amount of incident light, which is in accordance with Krumbein and Potts (1978).

Of the thirteen identified genera, the genus that presents the most different species is *Gloeocapsa* with four, followed by *Cyanosaccus* and *Leptolyngbya* with three species each, then by *Chroococcus* and *Pleurocapsa* with two each. The

Table 1. Location of cyanobacteria at Gelada Cave and environmental conditions showing maxima and minima of PAR, temperature, and relative humidity to which the different taxa grow. Numbers show sampling sites.

		P.A.R. ($\mu E.m^{-2}.s^{-1}$)		Temperature (°C)		Relative Humidity (%)	
Cyanobacteria	Sampling Site	max	min	max	min	max	min
Aphanothece saxicola	6,10,	0.004	0.0008	14.3	5.5	91.0	76.0
Asterocapsa divina	1,2,3,4,5,6,7,8,11,13	0.03	0.001	18.0	5.4	95.0	55.0
Chroococcidium sp	4	0.01	0.004	16.0	5.4	84.0	77.0
Chroococcus spelaeus	1,4,5,6,14	0.02	0.003	18.0	5.4	92.0	55.0
Chroococcus westii	6,7,8,14	0.01	0.001	14.3	5.5	91.0	71.0
Cyanobacterium cedrorum	5	0.003	0.005	15.5	5.7	92.0	73.0
Cyanosaccus aegeus	1,6,7,10,14	0.02	0.0008	18.0	5.5	91.0	55.0
Cyanosaccus atticus	11,18	0.03	0.002	13.4	5.6	90.0	71.0
Cyanosaccus sp	3	0.03	0.002	16.4	5.6	80.0	78.0
Cyanostylon microcystoides	1,2,5,8	0.03	0.001	18.0	5.7	92.0	55.0
Gloeocapsa biformis	1,2,5,15	0.03	0.002	18.0	5.5	92.0	55.0
Gloeocapsa nigrescens	3	0.03	0.002	16.4	5.6	80.0	78.0
Gloeocapsa novacekii	2,8,17	0.03	0.0008	18.0	5.8	85.0	67.0
Gloeocasa rupicola	6,12,15,17,19	0.06	0.0008	14.3	5.5	91.0	69.0
Leptolyngbya "Albertano/ Kováčik-red"	3,4,7,10,11,12	0.03	0.0008	16.4	5.4	90.0	77.0
Leptolyngbya carnea	9	0.003	0.001	12.3	6.3	86.0	82.0
Leptolyngbya leptotrichiformis	2,5,6,7,9,11,13,18	0.03	0.001	17.5	5.5	95.0	67.0
Pleurocapsa sp	16	0.009	0.0009	13.6	5.7	84.0	73.0
Pleurocapsa minor	8, 9,10,11	0.008	0.0008	13.1	5.6	90.0	81.0
Pseudocapsa dubia	1,2,3,4,8	0.03	0.001	18.0	5.4	85.0	55.0
Scytonema julianum	5,6,10,11,13,19	0.06	0.0008	15.5	5.5	95.0	69.0
Symphyonema cavernicolum	18	0.03	0.002	13.4	5.8	83.0	71.0

remaining genera: *Aphanothece*, *Asterocapsa*, *Chroococcidium*, *Cyanobacterium*, *Cyanostylon*, *Pseudocapsa*, *Scytonema* and *Symphyonema* presented one species each.

The fact that four *Gloeocapsa* species were present at the Gelada Cave indicates that the algal colonization on the walls is at an intermediate stage, and coincides with Fritsch (1907), Diels (1914), Häyren (1940), Garty (1990) and Pentecost (1992), who all considered these genera to be pioneers in rock colonization. This contrasts with similar works in which *Gloeocapsa* appears less abundantly (Iliopoulou-Georgoudaki et al., 1993, Asencio and Aboal, 2000a, and Beltrán and Asencio, in press).

Of the twenty-two species identified, the most common are *Asterocapsa divina* found at ten points, *Leptolyngbya leptotrichiformis* at eight points, and *Scytonema julianum* at six points, while *Chroococcidium* sp, *Cyanobacterium cedrorum*, *Cyanosaccus* sp, *Gloeocapsa nigrescens*, *Leptolyngbya carnea*, *Pleurocapsa* sp and *Symphyonema cavernicolum* were encountered at only one point each.

Those species which withstand less constant environmental conditions at the Gelada Cave are: *Cyanosaccus aegeus* (0.02–0.0008 $\mu E.m^{-2}.s^{-1}$, 91.0–55.0%, 18.0–5.5 °C), *Gloeocapsa novacekii* (0.03–0.0008 $\mu E.m^{-2}.s^{-1}$, 85.0–67.0%, 18.0–5.8 °C), *Gloeocapsa rupicola* (0.06–0.0008 $\mu E.m^{-2}.s^{-1}$, 91.0–69.0%, 14.3–5.5 °C), *Leptolyngbya "Albertano/Kováčik-red"* (0.03–0.0008 $\mu E.m^{-2}.s^{-1}$, 90.0–77.0%, 16.4–5.4 °C) and *Scytonema julianum* (0.06–0.0008 $\mu E.m^{-2}.s^{-1}$, 95.0–69.0%, 15.5–5.5 °C), whereas *Cyanobacterium cedrorum* (0.003–0.005 $\mu E.m^{-2}.s^{-1}$, 92.0–73.0%, 15.5–5.7 °C) and *Leptolyngbya carnea* (0.003–0.001 $\mu E.m^{-2}.s^{-1}$, 86.0–82.0%, 12.3–6.3 °C) withstand more constant environmental conditions.

Scytonema julianum (Fig. 2) can resist extreme oscillations. It grows on well lit cave walls with maximum values of 2000 $\mu E.m^{-2}.s^{-1}$ and under very low light conditions in some caves, where minimum values of 0.007 $\mu E.m^{-2}.s^{-1}$ were registered (Leclerc et al., 1983; Couté and Bury 1988 and Aboal et al. 1994).

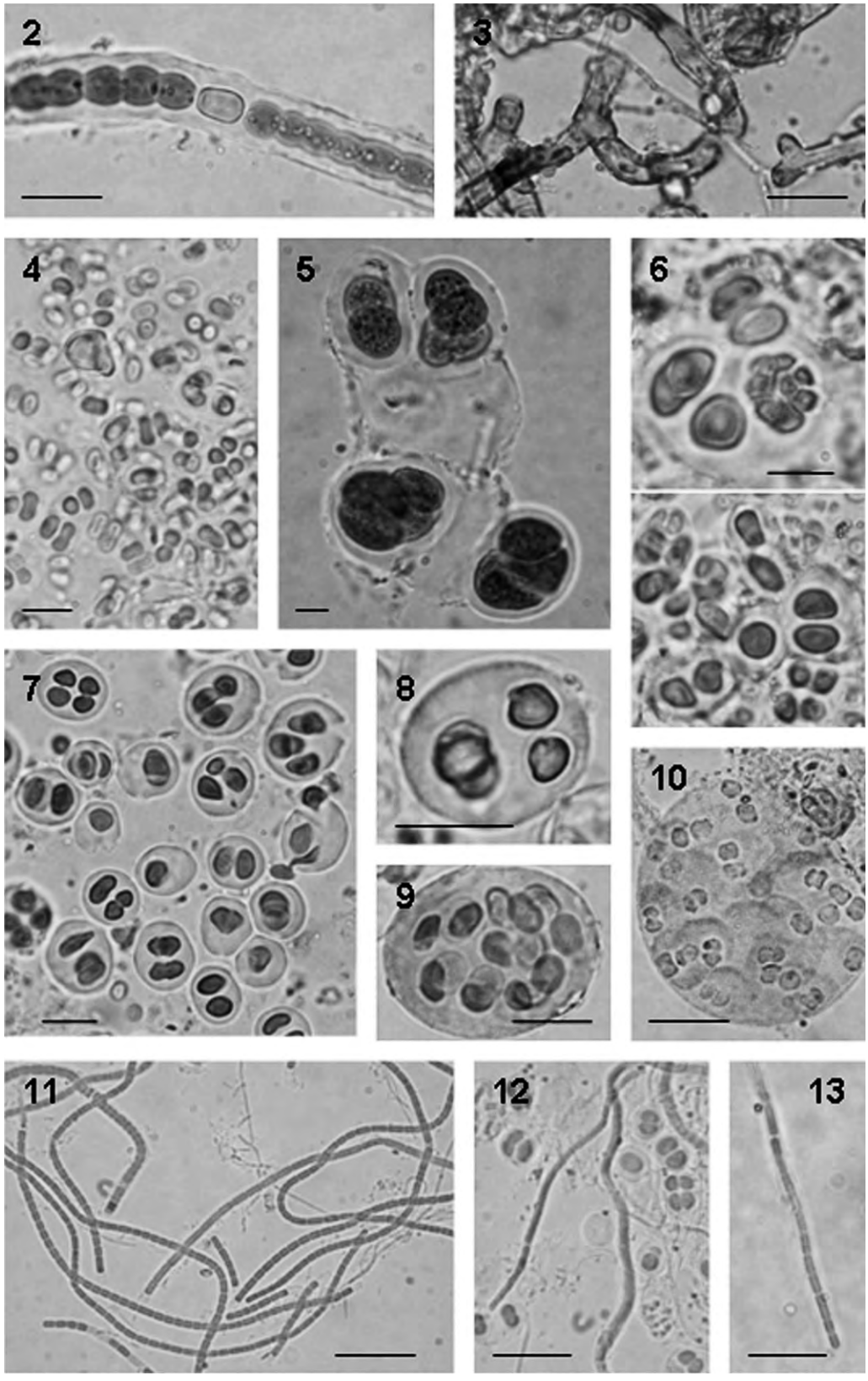

Plate 1. (Figures 2–13) Light micrographs [scale bar: 10 µm] of: 2- *Scytonema julianum*, 3- *Symphyonema cavernicolum*, 4- *Cyanobacterium cedrorum*, 5- *Cyanosaccus aegeus*, 6- *Cyanosaccus atticus*, 7- *Cyanostylon microcystoides*, 8- *Gloeocapsa nigrescens*, 9- *Gloeocapsa novacekii*, 10- *Gloeocapsa rupicola*, 11- *Leptolyngbya "AlbertanolKováčik-red"*, 12- *Leptolyngbya carnea*, 13- *Leptolyngbya leptotrichiformis*.

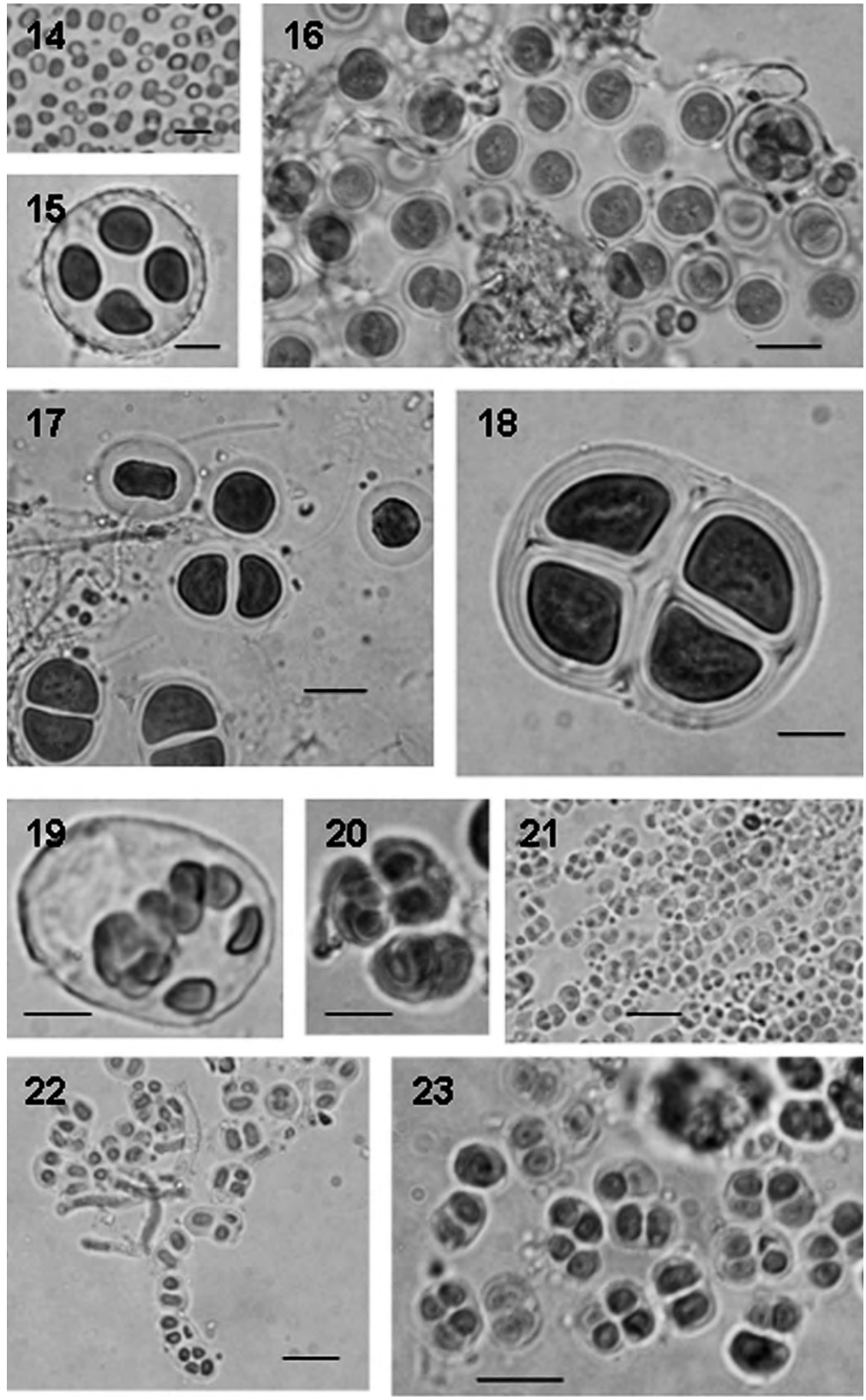

Plate 2. (Figures 14–23) Light micrographs [scale bar: 10 µm] of: 14- *Aphanothece saxicola*, 15- *Asterocapsa divina*, 16- *Chroococcidium* sp, 17- *Chroococcus spelaeus*, 18- *Chroococcus westii*, 19- *Cyanosaccus* sp, 20- *Gloeocapsa biformis*, 21- *Pleurocapsa* sp, 22- *Pleurocapsa minor* 23- *Pseudocapsa dubia*.

Table 2. Characterization, composition and location of cyanobacteria communities at Gelada Cave. Numbers show sampling sites.

Sampling Sites	Cyanobacterial Comunities	Patina
1	*Asterocapsa divina*, *Chroococcus spelaeus*, *Cyanosaccus aegeus*, *Cyanostylon microcystoides*, *Gloeocapsa biformis*, *Pseudocapsa dubia*	greenish-bluish
2	*Asterocapsa divina*, *Cyanostylon microcystoides*, *Gloeocapsa biformis*, *G. novacekii*, *Leptolyngbya leptotrichiformis*, *Pseudocapsa dubia*	greyish
3	*Asterocapsa divina*, *Cyanosaccus* sp, *Gloeocapsa nigrescens*, *Leptolyngbya ''Albertano/Kováčik-red''*, *Pseudocapsa dubia*	greyish
4	*Asterocapsa divina Chroococcidium* sp, *Chroococcus spelaeus*, *Leptolyngbya ''Albertano/Kováčik-red''*, *Pseudocapsa dubia*	greyish
5	*Asterocapsa divina Chroococcus spelaeus*, *Cyanobacterium cedrorum*, *Cyanostylon microcystoides*, *Gloeocapsa biformis*, *Leptolyngbya leptotrichiformis*, *Scytonema julianum*	bluish-greyish
6	*Aphanothece saxicola*, *Asterocapsa divina*, *Chroococcus spelaeus*, *Ch. westii*, *Cyanosaccus aegeus*, *Gloeocapsa rupicola*, *Leptolyngbya leptotrichiformis*, *Scytonema julianum*	bluish-greyish
7	*Asterocapsa divina*, *Chroococcus westii*, *Cyanosaccus aegeus*, *Leptolyngbya ''Albertano/Kováčik-red''*, *L. leptotrichiformis*	brownish-grey
8	*Asterocapsa divina*, *Chroococcus westii*, *Cyanostylon microcystoides*, *Gloeocapsa novacekii*, *Pleurocapsa minor*, *Pseudocapsa dubia*	greenish-bluish
9	*Leptolyngbya carnea*, *Leptolyngbya leptotrichiformis*, *Pleurocapsa minor*	brownish-grey
10	*Aphanothece saxicola*, *Cyanosaccus aegeus*, *Leptolyngbya ''Albertano/ Kováčik-red''*, *Pleurocapsa minor*, *Scytonema julianum*	bluish-greyish
11	*Asterocapsa divina*, *Cyanosaccus atticus*, *Leptolyngbya ''Albertano/ Kováčik-red''*, *Leptolyngbya leptotrichiformis*, *Pleurocapsa minor*, *Scytonema julianum*	bluish-greyish
12	*Gloeocapsa rupicola*, *Leptolyngbya ''Albertano/Kováčik-red''*	brownish-grey
13	*Asterocapsa divina*, *Leptolyngbya leptotrichiformis*, *Scytonema julianum*	bluish-greyish
14	*Chroococcus spelaeus*, *Chroococcus westii*, *Cyanosaccus aegeus*	greenish-bluish
15	*Gloeocapsa biformis*, *Gloeocapsa rupicola*	greenish-bluish
16	*Pleurocapsa* sp	greenish-bluish
17	*Gloeocapsa novacekii Gloeocapsa rupicola*	greenish-bluish
18	*Cyanosaccus atticus Leptolyngbya leptotrichiformis* and *Symphyonema cavernicolum*.	brownish-grey
19	*Gloeocapsa rupicola Scytonema julianum*	bluish-greyish

In contrast, other filamentous cyanobacteria, such as *Symphyonema cavernicolum* (Fig. 3), cited for the second time in such settings, require more stable temperature, relative humidity, and PAR values. This species at the Gelada Cave withstands PAR values below the minimum recorded at the La Serreta Cave during its epilithic development (Asencio and Aboal, 2000a). This confirms that this species does not withstand high light intensity values and implies that it develops chasmoendolithically when light peaks are very high (Asencio et al., 1996).

Of the twenty-two species identified, ten: *Cyanobacterium cedrorum* (Fig. 4), *Cyanosaccus aegeus* (Fig. 5), *C. atticus* (Fig. 6), *Cyanostylon microcystoides* (Fig. 7), *Gloeocapsa nigrescens* (Fig. 8), *G. novacekii* (Fig. 9), *G. rupicola* (Fig. 10), *Leptolyngbya ''Albertano/Kováčik-red''* (Fig. 11), *L. carnea* (Fig. 12), and *L. leptotrichiformis* (Fig. 13) have not been previously cited in cave settings, but in places with weak incident radiation. Therefore, these results confirm the importance of light in the distribution of algae species and coincide with those of Jaag (1945) and Zehnder (1953).

Microscopic observations revealed that cyanobacteria are arranged in a particular assemblage named patinas which are blue, brown, green, or gray and continuous, and are arranged mosaically inside the Gelada Cave. These communities contain coccoid forms that are frequently accompanied by filamentous forms that are irregularly distributed and do not present stratification.

We may assume two different areas at the Gelada Cave. a) One area is the entrance level, where the microclimate is influenced by the exterior and attenuated light, temperature, and relative humidity fluctuate throughout the year. Patina is greenish-bluish formed by coccoid species only, and there are also grayish patina constituted by coccoid and filamentous species. b) The second area is the inside level with a

stable temperature and relative humidity and very low light. The patina found are greenish-bluish formed by only coccoids species, brownish-gray patina constituted by coccoid forms and filamentous forms, and bluish-grayish patina formed by coccoid forms and filamentous forms where *Scytonema julianum* predominates.

The points in the Gelada Cave where the largest number of species grow were 6 and 5 with eight and seven species respectively, and the lowest number was at 16 with only one species (Table 2). The diversity of cyanobacteria communities diminishes with decreasing light.

The occurrence of a particular assemblage of cyanobacteria in the samples taken at the Gelada Cave suggests some stability of species composition in these communities. The network of filaments may contribute to maintain levels of moisture during periods in which the relative humidity of the air is low, thus favoring all community members.

There was a larger number of species growing at the sampling locations facing west given the presence of holm oaks, which prevent sun rays from passing to the sampling locations facing east. The primary common stress factor on the distribution of algal communities in the Gelada Cave is light shortage, followed by humidity, lack of nutrients and temperature, which is in accordance with Smith and Olson (2007) for cave-like environments.

ACKNOWLEDGEMENTS

We sincerely thank N. Espinosa, P. Espinosa, T. Espinosa and L. Serra for their help in the field and H. Warburton for his assistance in the English version of the text.

REFERENCES

Aboal, M., Asencio, A.D., and Prefasi, M., 1994, Studies on cave cyanophytes from southeastern Spain: *Scytonema julianum* Richter: Archiv für Hydrobiology Algological Studies, v. 75, p. 31–36.

Aboal, M., Asencio, A.D., and López-Jiménez, E., 2003, Morphological, ultrastructural and ecological study of *Asterocapsa divina* Komárek (Chroococcaceae, Cyanobacteria) from a cave of Southeastern Spain: Archiv für Hydrobiology/Algological Studies, v. 109, p. 57–65.

Anagnostidis, K., Economou-Amilli, A., and Pantazidou, A., 1981, Studies on the microflora of the cave Perama, Ioannina, Greece: Bulletin Society Speleological Greece, v. 18, p. 458–530.

Anagnostidis, K., and Pantazidou, A., 1985, *Cyanosaccus aegaeus* n. sp., a new marine endolithic cyanophyte from the Aegean Sea, Hellas (Greece): Archiv für Hydrobiology/Algological Studies, v. 38/39, p. 105–114.

Anagnostidis, K., and Pantazidou, A., 1988, Endolithic cyanophytes from the saline thermal springs of Aedipsos, Hellas (Greece): Archiv für Hydrobiology/Algological Studies, v. 50–53, p. 555–559.

Ariño, X., Hernández-Mariné, M., and Saíz-Jiménez, C., 1997, Preliminary investigations on epilithic cyanophytes from a Roman necropolis: Archiv für Hydrobiology/Algological Studies, v. 75, p. 71–74.

Asencio, A.D., 1997, Flora algal y condiciones ambientales de las cuevas y abrigos con pinturas rupestres de la Región de Murcia (SE España). [Ph.D.thesis]: Universidad de Murcia, 382 p.

Asencio, A.D., and Aboal, M., 1996, Cyanophytes from Andragulla abrigo (Murcia, SE Spain) and their environmental conditions: Archiv für Hydrobiology/Algological Studies, v. 83, p. 55–72.

Asencio, A.D., Aboal, M., and Hoffmann, L., 1996, A new cave-inhabiting blue-green alga: *Symphyonema cavernicolum* sp. nova (Mastigocladaceae, Stigonematales): Archiv für Hydrobiology/Algological Studies, v. 83, p. 73–82.

Asencio, A.D., and Aboal, M., 2000a, Algae from La Serreta cave (Murcia, SE Spain) and their environmental conditions: Archiv für Hydrobiology/Algological Studies, v. 96, p. 59–72.

Asencio, A.D., and Aboal, M., 2000b, A contribution to knowledge of chasmoendolithic algae in cave-like environments: Archiv für Hydrobiology/Algological Studies, v. 98, p. 133–151.

Beltrán, J.A., and Asencio, A.D., 2009, Cyanophytes from the L'Aigua cave (Alicante, SE Spain) and their environmental conditions: Archiv für Hydrobiology/Algological Studies (in press).

Caiola, M.G., Billi, D., and Friedmann, E.I., 1996, Effect of desiccation on envelopes of the cyanobacterium *Chroococcidiopsis* sp (Chroococcales): European Journal of Phycology, v. 31(1), p. 97–105.

Cañaveras, J.C., Sánchez-Moral, S., Soler, V., and Saíz-Jiménez, C., 2001, Microorganisms and microbially induced fabrics in cave walls: Geomicrobiology Journal, v. 18, p. 223–240.

Chang, T.P., and Chang-Schneider, H., 1991, Algen in vier süddeutschen Höhlen: Berichte der Bayerischen Botanischen Gesellschaft, v. 62, p. 221–229.

Couté, A., and Bury, E., 1988, Ultrastructure d'une cyanophycée aérienne calcifiée cavernicole: *Scytonema julianum* (Frank) Richter (Hormogonophycideae, Nostocales, Scytonemataceae): Hydrobiologia, v. 160, p. 219–239.

Diels, L., 1914, Die Algen Vegetation der südtiroler Dolomitriffe. Ein Beitrag zur Ökologie der Lithophyten: Verhandlungen der Deutschen Botanischen Gesellschaft, v. 32, p. 502–526.

Dor, I., and Dor, Y., 1999, Cyanobacterial flora of the Soreq stalactite Cave (Israel) and way of its control: Archiv für Hydrobiology/ Algological Studies, v. 129, p. 115–118.

Domínguez, S.G., and Asencio, A.D., 2009, Distribution of chasmoendolithic Cyanobacteria in gypsiferous soils from semi-arid environments (SE Spain) by chemicals and physical parameters: Nova Hedwigia, (in press).

Friedmann, E.I., 1972, Ecology of lithophytic algal habitats in Middle Eastern and North American deserts, *in* Rodin, L.E., ed., Ecophysiological foundation of ecosystems productivity in arid zones, Nauka, U.S.S.R. Academic Sciences, Leningrad, p. 182–185.

Friedmann, E.I., 1979, The genus *Geitleria* (Cyanophyceae or Cyanobacteria): Distribution of *G. calcarea* and *G. floridana* n. sp.: Plant Systematics and Evolution, v. 131, p. 169–178.

Fritsh, F.E., 1907, A general consideration of the subaerial and freshwater algal flora of Ceylon. A contribution to the study of tropical algal ecology. Part I. –Subaerial algae and algae of the inland freshwaters, *in* Proceedings of the Royal Society of London, v. 79, p. 197–254.

Garbacki, N., Ector, L., Kostikov, I., and Hoffmann, L., 1999, Contribution à l'étude de la flore des grottes de Belgique: Belgium Journal of Botany, v. 132, p. 43–76.

Garty, J., 1990, Influence of epilithic microorganisms on the surface temperature of building walls: Canadian Journal of Botany, v. 68, p. 1349–1353.

Golubic, S., 1967, Algenvegetation der Felsen, *in* Elster, H.J., and Ohle, W., eds., Die Binnengewässer: E. Schweizerbart'sche Verlagsbuchhandlung, Stuttgart, p. 23–183.

Gracia-Alonso, C.A., 1974, *Geitleria calcarea* Friedmann nueva alga cavernicola para España: Speleon, v. 21, p. 133–136.

Häyren, E., 1940, Die Algenvegetation der Sickerwasserstreifen auf den Felsen in Südfinnland: Societas Scientiarum Fennicae Commentationes Biologicae, v. 7, p. 1–19.

Hernández-Mariné, M., and Canals, T., 1994, *Herpyzonema pulverulentum* (*Mastigocladaceae*), a new cavernicolous atmophytic and lime-incrusted cyanophyte: Archiv für Hydrobiology/Algological Studies, v. 75, p. 123–136.

Hernández-Mariné, M., Asencio, A.D., Canals, A., Ariño, X., Aboal, M., and Hoffmann, L., 1999, Discovery of populations of the lime-incrusting genus *Loriella* (Stigonematales) in Spanish caves: Archiv für Hydrobiology/Algological Studies, v. 94, p. 121–138.

Hoffmann, L., 1989, Algae of terrestrial habitats: Botanical Review, v. 55, p. 77–105.

Iliopoulou-Georgoudaki, J., Pantazidou, A., and Theoulakis, P., 1993, An assessment of cleaning photoautotropic microflora: the case of Perama cave, Ioannina Greece: Mémories de Biospéologie, v. 20, p. 117–120.

Jaag, O., 1945, Untersuchungen über die Vegetation und Biologie der Algen des nackten Gesteins in den Alpen, im Jura und schweizerischen Mittelland: Beiträge zur Kryptogamenflora der Schweiz, v. 9, p. 1–560.
Komárek, J., 1993, Validation of the genera *Gloeocapsopsis* and *Asterocapsa* (Cyanoprokaryota) with regard to species from Japan, Mexico and Himalayas: Bulletin National Science Museum, Tokyo, Ser. B, v. 19, p. 19–37.
Komárek, J., and Anagnostidis, K., 1999, Süsswasserflora von Mitteleuropa. Cyanoprokaryota 1. Chroococcales, Gustav Fischer Verlag, Stuttgart, Jena, New York, 548 p.
Komárek, J., and Anagnostidis, K., 2005, Cyanophyta part II: *Oscillatoriales*, *in*, Büdel, B., Gärtner, G., Krienitz, L., and Schagerl, M., eds., Süsswasserflora von Mitteleuropa 19/2: 1–759, Gustav Fischer, Jena,
Krumbein, W.E., and Potts, M., 1978, Light penetration, salinity and other growth regulating factors of four stromatolitic environments along the shores of the Gulf of Aqaba (Sinai), in: Friedmann, G.M., ed., Abstracts 10th International Congress on Sedimentology 1. Jerusalem. 363 p.
Leclerc, J.C., Couté, A., and Dupuy, P., 1983, Le climat annuel de deux grottes et d'une église du Poitou, où vivent des colonies pures d'algues sciaphiles: Cryptogamie, Algologie, v. 4, p. 1–19.
Margalef, R., 1952, Algas de agua dulce del noroeste de España: Publicaciones del Instituto de Biología Aplicada, v. 22, p. 43–152.
Nienow, J.A., 1996, Ecology of subaerial algae: Nova Hedwigia, v. 112, p. 537–552.
Palik, P., 1938, Adatok a Bukk-Hegység Lithophyta Algavegetátiójához. (Beiträge zur Kenntnis der Lithophyten Algenvegetation des Bükkgebirges): Index Horti Botanici Universitatis Budapestinensis, v. 3, p. 3–10.
Pentecost, A., 1992, A note on the colonization of limestone rocks by Cyanobacteria: Archiv für Hydrobiology, v. 124, p. 167–172.
Poulicková, A., and Hasler, P., 2007, Aerophytic diatoms from caves in central Moravia (Czech Republic): Preslia, v. 79, p. 185–204.
Potts, M., 1999, Mechanisms of desiccation tolerance in cyanobacteria: European Journal of Phycology, v. 34, p. 319–328.
Potts, M., and Friedmann, E.I., 1981, Effects of water stress on cryptoendolithic cyanobacteria from hot desert rocks: Archiv für Mikrobiologie, v. 130, p. 267–271.
Rifón-Lastra, A.B., 2000, Algas epilíticas en monumentos de interés histórico de Galicia. [Ph.D.thesis], Universidade da Coruña, 282 p.
Rippka, R., Deruelles, J., Waterbury, J.B., Herdman, M., and Stanier, R.Y., 1979, Generic assignments, strain histories and properties of pure cultures of cyanobacteria: Journal of General Microbiology, v. 111, p. 1–61.
Ruíz-Sánchez, I., Marín-Girón, F., Ojeda, F., Marín-Olalla, F., Berros, J., and Marín-Olalla, E., 1991, Estudio macroscópico "in situ" y microscópico-ecológico de pequeñas zonas de flora verde (algas verdes y verdeazuladas) del interior de la Cueva de Nerja, *in*: Marín, F., and Carrasco, F., eds., Investigación biológica y edafológica de la cueva de Nerja, Trabajos sobre la cueva de Nerja, v. 2, p. 113–125.
Seckt, H., 1938, Estudios hidrobiológicos en la Argentina. Schizophyceae: Boletín de la Academia Nacional de Ciencias de Córdoba, v. 25, p. 383–429.
Skuja, H., 1970, Alghe cavernicole nelle zone illuminate delle grotte di Castellana (Murge di Bari).-Le Grotte d'Italia, Ser. 4, v. 2, p. 193–202.
Smith, T., and Olson, R., 2007, A taxonomic survey of lamp flora (Algae and Cyanobacateria) in electrically lit passages within Mammoth cave national park, Kentucky: International Journal of Speleology, v. 36, p. 105–114.
Uher, B., and Kovacik, L., 2002, Epilithic cyanobacteria of subaerial habitats in National Park Slovak Paradise (1998–2000): Bulletin Slovenskej Botanickej Spoločnosti Bratislava, v. 24, p. 25–29.
Uher, B., Aboal, M., and Kovacik, L., 2005, Epilithic and chasmoendolithic phycolflora of monuments and buildings in South-Eastern Spain: Cryptogamie, Algologie, v. 26(3), p. 275–358.
Vinogradova, O.N., Kovalenko, O.V., Wasser, S.P., Nevo, E., and Weinstein-Evron, M., 1998, Species diversity gradient to darkness stress in blue-green algae/cyanobacteria: a microscale test in a prehistoric cave, Mount Carmel, Israel: Israel Journal of Plant Sciences, v. 46, p. 229–238.
Zehnder, A., 1953, Beitrag zur Kenntnis von Mikroklima und Algenvegetation des nackten Gesteins in den Tropen: Berichte der Schweizerischen Botanischen Gesellschaft, v. 63, p. 5–26.

APPENDIX 1.
TAXONOMIC LIST OF CYANOBACTERIAL FLORA FROM GELADA CAVE

Aphanothece saxicola Nägeli Fig. 14
Cylindrical cells, 2.0–3.0 μm wide and 2.5–3.5 μm long, grouped in a gelatinous mass with no clear shape. With the sheath, they can become 2.5–3.5 μm wide and 3.0–4.0 μm long. This species was cited by Seckt (1938), Margalef (1952), Dor and Dor (1999), Smith and Olson (2007) and by Beltrán and Asencio (in press) as an epilithic species on cave walls.

Asterocapsa divina Komárek Fig. 15
Spherical cells, 4.0–5.0(−6.0) μm, surrounded by a hyaline sheath, ornamented with wart-like structures, reaching a diameter of 6.5–8.0(−9.0) μm. They group to form colonies reaching 30.0 μm. Komárek (1993) described this species on limestone rocks in Mexico. Aboal et al (2003) found this species in a cave in Murcia, Spain.

***Chroococcidium* sp** Fig. 16
Spherical, bluish-greenish 7.6 μm-diameter cells, which may form groups as colonies of up to 14.0 μm. They are arranged as an undefined gelatinous mass.

Chroococcus spelaeus Ecergovic Fig. 17
Spherical, 9.0–10.0 μm-diameter, violet or dark green cells surrounded by a hyaline sheath which reaches 15.0 μm. After division, groups of 2–4 cells appear with a diameter of up to 20.0 μm. Komárek and Anagnostidis (1999) cited this species as aerophytic, and they found it on humid rocks in Croatia. Poulíčková and Hašler (2007) noticed it in caves in the Czech Republic.

Chroococcus westii Boye-Petersen Fig. 18
Violet spherical cells of 11.0 μm diameter, surrounded by a lamellate hyaline sheath reaching 15.0 μm. After division, groups of 2 to 4 cells appear to reach a diameter of 20.0–25.0 μm. Komárek and Anagnostidis (1999) cited this species as subaerophytic and found it on humid rocks in mountainous areas. Garbacki et al (1999) referred to it in caves in Belgium.

Cyanobacterium cedrorum (Sauvageau) Komárek et al. Fig. 4
Cylindrical bluish-greenish cells, either alone or in pairs, 4.5 μm long and 2.0 μm wide.
Komárek and Anagnostidis (1999) cited this species as being subaerophytic on humid rocks of warm areas of the temperate zone and in tropical countries. Uher et al (2005) noted it on monuments in Murcia, Spain.

***Cyanosaccus* sp** Fig. 19
Spherical or pyriform purple cells, 6.0 μm. They are single or form groups of 2–4, surrounded by a gelatinose, hyaline, penduculated glass-shaped sheath of up to 20.0 μm wide. Presence of spherical nanocytes, 2.5(−3.0) μm diameter.

Cyanosaccus aegeus Anagnostidis et Pantazidou Fig. 5
Ellipsoidal or pyriform violet cells with a granular content, measuring 12.0 × 9.0 μm. They are single or form groups of 2–4, surrounded by a mucilaginous, colourless and

penduculated sheath. These structures, measuring as much as 37.0 μm wide, form groups of 4 and appear dendriform. Anagnostidis and Pantazidou (1985) described this species as endolithic on carbonate rocks of the Aegean Sea. Komárek and Anagnostidis (1999) cited it on the coast of South Africa.

Cyanosaccus atticus Anagnostidis et Pantazidou Fig. 6

Spherical or pyriform purple cells of around 5.4 μm. They are single or form groups of 2 to 4, surrounded by a mucilaginous, hyaline and pedunculated sheath of up to 15.0–20.0 μm wide. Presence of spherical, 1.5(−2.0) μm-diameter nanocytes. Anagnostidis and Pantazidou (1988) described this species as endolithic on carbonated rocks of the Aegean Sea.

Cyanostylon microcystoides Geitler Fig. 7

Reddish, spherical 4.0 μm-diameter cells which are either alone or form groups of 2–4 cells, surrounded by a mucilaginous and hyaline sheath which extends to become penduculated. Komárek and Anagnostidis (1999) referred to this species on the walls of alpine lakes and waterfalls in Central Europe.

Gloeocapsa biformis Ecergovic Fig. 20

Bluish-greenish spherical cells with a diameter of 3.0–4.0 μm, surrounded by a hyaline or yellowish sheath that reach up to 5.0–6.0 μm. Golubic (1967) found this species inside a cave in Croatia. Anagnostidis et al. (1981) mentioned it in the Perama Cave at Ioannina in Greece. Chang and Chang-Schneider (1991) found it in caves in Germany, while Ilipoulou-Georgoudaki et al. (1993) referred to it in a cave in Greece. Asencio and Aboal (1996) found it in a cave in Murcia, Spain. Garbacki et al. (1999) cited it in a cave in Belgium, whereas Beltrán and Asencio (in press) noticed it in a cave in Alicante, Spain.

Gloeocapsa nigrescens Nägeli in Rabenhorst Fig. 8

Spherical cells, 4.0–5.0 μm, surrounded by a reddish sheath reaching 6.0–7.0 μm. They group to colonies with a diameter of 10.0–20.0 μm. Komárek and Anagnostidis (1999) cited this species as aerophytic on calcareous rocks in poorly illuminated areas and with a high atmospheric humidity. It was cited by Uher and Kováčik (2002) in epilithic subaerial populations of Slovakia.

Gloeocapsa novacekii Komárek et Anagnostidis Fig. 9

Spherical cells, 5.2 μm, surrounded by a hyaline or dark red-coloured sheath reaching 6.5 μm, which groups to form colonies, 11.0–35.0μm, with colourless or reddish mucilaginous, non-lamellated sheaths. Komárek and Anagnostidis (1999) referred to this species as aerophytic on periodically dampened serpentine rocks in the Czech Republic. Rifón-Lastra (2000) cited on monuments of historic interest in Galicia, Spain. Domínguez and Asencio (in press) also cited it in gypsum areas of Alicante, Spain.

Gloeocapsa rupicola Kützing Fig. 10

Bluish-greenish spherical cells measuring 3.0–4.0 μm, surrounded by a lamellated, 6.0 μm-diameter reddish sheath. They may group to form colonies measuring 35.0–50.0 μm. Komárek and Anagnostidis (1999) described this species as being aerophytic on periodically dampened rocks and on mountain walls in Central Europe. Domínguez and Asencio (in press) cited it in gypsum areas of Alicante, Spain.

Leptolyngbya "AlbertanolKováčik-red" Fig. 11

Filaments with a diameter of 3.0 μm formed by a hyaline sheath and a constricted trichome formed by 2.0 μm-diameter and 2.0 μm-long brownish-reddish cells. Conical apical cell. Komárek and Anagnostidis (2005) cited this species as subaerophytic on humid walls of poorly illuminated areas.

Leptolyngbya carnea (Kützing ex Lemmermann) Anagnostidis et Komárek Fig. 12

Densely interwoven filaments, 4.0 μm, made up of a hyaline sheath and non-constricted trichome with reddish 3.0 μm isodiameterical cells. Rounded apical cell. Uher and Kováčik, (2002) cited this species in subaerial epilithic habitats in Slovakia. Komárek and Anagnostidis (2005) noted it as a subaerophytic species on the walls of greenhouses and on drenched rocks in Central Europe and in North America.

Leptolyngbya leptotrichiformis (Krieger) Anagnostidis et Komárek in Anagnostidis Fig. 13

Filaments, 2.0–3.0 μm wide, with a hyaline sheath which surrounds the trichome made up of cells that are longer than they are wide, 2.0 μm long and 1.0 μm wide. Rounded apical cell. Komárek and Anagnostidis (2005) cited this species as an aerophytic species on walls made out of humid rocks in Greece.

***Pleurocapsa* sp** Fig. 21

Colonies made up of bluish-greenish pseudofilaments, 3.0–4.0 μm, joined laterally by gelatinous hyaline sheaths. Rounded 2.0 μm-diameter cells. Nanocytes, 0.8 μm, group as cenobio with a diameter of 5.0 μm.

Pleurocapsa minor Hansgirg Fig. 22

Colonies formed of bluish-greenish pseudofilaments with a diameter of 3.0–9.0 μm with gelatinous hyaline sheaths which surround the 3.0–4.0 μm-diameter cells. This species has been cited in the Perama Cave at Ioannina in Greece (Anagnostidis et al., 1981). It has also been observed in the L'Aigua Cave in Alicante, Spain (Beltrán and Asencio, in press).

Pseudocapsa dubia Ercegovic Fig. 23

Spherical cells of a 4.0 μm diameter surrounded by a hyaline sheath, reaching a size of 5.0 μm. Cells vary in number and group in more or less rounded colonies, reaching 11.0–19.0 μm. Nanocytes with a diameter of 1.5–2.0 μm. Palik (1938) mentioned *Pseudocapsa dubia* in a cave in Hungary and Skuja (1970) observed it in a cave in Italy. Ariño et al. (1997) found it on Roman tombs in Seville, Spain, while Asencio (1997) cited it as an epilithic and casmoendolithic species in several caves in Murcia, Spain. It also appeared in the L'Aigua Cave in Alicante, Spain (Beltrán and Asencio, in press).

Scytonema julianum (Meneghini ex Frank) Richter Fig. 2
Greenish-bluish filament, 10.5 μm wide, surrounded by a considerably thick calcium carbonate sheath with which the filament reaches 13.0 μm. Hyaline sheath. Trichome formed by cells measuring 5.5–6.5 μm wide by 5.0–6.0 μm long. Rectangular heterocytes (5.0 μm × 7.0 μm). Friedmann (1979) cited this species on the walls of calcareous caves. Couté and Bury (1988) found it in numerous calcareous caves in France, while Hoffmann (1989) considered it characteristic of areas close to cave entrances. Iliopoulou-Georgoudaki et al. (1993) referred to it in a cave in Greece and Aboal et al. (1994) found it in a cave in Murcia, Spain. Ariño et al (1997) also cited it on Roman tombs in Seville, Spain. Cañaveras et al (2001) found it in caves at Altamira and Tito Bustillo, Santander, Spain, whereas Smith and Olson (2007) mentioned it in a cave in Kentucky, USA. Finally, Beltrán and Asencio (in press) found it at the L'Aigua Cave in Alicante, Spain.

Symphyonema cavernicolum Asencio, Aboal and Hoffmann Fig. 3
Filaments, diameter 5.0 μm, made up of constricted trichomes with tapering ends and with brownish cells measuring 4.0 μm wide and 11.0 μm long, surrounded by a hyaline sheath with calcium carbonate incrustations. They present genuine V-, Y- and T-shaped branches (infrequent). This species was described by Asencio et al. (1996) in cave settings in Murcia, Spain.

S. Šebela, J. Vaupotič, B. Košťák, and J. Stemberk – Direct measurement of present-day tectonic movement and associated radon flux in Postojna Cave, Slovenia. *Journal of Cave and Karst Studies,* v. 72, no. 1, p. 21–34. DOI: 10.4311/jcks2009es0077

DIRECT MEASUREMENT OF PRESENT-DAY TECTONIC MOVEMENT AND ASSOCIATED RADON FLUX IN POSTOJNA CAVE, SLOVENIA

Stanka Šebela[1], Janja Vaupotič[2], Blahoslav Košťák[3], and Josef Stemberk[3]

Abstract: Micro-tectonic deformations have been monitored continuously in 3D in Postojna Cave, Slovenia with TM 71 extensometers since 2004. Two instruments, 260 m apart, were installed on the Dinaric oriented (NW-SE) fault zone that is situated about 1,000 m north of the inner zone of the regionally important Predjama Fault. Monitoring on both instruments has shown small tectonic movements (i.e., a general dextral horizontal movement of 0.05 mm in four years [Postojna 1] and extension of 0.03 mm in four years [Postojna 2]). Between the longer or shorter calm periods, eleven extremes have been recorded regarding characteristic changes in displacement. The largest short-term movement was a compression of 0.04 mm in seven days, detected in March 2005, which coincided with the 25 km distant Ilirska Bistrica earthquake ($M_L = 3.9$). About two months before the earthquake an extension of 0.05 mm occurred and one month before the earthquake the strain changed into a compression of 0.05 mm. The largest permanent peak was detected at the end of 2004. Along the *y*-axis (Postojna 1) there was a dextral horizontal movement of 0.075 mm in one month (November 10 to December 15, 2004). After the sinistral horizontal movement of 0.02 mm (December 15–27, 2004), the *y*-axis retained its permanent position on 0.05 mm, where it remained for more than a year. Regarding the extremes, ten earthquakes were selected that coincided with tectonic micro-displacements. In terms of speleogenesis, the monitored fault zone represents a stable cave environment. Because radon flux is known to change significantly during tectonic and seismic activities, radon air concentrations were monitored in parallel since 2006. During horizontal movements, either dextral or sinistral, radon pathways underground were partly closed, thus hindering radon migration and reducing its concentration in the cave air. Extension movements do not appear to have affected radon transport. Alternatively, the compression process (Postojna 2, February–August 2007) appears to have opened some new routes for radon transport, facilitating radon migration and increasing its concentration in air.

Introduction

Caves are very special environments where traces of different speleological events can be preserved for over 10^6 years. However, caves are also dynamic environments. Karst waters forming underground passages use preferentially structural geological elements such as bedding planes, especially slipped bedding planes, fissures, faults, folds, etc. (Knez, 1996; Šebela, 1998; Kogovšek and Šebela, 2004; Šebela et al., 2004; Petrič and Šebela, 2004). In most studied cases, geological structures guiding the caves are no longer active. Some examples of active tectonics in karst described from different countries are included in Bini et al., 1992; Gilli and Delange, 2001; Mocchiutti and D'Andrea, 2002; and Plan et al., 2005.

Active tectonic structures in Postojna Cave have been monitored with TM 71 extensometers since 2004 (Šebela, 2005; Šebela et al., 2005; Gosar et al., 2007). Our goal was to detect the size and mechanism of tectonic movements along a well-expressed fault zone in the longest Slovenian cave and to evaluate the coincidence with seismic activity in that karst massif.

Beginning in 2006, we extended our study to include radon (^{222}Rn) as an indicator of tectonic and seismic activity. This radioactive noble gas originates from radioactive decay of ^{226}Ra in the ^{238}U radioactive decay chain in the Earth's crust. Only a fraction of the radon atoms created in a mineral grain emanate into the void space between grains, where they are dissolved either in water or in carrier gases, such as helium or nitrogen, and are thus transported by advection toward the ground surface and the atmosphere (Nero, 1988). This transport is influenced by a number of geophysical and geochemical parameters (Etiope and Martinelli, 2001).

Because in the area of faults the material is crushed, and hence more permeable to radon, the level of radon activity, either in the outdoor air or in soil gas at a fault, is generally

[1] Karst Research Institute SRC SASA, Titov trg 2, 6230 Postojna, Slovenia, sebela@zrc-sazu.si
[2] Jožef Stefan Institute, Jamova cesta 39, 1000 Ljubljana, Slovenia, Janja.Vaupotic@ijs.si
[3] Institute of Rock Structure and Mechanics, Academy of Sciences of the Czech Republic, V Holešovičkách 41, 18209 Prague, Czech Republic, košťák@irsm.cas.cz, stemberk@irsm.cas.cz

elevated. Changes in fault activity result in changing radon levels (Virk et al., 1997; Wu et al., 2003). In addition, the phenomena preceding and accompanying an earthquake can significantly change the radon pathways underground and thus govern radon levels appearing at the surface (Etiope and Martinelli, 2001). Thus, if radon is monitored in the outdoor air, soil gas, or thermal water, and a long-term time series of the resulting data is analyzed, in addition to regular fluctuations in radon levels ascribed to the effects of environmental conditions (e.g., temperature, barometric pressure), some anomalous increases or decreases in radon level may be observed and attributed to seismic events (Etiope and Martinelli, 2001).

In this study, radon was monitored continuously in Postojna Cave, together with measurements of micro movements. Micro tectonic movements and radon concentrations in air, observed at two sites at the Dinaric oriented (NW-SE) fault in the Postojna Cave, are examined in relation to seismic activity in the area. This is the first such comparative study between micro tectonic movements and radon air concentration to be investigated in a cave in Slovenia.

GEOLOGY AND SEISMICITY OF THE STUDY AREA

Slovenia is situated in the NE corner of the Adria-Europe collision tectonic zone. The Istria Peninsula (Fig. 1) contains the only outcrop of Adria microplate in the northern Adriatic region. The thrust belts of the Dinarides and Southern Alps form a rim of high topography around Adria. Major Dinaric (NW-SE) strike-slip faults cut and displace fold and thrust structures. Slovenia has considerable seismicity (Vrabec and Fodor, 2006), and this complex and neotectonically active region is of special interest because of the Classical Karst-Kras area (Fig. 2A).

Paleomagnetic data indicate that the motion of the Adriatic microplate has been associated with an approximately 30° counterclockwise rotation (Márton et al., 2003) since the late Miocene or Pliocene. GPS measurements suggest sharp (some mm/year) dextral (transpressive) movements along the Sava Fault and Periadriatic Lineament (Fig. 1), showing that the side intrusion in the northeast Alps is still active (Weber et al., 2004).

The strongest earthquakes that have occurred in Slovenia in recent years were situated along the Ravne Fault (Bajc et al., 2001; Kastelic and Cunningham, 2006). Slovenia is considered to exhibit moderate seismicity, and the External Dinarides (Fig. 1), in particular, are characterized by moderate historic and recent seismicity. Regarding the fault plane solutions, it is evident that the governing stress in the region runs in an approximate N-S direction (Poljak et al., 2000).

According to a geological interpretation based on the analysis of repeated levelling line campaigns data along the Sečovlje-Bled polygon in western Slovenia, the active

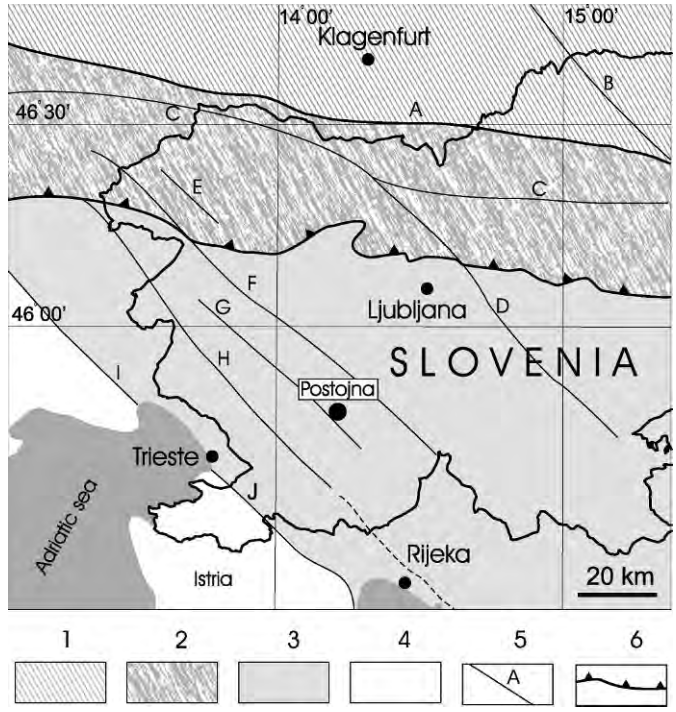

Figure 1. Tectonic situation of W Slovenia. 1-Eastern Alps (Alps), 2-Southern Alps (Dinarides), 3-External and Internal Dinarides, 4-Adriatic foreland, 5-Faults (A-Periadriatic Lineament, B-Labot Fault, C-Sava Fault, D-Stična Fault, E-Ravne Fault, F-Idrija Fault, G-Predjama Fault, H-Raša Fault, I-Palmanova Fault, J-Karst thrust edge), 6-Southalpine thrust front (after Poljak, 2007 and Placer, 1999).

tectonic structures (vertical movement) include at a minimum: a juvenile syncline between Strunjan and Koper, the Kras (Fig. 2A) Imbricate Structure, The Divača Fault, the Raša Fault, the Southalpine Front (Fig. 1), and the Julian Alps thrust (Rižnar et al., 2007). The Ravne Fault was responsible for the 1998 (M_W = 5.6) and 2004 (Krn, M_W = 5.2) earthquakes and appears to be an outstanding example of an actively propagating strike-slip fault cutting through pre-existing mountainous terrain (Kastelic and Cunningham, 2006).

LiDAR mapping to image seismogenic strike-slip faults in the Julian Alps in Slovenia was performed along the Idrija and Ravne Faults (Cunningham et al., 2006). One site (Kapa) in the Idrija LiDAR survey area may indicate some surface rupturing and other landscape features typically associated with strike-slip faulting. The Tolminka springs basin on the Ravne Fault is an example of a localized and active transtensional basin constructed within an overall transpressional system (Cunningham et al., 2006).

The strongest seismic event in the last 100 years around Postojna was the Cerknica earthquake (1926) (M_m = 5.2) that probably originated on the Idrija Fault (Ribarič, 1982). The epicenter was 10 km east of Postojna. The

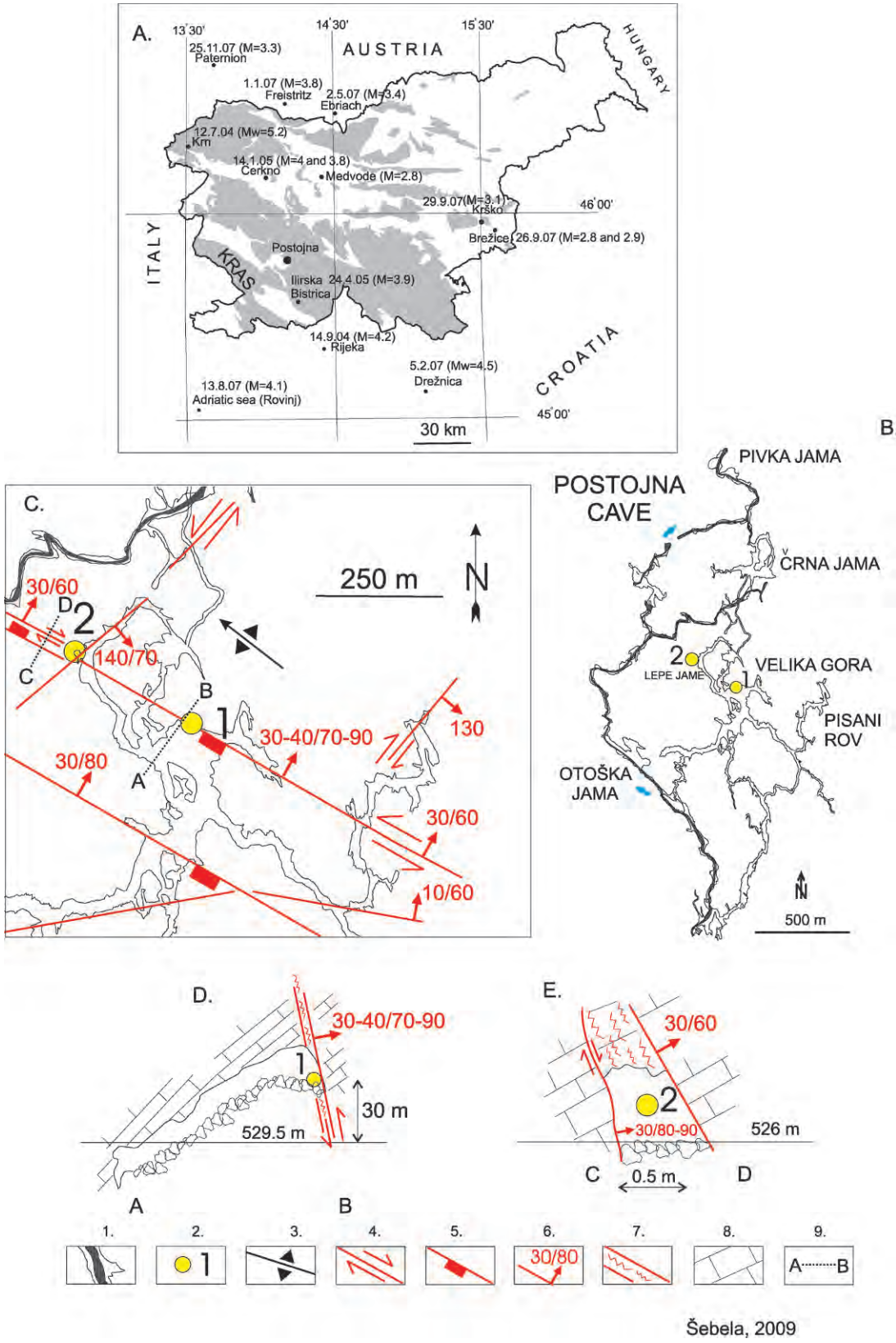

Figure 2. Tectonic structure of Postojna Cave. A.-The position of Postojna and Kras in Slovenia with epicenters of the stronger earthquakes. Grey areas are karst outcrops, B.-The passages of Postojna Cave with monitoring sites (1-Postojna 1, 2-Postojna 2), C.-Structural-geological map of the monitoring sites, D.-AB cross section, E.-CD cross section, 1-Underground river Pivka, 2-Monitoring sites: 1 (Postojna 1) and 2 (Postojna 2), 3-Postojna Anticline, 4-fault with horizontal (dextral) displacement, 5-fault with vertical displacement, 6-strike and dip of fault, 7-fault zone, 8-Upper Cretaceous limestone, 9-cross section.

newspaper *Edinost* (Anonymous, 1926) reported that in Postojna Cave a large stalagmite, one meter in diameter, collapsed due to the earthquake.

EXPERIMENTAL SETTING

SITE DESCRIPTION

The Postojna Cave (Fig. 2B), with 20 km of galleries, is the longest known cave system in Slovenia. The passages are developed in an approximately 800-m-thick package of Upper Cretaceous bedded limestones (Šebela, 1998).

The cave is situated between two important Dinaric faults, the Idrija Fault on the north and the Predjama Fault on the south (Fig. 1). The tectonic structure of the area between these faults is characteristic of a transition zone between two dextral strike-slip faults. In Postojna Cave, we can distinguish older overthrusting and folding deformations and younger faulting deformations. Overthrusting took place after the deposition of Eocene flysch. During the Miocene and Pliocene, the overthrusting was accompanied by folding. The principal folding deformation in the cave is the Postojna Anticline. Cave passages are developed in both flanks of the anticline (Fig. 2C) and follow the strike and dip of the bedding-planes, especially those with interbedded slips (Čar and Šebela, 1998).

The northern edge of Velika Gora (Fig. 2C and 2D) is developed along the Dinaric oriented (NW-SE) reverse fault zone, with traces of vertical displacement for some meters (Fig. 2C, monitoring site Postojna 1). The same fault zone from Velika Gora can be traced in some parts of the cave, but other parts do not exhibit the same tectonic characteristics. In the SE part of the cave, a horizontal sinistral movement with 60° dip angle for fault zone NW from Velika Gora is observed. The same fault zone exhibits vertical and horizontal displacements (Fig. 2C, monitoring site Postojna 2) and is cut by the cross-Dinaric fault zone (Sasowsky et al., 2003). Different tectonic activities are observed on the same Dinaric-oriented fault zone, sometimes with four individual tectonic phases.

The locations for installation of the extensometers in Postojna Cave were selected to evaluate if the monitored fault is tectonically active and to determine whether the tectonic activity has any influence on speleogensis. The two devices were installed in the same fault zone but on different fault planes. Postojna 1 was installed at the contact point between a fault plane (dip angle 70–90° to the NE) and a collapse block, partly covered with flowstone (Figs. 2D and 3). The second device (Postojna 2) was installed in a narrow natural passage, which was enlarged artificially 30-years-ago, between two fault planes that are about one half meter apart (Figs. 2E and 4). The northern fault plane dips to the NE at 60° and has horizontal striation, representing dextral movement. The southern one constitutes the normal fault, dipping towards the NE by 80–90° and shows vertical striation. The fault zone being monitored is about 1,000 m north of the inner zone of the

Figure 3. Monitoring site Postojna 1 with TM 71 instrument (photo S. Šebela).

Predjama Fault (Fig. 1). Postojna 1 is 68 m below ground surface and Postojna 2 is 60 m below ground surface and about 1,400 m from the entrance to the cave.

MEASUREMENT TECHNIQUES

MEASUREMENT OF MICRO MOVEMENTS

We employed a TM 71 extensometer, developed by Blahoslav Košťák (Košťák, 1969). This is a mechano-optical instrument that measures displacement in three dimensions (x, y and z). It works on the principle of the Moiré optical effect, which changes when two transparent plates move (Košťák, 1977; 1991). Each plate is fixed into the outcrop of a fault plane or fissure. The instrument is very robust and simple, and needs no source of energy. This is good for long-term observations under varying

Figure 4. Monitoring site Postojna 2 with TM 71 instrument (photo S. Šebela).

meteorological conditions (Avramova-Tacheva and Košťák, 1995). The characteristic of the TM 71 is long-term measurement of movements accurate to within 0.01 mm.

Measurements at Postojna 1 began May 26, 2004 and at Postojna 2 on February 26, 2004. The instruments are set permanently at the sites and their readings are taken generally once a month. Because the cave temperature is stable throughout the year (9 °C to 11 °C), any influence of temperature on data records can be disregarded. The measurements have an evaluation accuracy of 0.01 mm in all three displacement co-ordinates, x, y and z.

Measurement of Radon

Barasol probes (MC-450, ALGADE, France) were used during the first two years, and then replaced by Radim 5 WP monitors (SMM Company, Prague, Czech Republic). The Barasol probe is designed primarily for radon measurements in soil gas. The probe gives radon concentration, based on alpha spectrometry of radon decay products in the energy range of 1.5 MeV to 6 MeV using an implanted silicon detector. The detector sensitivity is 50 Bq m^{-3} with a sampling frequency of four times an hour. In addition to radon concentration, the probe also records temperature and barometric pressure. The Radim 5 monitor is used mostly for radon measurements of indoor air. It determines radon concentration by measuring gross alpha activity of the decay products ^{218}Po and ^{214}Po, collected electrostatically on the surface of a semiconductor detector. The sensitivity is about 50 Bq m^{-3} and the sampling frequency is twice an hour. Data are stored in the inner memory of both instrument and then transferred to a personal computer for further evaluation, usually once every two months. Instruments are checked regularly, using a portable AlphaGuard radon monitor (Genitron, Germany) as a reference instrument. Radon measurements were collected from the beginning of April through October 2007 at Postojna 1 (Fig. 7) and from October 2006 through October 2007 at Postojna 2 (Figs. 8 and 9).

Hourly average values of the outdoor air temperature at the Postojna meteorological station were obtained from the Office of Meteorology of the Environmental Agency of the Republic of Slovenia. Data on seismic events were obtained from the Office of Seismology of the same Agency. We considered only those earthquakes for which the magnitude M_L was higher than 2 and the distance R between our measurement site and the epicenter was less than 3 times Dobrovolsky's (Dobrovolsky et al., 1979) radius R_D, defined by $R_D = 10^{0.43 \times M_L}$. Origin 6.1 Data Analysis and Graphing Software were used for statistical data evaluation and presentation.

Results and Discussion

Micro Displacements

The measurement results include three coordinates, x, y, z, which are principally perpendicular to the observed fault zone (i.e., $+x$ represents compressive movement of the monitored fault zone, $+y$ represents sinistral-lateral movement, and $+z$ vertical movement) relative shear in the fault: N subsidence or S uplift. Displacements recorded at both sites (Figs. 5 and 6) are generally small, the range of movements being within 0.1 mm (+0.02 to −0.075). The plots show a number of sharp peaks. However, the development of such peaks in individual coordinates generally could not be matched between the two monitored sites. Some peaks are thus due to records close to the limits of recording accuracy. A certain similarity, however, can be observed between the two sites regarding the trend of development and periods of unrest. The total length of the displacement vector at each of the two sites developed parallel increasing short-term trends of about 0.1 mm yr^{-1} in the period July 2004–March 2005; later the trend fell to zero.

Detailed analysis of the individual coordinates show evidence of some periods of unrest alternating with more quiet periods. Movements detected in the y- and z-axes for both instruments were simultaneous, which suggests real tectonic movements. In general, unrest was recorded from the start of measurements at the beginning of 2004 until about March 2005, and then again during the period from October 2006 to January 2008.

Extremes (E) of the periods of unrest (Figs. 5 and 6) are indicated at the following periods/sites/coordinates/dates:

(a) E1: Postojna 2/$x \rightarrow -0.055$ mm/March–June 2004 (March 11 to June 29, extension; June 29 to July 13, compression; Krn earthquake July 12, 2004);
E2: Postojna 1/$z \rightarrow -0.03$ mm/May–June 2004;

(b) E3: Postojna 1/$x \rightarrow -0.04$ mm/July 30 to December 15, 2004 (extension); x $\rightarrow -0.02$ mm/December 27, 2004 to January 26, 2005 (extension);
E4: Postojna 1/ $y \rightarrow -0{,}075$ mm/November 10, 2004 to December 15, 2004 (dextral horizontal movement); December 15 to December 27, 2004 (sinistral horizontal movement)-permanent change of 0.05 mm;
E5: Postojna 2/ $z \rightarrow -0.03$ mm/September–November 2004;
E6: Postojna 2/$z \rightarrow -0.05$ mm/February–March 2005 (+0.04 mm in 7 days);
E7: Postojna 2/$x \rightarrow -0.04$ mm/January–March 2005; January 14 to March 22, 2005 (extension); March 22 to May 6, 2005 (compression); Ilirska Bistrica earthquake April 24, 2005;
E8: Postojna 2/$y \rightarrow -0.04$ mm/January–March 2005; January 14, to February 23, 2005 (dextral horizontal movement); March 29 to May 6, 2005 (sinistral horizontal movement); Cerkno earthquakes January 14, 2005; Ilirska Bistrica earthquake April 24, 2005;
E9: Postojna 1/$z \rightarrow -0.02$ mm/January–March 2005; (the value in the error limit);

(c) E10: Postojna 2/$y \rightarrow -0.025$ mm/October 2006–January 2007; October 13 to November 16, 2006

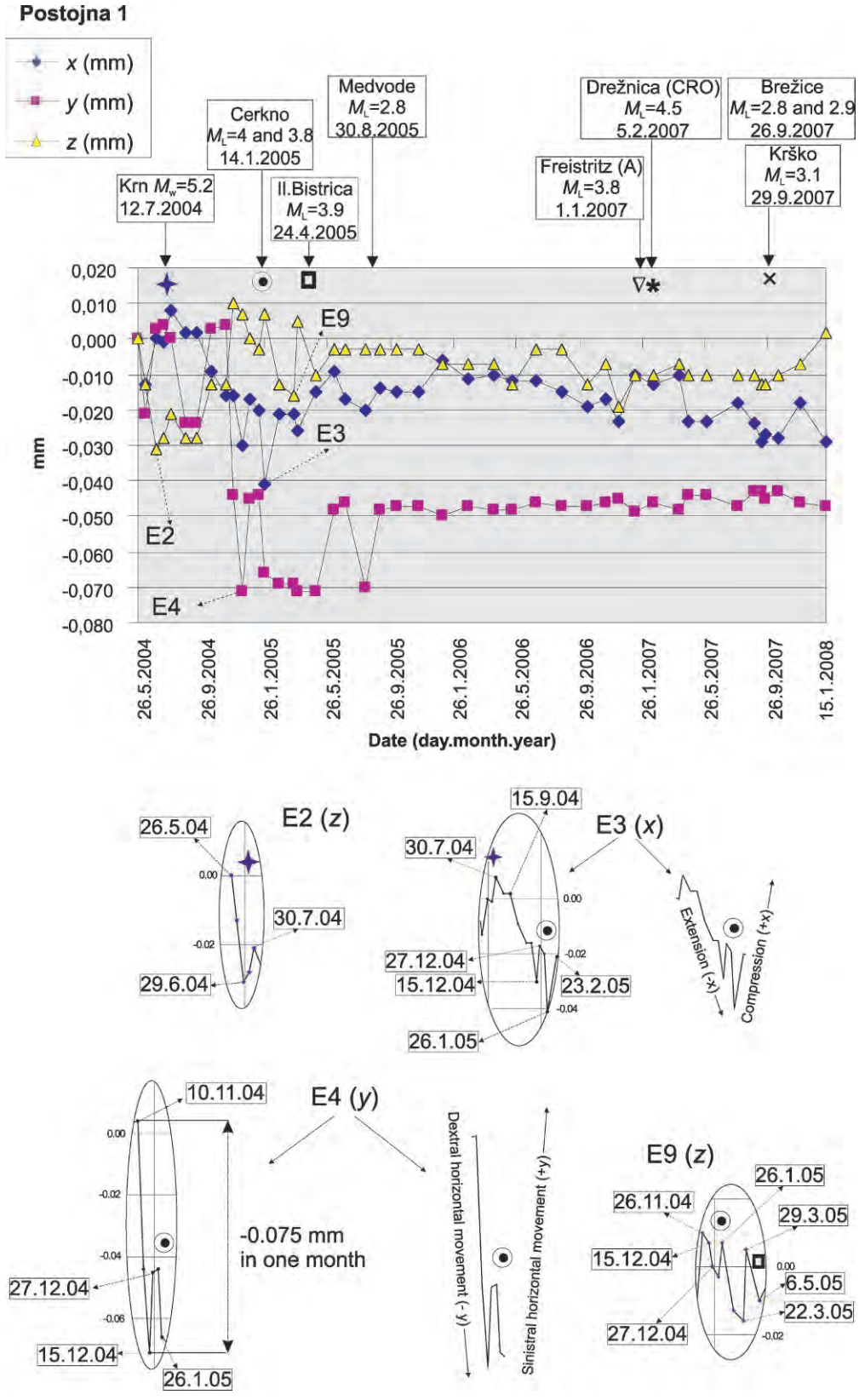

Figure 5. Displacements recorded by TM 71 at Postojna 1 monitoring site.

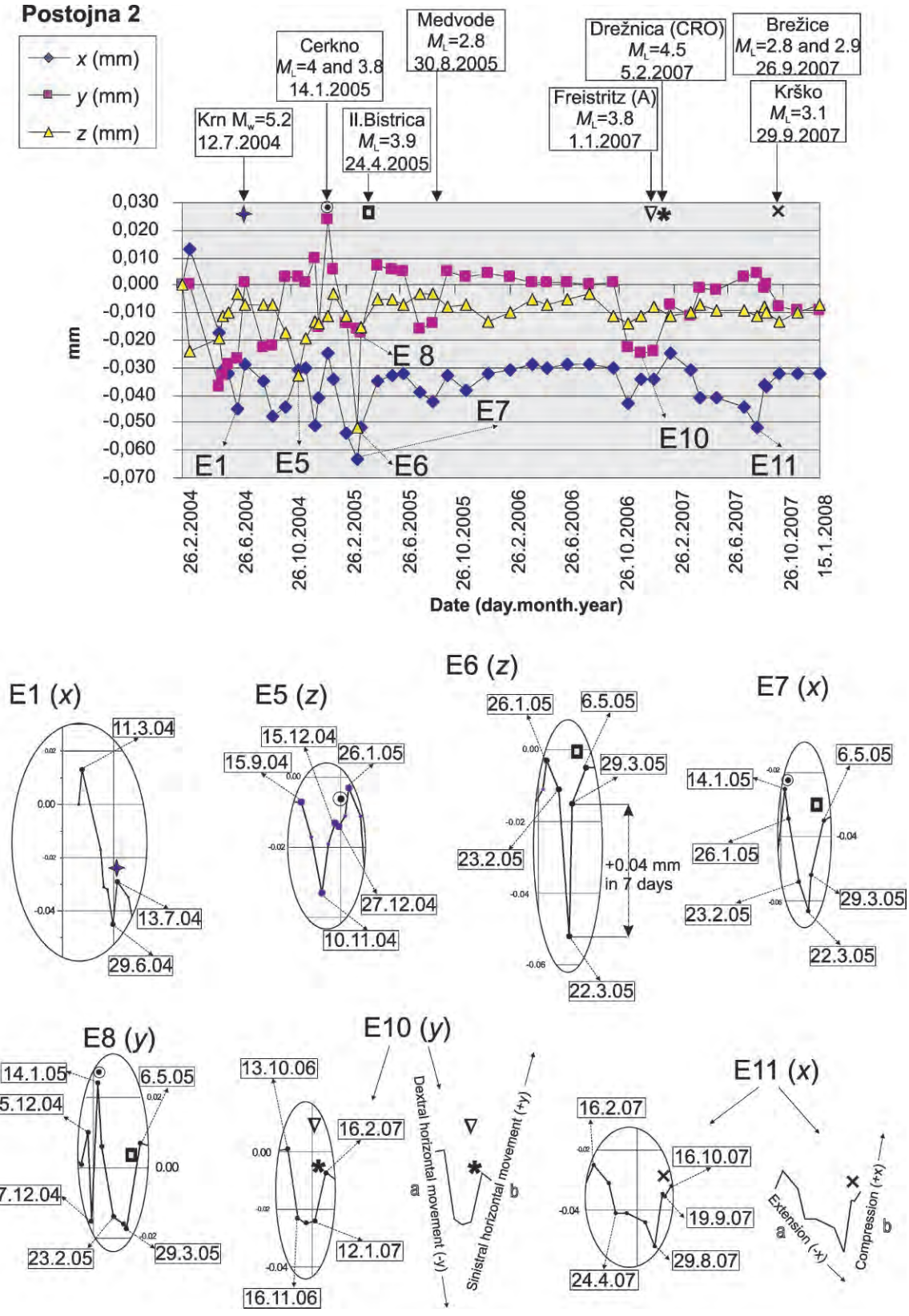

Figure 6. Displacements recorded by TM 71 at Postojna 2 monitoring site.

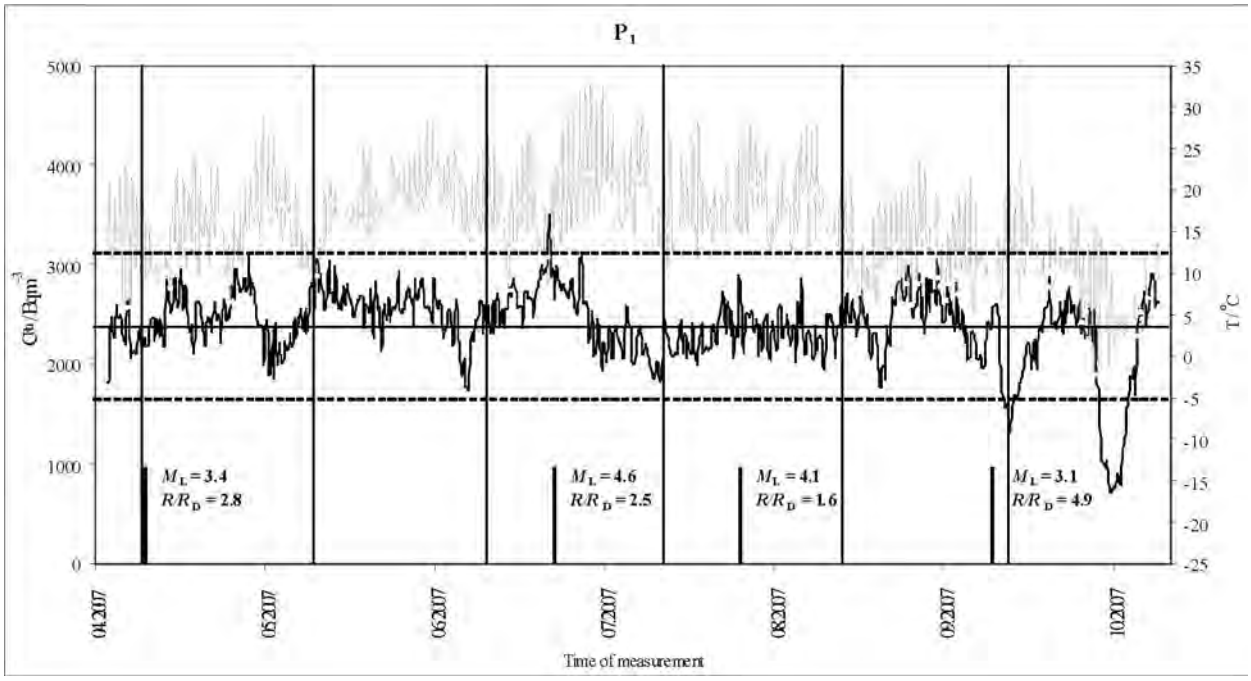

Figure 7. Time series plot of radon concentration in air (black line) at the Postojna 1 site and temperature of the outdoor air (grey line) at the Postojna Meteorological Station (April–October 2007); the relevant earthquakes are inserted, with M_L and R/R_D values indicated, $M_L = 3.4$ (Ebriach, Austria), $M_L = 4.6$ (38 km south from Zadar, Croatia), $M_L = 4.1$ (near Rovinj, Croatia), $M_L = 3.1$ (Krško, Slovenia) (see Table 1).

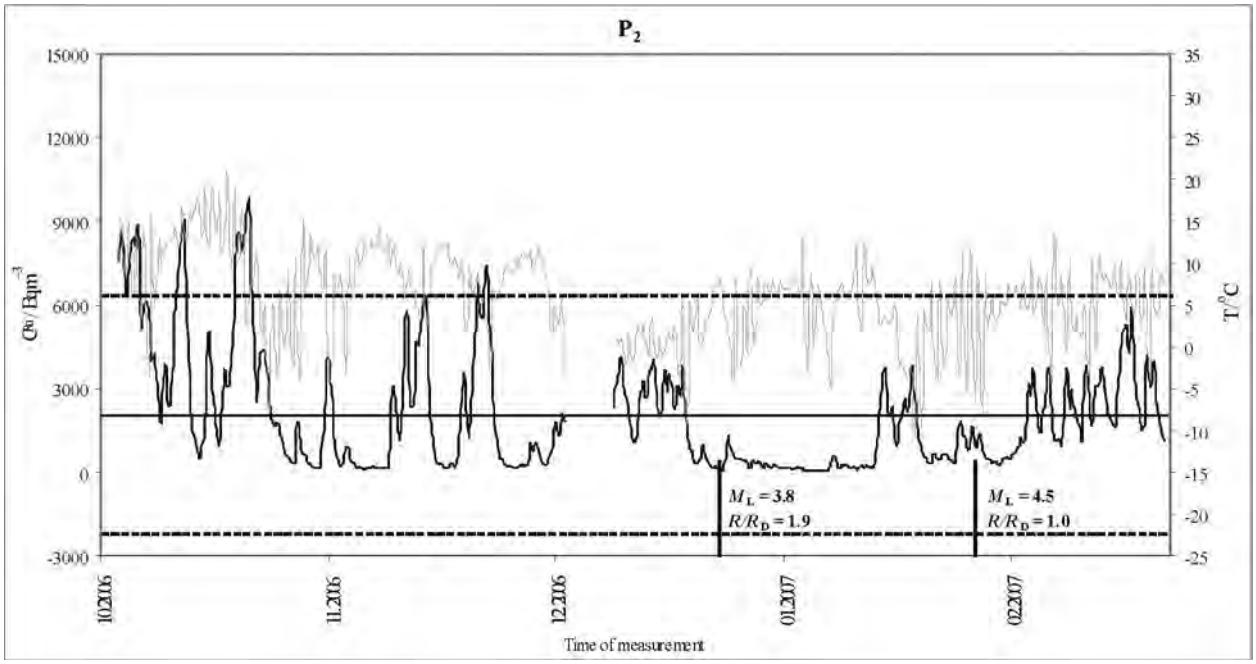

Figure 8. Time series plot of radon concentration in air (black line) at the Postojna 2 site and temperature of the outdoor air (grey line) at the Postojna Meteorological Station (October 2006–March 2007); the relevant earthquakes are inserted, with M_L and R/R_D values indicated, $M_L = 3.8$ (Freistritz, Austria), $M_L = 4.5$ (Drežnica, Croatia) (see Table 1).

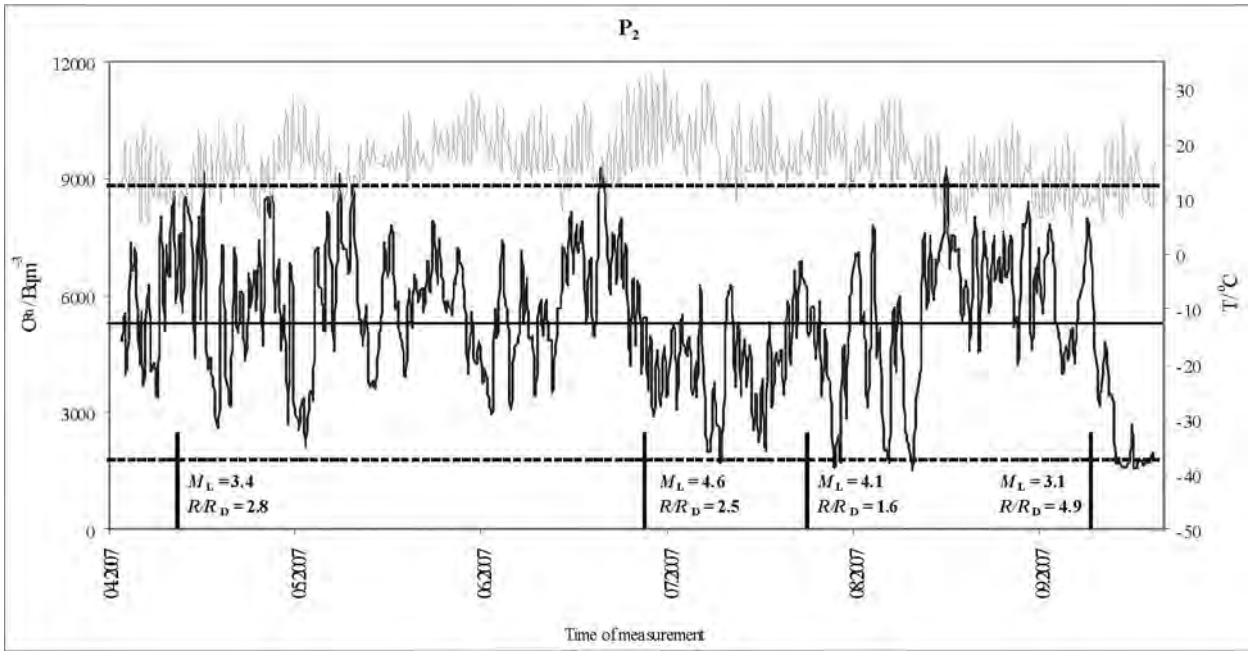

Figure 9. Time series plot of radon concentration in air (black line) at the Postojna 2 site and temperature of the outdoor air (grey line) at the Postojna Meteorological Station (April–October 2007); the relevant earthquakes are inserted, with M_L and R/R_D values indicated, $M_L = 3.4$ (Ebriach, Austria), $M_L = 4.6$ (38 km south from Zadar, Croatia), $M_L = 4.1$ (near Rovinj, Croatia), $M_L = 3.1$ (Krško, Slovenia) (see Table 1).

(dextral horizontal movement); January 12 to February 16, 2007 (sinistral horizontal movement); Freistritz earthquake (Austria) January 1, 2007; Drežnica earthquake (Croatia) February 5, 2007;
E11: Postojna 2/$x \rightarrow -0.035$ mm/February–August 2007; February 16 to August 29, 2007 (extension); August 29 to October 16, 2007 (compression).

When looking for earthquakes that might coincide with the registered displacements we found 10 events (Table 1, Figs. 5 and 6). The first was the Krn earthquake of July 12, 2004 ($M_w = 5.2$), which had an epicenter 70 km NW from the measuring sites. The earthquake occurred during the period of E1 and E2 when some fault opening along the x-axis at Postojna 2 (Fig. 6) and vertical movements along z-axis at Postojna 1 (Fig. 5) were recorded. Lateral movements observed at Postojna 1 and 2 during the (a) period were of special interest and were first reported by Šebela et al. (2005). Before the earthquake, the displacement along the y-axis corresponded to dextral lateral movement, and just before or during the earthquake, the movement changed to sinistral, with a step of about 0.03 mm (Šebela et al., 2005).

The second event, comprising two earthquakes (Cerkno, $M_L = 4.0$ and 3.8 on January 14, 2005), appeared in the (b) period, just after the extreme E4 in the y-axis (Fig. 5) that represents a dextral lateral slip of -0.075 mm. The most significant change in our observations appeared between November 10 and December 15, 2004. Between December 15, 2004 and Decemebr 27, 2004 movement on the y-axis was +0.03 mm (horizontal sinistral lateral slip). After the event, the step on the y-axis remained at about -0.05 mm, where it remains today. On December 26, 2006, the large Sumatra earthquake ($M_W = 9.2$) occurred. Can long-distant changes in stress and strain in the Earth's crust be an alternative cause of the big step or we registered just a coincidence? The slip registered on the y-axis at Postojna 2 was not as large as that registered at Postojna 1, even if we are observing the same fault zone, but not the same fault line. The movement on the y-axis (Postojna 2, first peak on E8) was -0.02 mm (dextral lateral slip from December 15 to December 27, 2004) and +0.04 mm (sinistral lateral slip from December 27, 2004 to January 14, 2005). During the Cerkno earthquakes, the TM 71 instrument registered significant movements on the z-axis (E5) at the Postojna 2 site (Fig. 6).

The extreme E6 on the z-axis (Fig. 6) appeared before the Ilirska Bistrica earthquake (April 24, 2005, $M_L = 3.9$) that was situated 25 km SE from Postojna. From March 22 until March 29, 2005, +0.04 mm was registered in seven days on the z-axis, the largest displacement recorded in one week. The Cerkno earthquakes and the Ilirska Bistrica earthquake occurred during three extremes (E6, E7 and E8; Postojna 2, Fig. 6). At Postojna 1, during the period of the Cerkno-Ilirska Bistrica earthquakes, we detected small displacements along the z (E9) and y-axes (-0.02 mm) (Fig. 5).

Table 1. Stronger earthquakes in Slovenia and neighbouring countries during the period of monitoring (sources: Ministry for Environment and Spatial Planning, Environmental Agency of the Republic of Slovenia, 2008, Seismology: http://www.arso.gov.si/potresi/ [accessed January 9, 2008] and European-Mediterranean Seismological Center, 2008, Database of Local Seismological Bulletins from European-Mediterranean Networks: http://www.emsc-csem.org/index.php?page=data&sub=base [accessed January 9, 2008]).

Date	Depth, km	M_L	Location	Air distance from Postojna
July 12, 2004	13	$M_w = 5.2$	Krn	70 km NW
September14, 2004	8,9 (?)	4.2	Fužine-Rijeka (Croatia)	50 km south
September 22, 2004	16	3.5	Zgornji Prekar	70 km NE
November 24, 2004	25	5.2	Manerba del Garda (Italia)	290 km W
November 25, 2004	15	5.2	Jabuka (Croatia)	310 km S
January 14, 2005	20	4	Cerkno	45 km NW
January 14, 2004	20	3.8	Cerkno	45 km NW
April 24, 2005	17	3.9	Ilirska Bistrica	25 km SE
August 30, 2005	18	2.8	Medvode	45 km NE
November 24, 2005	16	2.5	Postojna	5–10 km W
December 12, 2005	19	2.9	Žiri	30 km NW
January 30, 2006	12	2.1	Prestranek	10–15 km south
June 21, 2006	16	2.8	Gorski Kotar (Croatia)	70 km SE
August 30, 2006	22	2.4	Škofja Loka	45 km north
September 3, 2006	13	2	Podnanos	22 km W
September 24, 2006	15	2.2	Podnanos	22 km W
January 1, 2007	16	3.8	Freistritz/Bistrica v Rožu (Austria)	80 km north
February 5, 2007	10	$M_w = 4.5$	Drežnica (Croatia)	90 km south
May 2, 2007	16	3.4	Ebriach/Obirsko (Austria)	80 km NE
July 18, 2007	?	4.6	38 km south from Zadar (Croatia)	240 km SE
August 13, 2007	27	4.1	Adriatic sea, near Rovinj (Croatia)	95 km SW
September 26, 2007	3	2.8	Brežice	115 km E
September 26, 2007	5	2.9	Brežice	115 km E
September 29, 2007	10	3.1	Krško (Raka)	105 km E
November 25, 2007	12	3.3	Paternion (Austria)	107 km NW

M_L = local magnitude
M_W = moment magnitude

Between May 6, 2005 and October 13, 2006, the Postojna 2 monitoring site was very stable on all three axes. The only reliable disruption (Fig. 6) was from July 1 to October 7, 2005 during the Medvode earthquake (August 30, 2005, $M_L = 2.8$), being about 0.02 mm along *y*-axis. A displacement peak of about 0.02 mm was also recorded along the *y*-axis at Postojna 1 (Fig. 5), from July 1 to September 7, 2005.

The Postojna 1 site was very stable from June 9, 2005 until the beginning of 2007. Even during the earthquakes in 2007, significant movements were not detected, the *y*-axis in particular being very stable. During the third time (c) period (the year 2007), some movements on Postojna 2 (E10 and E11) were recorded. During the earthquakes in Austria (Freistritz, January 1, 2007, $M_L = 3.8$) and in Croatia (Drežnica, February 5, 2007, $M_L = 4.5$) we detected movement along the *y*-axis by −0.025 mm (E10). The Brežice (September 26, 2007, $M_L = 2.8$ and 2.9) and Krško earthquakes (September 29, 2007, $M_L = 3.1$) in Eastern Slovenia coincided with an extension along the *x*-axis of −0.035 mm from February 16 until August 29, 2007 and with a compression of +0.025 mm between August 29, 2007 and October 16, 2007. The fact that movements were recorded both before and after the earthquakes is important. Preceding movements, based on observation of micro-movements, have also been reported on several other occasions in Europe (Košťák et al., 2007; Stemberk and Košťák, 2007).

Monitoring results show small movements along all three axes. At Postojna 1 (Fig. 5), −0.05 mm dextral lateral movement (*y*-axis) was recorded over four years, and at Postojna 2 (Fig. 6), an extension of −0.03 mm over four years was recorded. The short-term rate of change averaged −0.05 mm yr^{-1} at Postojna 1 in the first year of monitoring (2004). The measurements for the *y*-axis in the year 2006 were very stable for both devices and show no movement at all.

The micro displacements determined in Postojna Cave were very small and frequently within the limits of error (0.01 mm). However, on the basis of some obvious extremes that generally coincided with seismic activity and of silent periods with almost no movement (Figs. 5 and

6), we believe that slow tectonic processes are being monitored within the aseismic fault zone.

In 2004 and the first part of 2005, some significant peaks, the largest being 0.075 mm in one month on the *y*-axis, were registered at Postojna 1 (Fig. 5, E4). From September 2005 till January 2008 (Fig. 5), the Postojna 1 monitoring site was very stable, especially along the *y*-axis. Because the extensometer is fixed between the collapse block and the fault wall of the collapse chamber (Fig. 3), we would expect some non-tectonic movements due to the instability of the collapse blocks, especially on the *z*-axis. The only two marked extremes along the *z*-axis (Fig. 5, E2 and E9) are very small, 0.020–0.025 mm, and coincided with the Krn, Cerkno and Ilirska Bistrica earthquakes. The stability of the largest collapse chamber in the cave, Velika Gora, is in this sense, very high.

The Postojna 2 site (Fig. 4) is in an artificially enlarged small natural passage, where the extensometer is fixed between two striated fault planes. The curves show some well-expressed peaks (Fig. 6), some of which coincide with earthquake activity. The highest extremes (E1 and E6, Fig. 6) do not exceed 0.05 mm. The calm period starting in September 2005 was interrupted at the end of September 2006. In 2007, two extremes (Fig. 6, E10 and E11) were concurrent with the Freistritz, Drežnica, Brežice and Krško earthquakes.

Even though we are observing the same Dinaric-oriented fault zone, the same response is not, in general, observed at the two monitoring sites that are separated 260-m-horizontally and 33.5-m-vertically (Fig. 2). One of the causes can be that the Dinaric-oriented fault is cut by a relatively younger cross-Dinaric fault (Sasowsky et al., 2003). Another fact is that the same fault zone is not necessarily tectonically active to the same degree along its length. Along the monitored fault zone we have found traces of at least four different old movements, but recent, very slow tectonic movements, that are showing a general horizontal dextral-lateral movement (Postojna 1) and extension (Postojna 2), are in agreement with the active tectonic situation on Dinaric faults in SW Slovenia. The earthquakes (Table 1) with lower magnitudes, even those close (5–22 km) to the monitoring sites, do not coincide with the micro-tectonic movements.

Radon Levels

Time series of radon activity concentrations (C_{Rn} in Bq m^{-3}) were measured at Postojna 1 and Postojna 2 (Figs. 7, 8 and 9) and recorded in parallel with the outdoor air temperature. C_{Rn} at Postojna 1 (Fig. 7) showed regular diurnal fluctuations, as previously observed at other locations in the cave (Vaupotič et al., 2001). The arithmetic mean of C_{Rn} over the whole period of monitoring is 2380 ± 376 Bq m^{-3}. During this time, no unrest was recorded at Postojna 1 and no effect of the unrest at Postojna 2 on radon level at Postojna 1 can be seen (extension until August 29 and compression from August 29 to October 16, 2007; Fig. 6). None of the earthquakes on May 2, 2007 (M_L = 3.4, R/R_D = 2.8), July 18, 2007 (M_L = 4.6, R/R_D = 2.5) or August 13, 2007 (M_L = 4.1, R/R_D = 1.6) appear to have had any connection, although their magnitudes were relatively high for the region and their R/R_D values quite low (Zmazek et al., 2003). The decrease in C_{Rn} after September 26, 2007 (Fig 7) cannot be paralleled with earthquakes that occurred in the period September 26, 2007 to September 29, 2007 because their epicenters were too far away (R/R_D between 4.8 and 7.1) although their magnitudes were not so low for the region (M_L from 2.1 to 3.1). This decrease in C_{Rn} was most probably caused by decreases in outdoor air temperature. It is well known that radon level in the Postojna Cave is governed mainly by the so called chimney effect (Vaupotič et al., 2001; Vaupotič, 2008). The cave system behaves as a huge fireplace: when the outdoor air temperature falls below the temperature of the cave, the air current from the warmer cave carries radon-rich air towards the outdoor air, causing fresh outdoor air with low radon levels to enter the cave and reducing the C_{Rn} in the cave. This occurred at Postojna 1 towards the end of September 2007 (Fig. 7) when the outdoor air temperature, which was below 0 °C for several days, fell far below the cave temperature. The arithmetic mean of C_{Rn} without the contribution after September 26, 2007 is 2445 ± 275 Bq m^{-3} and may be considered as the summer radon level at Postojna 1.

During radon monitoring at Postojna 2, two tectonic unrest periods were observed, E10(*y*) and E11(*x*) (Fig. 6). These may be further subdivided: E10(*y*) into (1) E10a(*y*): dextral horizontal movement starting on October 13, 2006 (before radon measurement had started) and ending on November 16, 2006, and (2) E10b(*y*) sinistral horizontal movement from January 12 to February 16, 2007); and E11(*x*) into (1) E11a(*x*) extension from February 16 to August 29, 2007, and (2) E11b(*x*) compression from August 29 to October 16, 2007. The diurnal variations in C_{Rn} are different from those observed at Postojna 1, thus presumably indicating the effect of micro movements on the transport of radon and its entry into the cave air.

The overall arithmetic mean C_{Rn}(tot) for Postojna 2 (Figs. 8 and 9) during the entire period of monitoring (October 2006–October 2007) is 3853 ± 2527 Bq m^{-3}, being about 60% higher than at Postojna 1. The standard deviation is high because of larger fluctuations than at Postojna 1 (Fig. 7). The winter arithmetic mean radon concentration C_{Rn}(w) = 1492 ± 1334 Bq m^{-3} was calculated from the beginning of December 2006 to the end of February 2007, and the summer mean C_{Rn}(s) = 4857 ± 1681 Bq m^{-3} from the beginning of July to the end of August 2007. The ratio C_{Rn}(w)/C_{Rn}(tot) = 0.39 is much lower than, and C_{Rn}(s)/C_{Rn}(tot) = 1.26 similar to other parts of the cave (Vaupotič, 2008). This low C_{Rn}(w)/C_{Rn}(tot) value could have been caused by micro movements, as well as the chimney effect. At the beginning of the plot in Figure 8 C_{Rn}, values are high, start to decrease as

E10a(y) approaches its end, and are very low at the end of this period, although the outdoor temperature was above 10 °C and, hence, the chimney effect could not be operative. Soon after that, two C_{Rn} peaks appear at the temperature minima, which is contrary to expectations based on the chimney effect. C_{Rn} then remains constantly low till almost the end of the E10b(y) unrest. There are periods of elevated C_{Rn} in the second halves of November and December 2006 and January 2007, and the beginning of February 2007, again at the temperature minima as before. Because no unrest was recorded during these times, these elevated Rn levels, except for those in the second half of November 2006, may be assumed as anomalies, possibly coinciding with earthquakes on January 1, 2007 (M_L = 3.8, R/R_D = 1.9) and February 5, 2007 (M_W = 4.5, R/R_D = 1.1), respectively. The November 2006 anomaly could not have been paralleled with the January 1, 2007 earthquake because the anomaly precedes the earthquake. The arithmetic means of C_{Rn} for the periods from October 13 to November 16, 2006 (E10a(y) unrest) and from January 12 to February 16, 2007 (E10b(y) unrest) are C_{Rn}(E10a) = 3267 ± 2925 Bq m^{-3} and C_{Rn}(E10b) = 1105 ± 1040 Bq m^{-3}. If the first average is compared with the summer average and the second with the winter average, the following ratios are obtained: C_{Rn}(E10a)/C_{Rn}(s) = 0.67 and C_{Rn}(E10b)/C_{Rn}(w) = 0.74. This suggests that horizontal movement (Fig. 6, E10), either dextral or sinistral, significantly reduced radon levels on the observed fault.

With the appearance of the E11a(x) unrest (from February 16 to August 29, 2007; Fig. 6), C_{Rn} starts to increase (Figs. 8 and 9), resulting in an arithmetic mean of the entire unrest of C_{Rn}(E11a) = 4314 ± 2273 Bq m^{-3}. This value is not significantly higher than C_{Rn}(tot), the ratio C_{Rn}(E11a)/C_{Rn}(tot) being 1.12, and it may therefore be concluded that extension did not influence radon transport. No radon anomalies have been observed during the earthquakes occurring on May 2, 2007 (M_L = 3.4, R/R_D = 2.8), July 18, 2007 (M_L = 4.6, R/R_D = 2.5) or August 13, 2007 (M_L = 4.1, R/R_D = 1.6), although their magnitudes were relatively high for the region and R/R_D values quite low (Zmazek et al., 2003).

On August 29, 2007, the E11(x) unrest continued but changed from extension to compression (E11b(x) from August 29 to October 16, 2007; Fig. 6). C_{Rn} started to increase, giving an arithmetic mean for this period C_{Rn}(E11b) = 5184 ± 2163 Bq m^{-3}. When on September 19, 2007 the compression process slowed down (Fig. 6), C_{Rn} started to decrease and reached very low values towards the end of E11b(x). As for Postojna 1, it is not believed that this decrease coincided with earthquakes that occurred in the period September 26, 2007 to September 29, 2007 because their epicenters were too far away (R/R_D between 4.8 and 7.1), although their magnitudes were not so low for the region (M_L from 2.1 to 3.1) (Zmazek et al., 2003). Because C_{Rn}(E11b) is significantly higher than C_{Rn}(tot), with C_{Rn}(E11b)/C_{Rn}(tot) = 1.35, it can be concluded that compression significantly facilitates radon transport, thus increasing its activity in air. If only the fast compression period (from August 29 to September 19, 2007; Fig. 6) is taken into account, the related C_{Rn} arithmetic mean is 6150 ± 1739 Bq m^{-3} and the effect of compression on radon transport is even more pronounced.

CONCLUSIONS

Recent studies of active tectonics in Slovenia (Cunningham et al., 2006; Poljak, 2007; Rižnar et al, 2007; Verbič, 2005; Vrabec and Fodor, 2006) suggest that some caves should preserve and generate traces of active tectonics. In this context, two TM 71 extensometers were installed in 2004 in Postojna Cave on the Dinaric-oriented fault zone, situated about 1,000 m to the north of the Predjama Fault (Fig. 1)

The measurements of tectonic micro-displacements showed small tectonic movements on both instruments, a general dextral horizontal movement of 0.05 mm in four years (Postojna 1, Figure 5) and an extension of 0.03 mm in four years (Postojna 2, Figure 6). Eleven extremes of characteristic changes in displacement were determined between variable calm periods. Contemporaneous with some stronger earthquakes (for example Krn earthquake, July 12, 2004, M_W = 5.2), unrest was detected. For example, movements of 0.03–0.075 mm were detected in the period of one month along the fault zone. However, after the earthquake, the rock generally returns to the same position as before the earthquake. Similar behavior was described in Slovakia (Briestenský et al., 2007) and other countries (Košťák et al., 2007) where we were monitoring a seismic fault zone and detecting the micro-tectonic changes in Earth's crust before, during and after the earthquakes.

The greatest short-term movement was a compression of 0.04 mm in seven days, detected in March 2005 and coincided with the 25 km distant Ilirska Bistrica earthquake (M_L = 3.9). About two months before the earthquake, an extension of 0.05 mm occurred, and one month before the earthquake the stress changed into a compression of 0.05 mm. The largest permanent shift was detected at the end of 2004. Along the y-axis (at Postojna 1), a dextral horizontal movement of 0.075 mm was observed in one month. After the sinistral horizontal movement of 0.02 mm (December 15, 2004 to December 27, 2004), the y-axis retained its position on 0.05 mm, where it is still today. Regarding the extremes, ten earthquakes that coincide with tectonic micro-displacements were selected. In the time frame of speleogenesis, the monitored fault zone today represents a stable cave environment.

During horizontal movement, either dextral or sinistral, radon pathways underground were partly closed, thus hindering radon migration and reducing its concentration in the cave air. Extension does not appear to have affected radon transport. Alternatively, the compression process

(Postojna 2, February–August 2007) appears to have opened some new routes for radon transport, thus facilitating radon migration and increasing its concentration in air. In the present state of knowledge, a more solid explanation of these findings is not possible.

The comparative study is ongoing. The observed fault zone transmits only very small tectonic movements, but long-term monitoring of different parameters could sufficiently explain the relations in Earth's karst massif related to changes in stress and strain before, during, and after the stronger earthquakes. Finally, we will continue our comparative research with other monitoring sites where we have results and ongoing data collection (Stemberk et al., 2003; Košťák et al., 2007; Stemberk and Košťák, 2007; Briestenský et al., 2007).

Acknowledgments

The authors thank Mr. Mladen Živčić (Office of Seismology of the Environmental Agency of the Republic of Slovenia) for suggesting the combined measurements of radon concentrations and micro-tectonic deformations within this study, and Mrs. Ina Cecić (the same Office) for providing the information on the earthquake in Postojna Cave from the *Edinost* newspaper (Anonymous, 1926). The study was part of the projects: COST 625, Slovenia-Czech Republic cooperation in science and technology (BI-CZ/06-07-011 and BI-CZ/08-09-015).

References

Anonymous, 1926, Iz tržaške pokrajine, Postojna, sedem dni potresa: Edinost, 8.jaunar 1926, Trst.

Avramova-Tacheva, E., and Košťák, B., 1995, Local three-dimensional extensiometric measurements for the determination of displacements in the Krupnik fault zone, Bulgaria: Acta Montana IRSM AS CR, series A, no. 8 (97), p. 87–98.

Bajc, J., Aoudia, A., Saraò, A., and Suhadolc, P., 2001, The 1998 Bovec-Krn mountain (Slovenia) earthquake sequence: Geophysical Research Letters, v. 28, no. 9, p. 1839–1842.

Bini, A., Quinif, Y., Sules, O., and Uggeri, A., 1992, Les mouvements tectoniques recents dans les grottes du Mont Campo dei Fiori (Lombardie, Italie): Karstologia, v. 19, p. 23–30.

Briestenský, M., Stemberk, J., and Petro, L., 2007, Displacements registered around the 13 March 2006 Vrbové earthquake M = 3.2 (Western Carpathians): Geologica Carpathica, v. 58, no. 5, p. 487–493.

Čar, J., and Šebela, S., 1998, Bedding planes, moved bedding planes, connective fissures and horizontal cave passages (examples from Postojnska Jama cave): Acta Carsologica, v. 27, no. 2, p. 75–95.

Cunningham, D., Grebby, S., Tansey, K., Gosar, A., and Kastelic, V., 2006, Application of airborne LiDAR to mapping seismogenic faults in forested mountainous terrain, southeastern Alps, Slovenia: Geophysical Research Letters, v. 33, L20308 p. doi:10.1029/2006GL027014.

Dobrovolsky, I.P., Zubkov, S.I., and Miachkin, V.I., 1979, Estimation of the zone of earthquake preparation zone: Pure and Applied. Geophysics, v. 117, p. 1025–1044.

Etiope, G., and Martinelli, G., 2001, Migration of carrier and trace gases in the geosphere: An overview: Physics of Earth Planet Interiors, v. 129, p. 185–204.

European-Mediterranean Seismological Center, 2008, Database of Local Seismological Bulletins from European-Mediterranean Networks: http://www.emsc-csem.org/index.php?page=data&sub=base [accessed January 9, 2008].

Gilli, E., and Delange, P., 2001, Utilisation des spélèothèmes comme indicateurs de néotectonnique ou de paléosismicité: Riviera 2000, Tectonique active et géomorphologie, Villefranche-sur-Mer: Revue d'Analyse Spatial-No. Spécial 2001, p. 79–90.

Gosar, A., Šebela, S., Košťák, B., and Stemberk, J., 2007, Micro-deformation monitoring of active tectonic structures in W Slovenia: Acta Geodynamics et Geomaterialia, v. 4, no. 1, p. 87–98.

Kastelic, V., and Cunningham, D., 2006, Multi-disciplinary investigation of active strike-slip fault propagation in the Julian Alps: The Ravne Fault, NW Slovenia: Geophysics. Research Abstracts, v. 8, p. 05018.

Knez, M., 1996, The bedding-plane impact on development of karst caves (An example of Velika Dolina, Škocjanske Jame Caves): Ljubljana, Zbirka ZRC, no. 14, 186 p.

Kogovšek, J., and Šebela, S., 2004, Water tracing through the vadose zone above Postojnska Jama, Slovenia: Environmental Geology, v. 45, no. 7, p. 992–1001.

Košťák, B., 1969, A new device for in-situ movement detection and measurement: Experimental Mechanics 9, p. 374–379.

Košťák, B., 1977, Terčové měřidlo TM-71 a jeho užití pro měření velmi pomalých pohybů na poruchách a trhlinách: Inž. Stavby, v. 25, no. 5, p. 213–218.

Košťák, B., 1991, Combined indicator using Moiré technique, *in* Proceedings of the. 3rd International Symposium on Field Measurements in Geomechanics, Oslo, Balkema, p. 53–60.

Košťák, B., Cacoń, S., Dobrev, N.D., Avramova-Tacheva, E., Fecker, E., Kopecký, J., Petro, L., Schweizer, R., and Nikonov, A.A., 2007, Observations of tectonic microdisplacements in Europe in relation to the Iran 1997 and Turkey 1999 earthquakes: Izvestiya – Physics of the Solid Earth, v. 43, no. 6, p. 503–516.

Márton, E., Ćosović, V., Drobne, K., and Moro, A., 2003, Palaeomagnetic evidence for Tertiary counterclockwise rotation of Adria: Tectonophysics, v. 377, p. 143–156.

Ministry for Environment and Spatial Planning, Environmental Agency of the Republic of Slovenia, 2008, Seismology: http://www.arso.gov.si/potresi/ [accessed January 9, 2008].

Mocchiutti, A., and D'Andrea, A., 2002, Morphologic evidence of recent and modern tectonic movements in some caves of the Friuli Prealps (northeastern Italy): Memoirs of the Society of Geology Italy, v. 57, p. 487–491.

Nero, A.V., 1988, Radon and its decay products in indoor air: an overview, *in* Nazaroff, W.W., and Nero, Jr., A.V., eds., Radon and its Decay Products in Indoor Air, New York, John Wiley & Sons, p. 1–53.

Petrič, M., and Šebela, S., 2004, Vulnerability mapping in the recharge area of the Korentan spring, Slovenia: Acta Carsologica, v. 33, no. 2, p. 151–168.

Placer, L., 1999, Structural meaning of the Sava folds: Geologija, v. 41, p. 191–221.

Plan, L., Spötl, Ch., Grasemann, B., Decker, D., Offenbecher, K.H., and Wiesmayr, G., 2005, Seismothems caused by neotectonic activity in the Eastern Alps, *in* 14th International Congress of Speleology, Final Programme & Abstract Book, p. 117–118.

Poljak, M., 2007, Structural-Tectonic Map of Slovenia 1:250.000, Ljubljana, Geological Survey of Slovenia, 52 p.

Poljak, M., Živčić, M., and Zupančič, P., 2000, The seismotectonic charateristics of Slovenia: Pure and Applied Geophysics, v. 157, p. 37–55.

Ribarič, V., 1982, Seismicity of Slovenia – Catalogue of Earthquakes (792 A.D.-1981): Ljubljana , SZ SRS Publication Ser. A, no. 1-1, 649 p.

Rižnar, I., Koler, B., and Bavec, M., 2007, Recent activity of the regional geologic structures in western Slovenia: Geologija, v. 50, no. 1, p. 111–120.

Sasowsky, I.D., Šebela, S., and Harbert, W., 2003, Concurrent tectonism and aquifer evolution >100,000 years recorded in cave sediments, Dinaric karst, Slovenia: Environmental Geology, v. 44, p. 8–13.

Šebela, S., 1998, Tectonic structure of Postojnska jama cave system: Ljubljana, Zbirka ZRC, no. 18, 112 p.

Šebela, S., 2005, Monitoring of active tectonic structures – Project COST 625: Acta Carsologica, v. 34, no. 2, p. 471–488.

Šebela, S., Slabe, T., Liu, H., and Pruner, P., 2004, Speleogenesis of selected caves beneath the Lunan Shilin and Caves of Fenglin Karst in

Qiubei, Yunnan: Acta Geologica Sinica (English edition.), v. 78, no. 6, p. 1289–1298.

Šebela, S., Gosar, A., Košťák, B., and Stemberk, J., 2005, Active tectonic structures in the W part of Slovenia - setting of micro-deformation monitoring net: Acta Geodynamics et Geomaterialia, v. 2, no. 1, p. 45–57.

Stemberk, J., Košťák, B., and Vilimek, V., 2003, 3D monitoring of active tectonic structures: Journal of Geodynamics, v. 36, no. 1–2, p. 103–112.

Stemberk, J., and Košťák, B., 2007, 3-D trend of aseismic creep along active faults in western part of the Gulf of Corinth Greece: Acta Geodynamics Geomater, v. 4, no. 1, p. 53–65.

Vaupotič, J., 2008, Nanosize radon short-lived decay products in the air of the Postojna Cave: Science of the Total Environment, v. 393, p. 27–38.

Vaupotič, J., Csiege, I., Radolić, V., Hunyadi, I., Planinić, J., and Kobal, I., 2001, Methodology of radon monitoring and dose estimates in Postojna Cave, Slovenia: Health Physics., v. 80, p. 142–147.

Verbič, T., 2005, Quaternary stratigraphy and neotectonics of the Eastern Krško Basin. Part 2: Neotectonics: Razprave IV, Razreda SAZU, v. 66, no. 1, p. 171–216.

Virk, H.S., Singh, M., and Ramola, R.C., 1997, Radon monitoring for uranium exploration, earthquake prediction and environmental health hazard in Himachal Pradesh, India: an appraisal: *in* Virk, H.S., ed., Rare gas geochemistry – applications in earth and environmental sciences, Amristar, Guru Nanak Dev University, p. 89–99.

Vrabec, M., and Fodor, L., 2006, Late Cenozoic Tectonics of Slovenia: Structural Styles at the Northeastern Corner of the Adriatic microplate: *in* Pinter, N., Grenerczy, G., Weber, J., Medak, D., and Stein, S., eds., Proceedings of the NATO Advanced Research Workshop on The Adria microplate: GPS Geodesy, Tectonics, and Hazards, Veszprem, Springer, Hungary 4–7 April 2004, NATO Science Series, IV, Earth and Environmental Sciences, v. 61, p. 151–168.

Weber, J.C., Vrabec, M., Stopar, B., and Dixon, T., 2004, New GPS constraints on Adria microplate kinematics, dynamics, and rigidity from the Istria peninsula, Slovenia and Croatia: GSA Abstracts with Programs, v. 36, no. 5

Wu, Y., Wang, W., Liu, H., Zhou, X., Wang, L., and Titus, R., 2003, Radon concentration: a tool for assessing the fracture network at Guanyinyan study area, China: Water SA, v. 29, p. 49–53.

Zmazek, B., Todorovski, L., Džeroski, S., Vaupotič, J., and Kobal, I., 2003, Application of decision trees to the analyis of soil gas radon data for earthquake predisction: Applied Radiation Isotopes, v. 58, p. 697–706.

G.L. Harley, P.P. Reeder, J.S. Polk, and P.E. van Beynen – Developing a GIS-based inventory for the implementation of cave management protocols in Withlacoochee State Forest, Florida. *Journal of Cave and Karst Studies,* v. 72, no. 1, p. 35–42. DOI: 10.4311/jcks2008lsc0063

DEVELOPING A GIS-BASED INVENTORY FOR THE IMPLEMENTATION OF CAVE MANAGEMENT PROTOCOLS IN WITHLACOOCHEE STATE FOREST, FLORIDA

Grant L. Harley[1], Philip P. Reeder[2], Jason S. Polk[3], and Philip E. van Beynen[2]

Abstract: The type of data collected during cave inventories includes a myriad of different parameters; however, the actual practice of field data collection lacks a modern, standardized method. The integration of GIS with methods associated with the inventory of cave resources and utilization patterns improve upon the previously utilized paper-form of inventory. This article discusses the development of a GIS-based method of cave inventory and how its implementation advanced cave management protocols in Withlacoochee State Forest (WSF), Florida. After realizing the need for a more sophisticated and secure method to inventory caves in WSF, an alternative data collection, storage, and manipulation method was expanded that allowed the input and storage of large amounts of spatially-referenced data. The overarching purpose of this study was to create a modernized and user-friendly GIS-based method of cave inventory that encompassed all aspects of the inventory (i.e., data collection, storage, manipulation, and post-processing) for the efficient management of caves in WSF. The GIS-based inventory developed for WSF caves is easily applied by state forest personnel and is aiding in the drafting of management plans for each cave they manage. Having rigorously tested this method in 19 caves, we feel it is applicable to cave systems in all karst areas.

Introduction

Geographic Information Systems (GIS) are used in a variety of fields such as urban and regional planning (Dai et al., 2001; Jankowski, 1989), criminology (Brantingham and Brantingham, 1995; Chainey and Ratcliffe, 2005), and natural sciences (Carrara et al., 1991; Goodchild, 1993). GIS is now being applied to various aspects of cave and karst science for its ability to integrate data storage with a spatial component. The integration of GIS with karst research has furthered the study of speleogenesis (Horrocks and Szukalski, 2002; Hung et al., 2002), cave ecosystems (Despain and Fryer, 2002), cave geomorphology and hydrology (Florea et al., 2003; Florea, 2006), the consideration of caves as a monetary resource for tourism (Ohms and Reece, 2002), cave archaeology (Moyes, 2002), and the human disturbance of karst environments (van Beynen and Townsend, 2005). In this paper, we present a new method for using GIS to inventory cave contents for resource management purposes.

More than 25% of the world's population either lives on or obtains drinking water from karst terranes, with caves being an integral component of karst landscapes (KWI, 2009). Understanding caves as natural systems and potential groundwater resources is the key to their management and protection, with the first step being to conduct a cave inventory (DuChene, 2006). However, cave inventories are not widely published in the popular and professional press, vary in both purpose and method, and are often subjective with respect to the amount and type of data included. Assimilating GIS with methodologies associated with the inventory of cave resources and utilization patterns could make the paper-form inventory of cave systems obsolete, thereby moving towards more comprehensive data collection and user flexibility.

This project was initiated through a collaborative effort between the Withlacoochee State Forest (WSF) and the Department of Geography at the University of South Florida. Prior to this project, state forest personnel had limited knowledge of their caves and expressed the need for a comprehensive cave management strategy. The research design for this study was to develop and test a method for conducting inventories in WSF terrestrial caves using GIS, thereby allowing state forest personnel to easily access and manipulate data, and provide a replicable method for future inventories of other cave systems in west-central Florida. Given the widespread lack of cave management in WSF, the inventory served as the first account of cave contents in WSF and the first step in developing ongoing management strategies.

[1] Department of Geography, University of Tennessee, 304 Burchfiel Geography Building, Knoxville, TN 37996, glharley@gmail.com
[2] Department of Geography, University of South Florida, 4202 E. Fowler Ave., Tampa, FL, 33620, preeder@cas.usf.edu, vanbeyne@cas.usf.edu
[3] Hoffmon Environmental Research Institute, Department of Geography and Geology, Western Kentucky University, 1906 College Heights Blvd., Bowling Green, KY, 42101, jason.polk@wku.edu

Figure 1. Gentle, rolling topography near Withlacoochee State Forest, Brooksville, Florida. In the background is an upland mesic-hardwood hummock adjacent to a sinkhole lowland in the foreground.

The overall purpose of this study was to create a modernized and user-friendly GIS-based method of cave inventory that encompasses all aspects of the inventory (i.e., data collection, storage, manipulation, and post-processing) for the efficient management of caves in WSF. This article presents a GIS-based method and database design the authors developed to facilitate cave inventories in WSF.

BACKGROUND: CAVE INVENTORY

Since the 1700s, cave inventories involved cataloging biota, archaeological sites, and fossil deposits (DuChene, 2006). A number of different groups have conducted cave inventories throughout the United States with varying objectives (Brown and Kirk, 1999; Douglas, 1999; DuChene, 2006). Data collected during these inventories included a wide variety of cave features and their attributes. However, the actual practice of field data collection has lacked a modern, standardized method. Although paper inventory forms are the most widely used and accepted tool for recording cave inventory data (DuChene, 2006), they are especially difficult to use in tight, wet, and muddy cave environments, as experienced in the preliminary stages of this project. These conditions made it necessary to utilize alternative means of data collection that could withstand the rigors of harsh cave conditions. Since the advent of GIS, researchers have realized the potential of combining cave inventory data and GIS (Knutson, 1997; Pfaff et al., 2000; McNeil et al., 2002; Moyes, 2002; Horrocks and Szukalski, 2002; Ohms and Reece, 2002; Despain and Fryer, 2002; Walz and Spoelman, 2005). By integrating GIS with previous forms of inventory, additional data can be collected in a quicker, more efficient manner, thus reducing the cost and staffing needs, and eliminating the aforementioned problems associated with paper inventory forms.

STUDY AREA

WSF is a vast stretch of land in west-central Florida that covers approximately 637 km^2 and spans four counties (Citrus, Pasco, Hernando, and Sumter). The karst features found in WSF include: springs, sinkholes, and terrestrial caves. Currently, there are 19 known caves located in WSF, all of which are developed within the Brooksville Ridge. The Brooksville Ridge is the largest of the ridges located in the Central Upland of the Florida Peninsula (White, 1970). Elevations vary throughout its length from 21 to 60 m above mean sea level. The topography is rolling hills with internal drainage occurring mostly through caves associated with the Floridan Aquifer System. Additionally, upland mesic-hardwood hummocks separate sinkhole lowlands that are mostly occupied by wetlands or lakes (Florea, 2006) (Fig. 1). The WSF caves are all located within the Citrus Tract, which is positioned on the border of Citrus and Hernando Counties (Fig. 2). WSF is state-owned, public land and any recreational activity requires a special-use permit, including cave access.

METHODS

LOCATING CAVES FOR INVENTORY

All 19 known caves within WSF were visited in the spring of 2007 in order to assemble a detailed record of

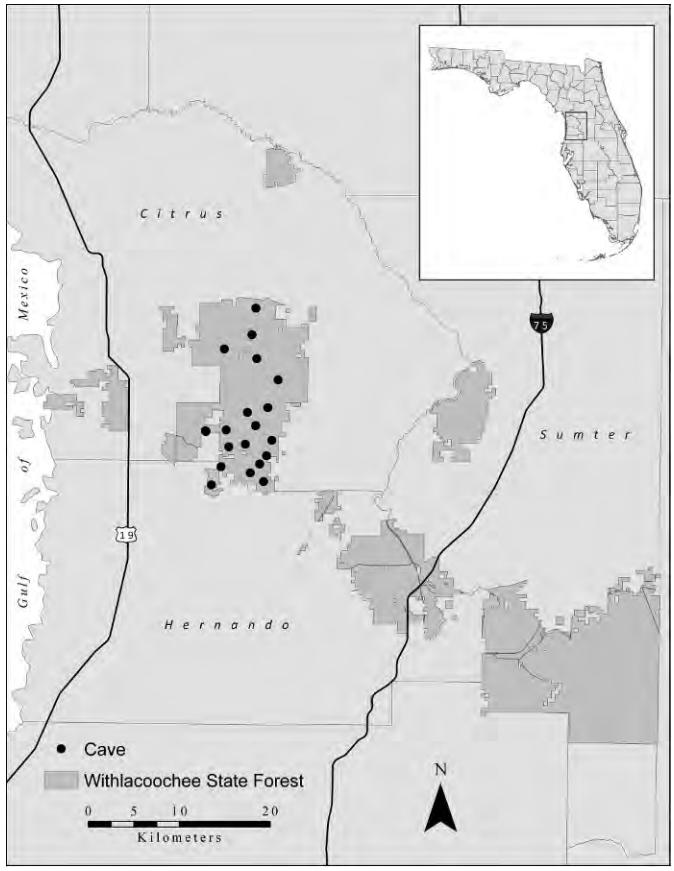

Figure 2. Location of caves within Withlacoochee State Forest, Florida.

Figure 3. A mobile GPS unit was linked with the PDA to facilitate the acquisition of cave locations.

resources using a GIS-based inventory. A Global Positioning System (GPS) was linked with ESRI ArcPad 7.1, which allowed for cave entrance location acquisition in the field and storage directly into the geodatabase (Fig. 3). ArcPad 7.1 is GIS software for mobile devices and provides the ability to collect field data in a reliable and efficient manner (Clarke et al., 2002). A mobile Haicom HI-303III GPS unit was used to locate cave entrances with known waypoints. However, caves with unknown waypoints were marked in the field using the mobile GPS unit. Because of the link between GPS and GIS, these caves were immediately added to ArcPad 7.1 and made available for inventory data input directly in the geodatabase.

Inventory Framework and Contents

The cave inventory framework is based on a paper inventory model described by O'Dowd and Broeker (1996). This inventory model was one of the most comprehensive inventory models available and proved to be easily adaptable to suit the objectives of this project. The inventory model was adjusted to comprehensively fit in a GIS geodatabase by creating categorized attributes with detailed descriptions and fields for data input. Cave-survey data containing stations were necessary to give cave resources a reference point during inventory. Each survey station was given an absolute location based upon the entrance GPS data. Several caves in WSF were previously surveyed and maps were acquired from the cartographers. However, the majority of caves were simultaneously surveyed and inventoried, which is a widely practiced and accepted method (Ohms and Reece, 2002; Horrocks and Szukalski, 2002; DuChene, 2006). For caves lacking an existing survey, one was conducted using a compass, inclinometer, and tape (Dasher, 1994). A detailed account of specific cave contents was inventoried at each survey station. Features within each cave located between survey stations were assigned to the closest survey station. These parameters are presented in the geodatabase data dictionary, which is used to describe each field and its possible values (Table 1).

Using GIS for Cave Inventory

Collecting and storing inventory data in the same step was a more efficient method that saved time and work and eliminated human error during the process of data transcription from paper forms. In order to facilitate data collection, ArcPad 7.1 was loaded onto a Dell Axim X51 personal digital assistant (PDA) (Fig. 4). An Aqua Quest

Table 1. Geodatabase Data Dictionary.

Attribute Name	Description
Name	All known names of cave
Inventory Date	Date the inventory was conducted
Inventory ID	Unique ID given to each cave for geodatabase identification
Township	Township in which cave is located (Public Land Survey System)
Range	Range in which cave is located (Public Land Survey System)
Section	Section in which cave is locate (Public Land Survey System)
County	Florida county in which cave is located
Personnel	People who conducted inventory
Cave Ownership	Ownership of cave. Values = Commercial, Private, Public, Government Park, Unknown Status
Equipment Needed	Equipment needed to cave. Values = Boat or Floatation, Diving Equipment, Handline, Kneepads, Cable ladder, Normal Speleo Gear, Shovel-Blasting, Rope or Vertical Equipment, Other special equipment, Unknown, Wet-Suit, Mask/ snorkel, None, NA
Other Equipment Needed	Same values as Equipment Needed (above) to list multiple equipment needs
Elevation	Elevation of cave entrance in meters above mean sea-level
Cave Map Status	Current status of cave map. Values = Improved map, New map/survey, Redraw of old map, In progress, No map, Complete map, Sketch only, not to scale
Cave Length	Current surveyed length of cave (m)
Cave Vertical Extent	Current surveyed vertical extent of cave (m)
Management Notes	Notes pertaining to the management of cave
Entry Status	Accessibility of cave. Values = Fees charged for entry, Destroyed or closed, Forbidden by owner, Locked/Gated, Navigable Waterway, Open access, Permission required, Waiver required, Temporarily blocked, Unknown status, NA
Multiple Entrances	Indicates whether there are multiple entrances to cave. Values = Y (Yes) or N (No)
Type Of Entrance: Vertical	Indicates type of cave entrance if vertical. Values = Artificial shaft, Bottleneck/ small but bells out, Chimney/climb, Very wide pit (+20 ft), Pit, Tight pit, Enlarged fissure, Tight squeeze, NA
Type Of Entrance: Horizontal/ Downward Sloping	Indicates type of cave entrance if horizontal or downward sloping. Values = Large horizontal (+ 20 ft), Stoop/duck walk, Crawl, Artificial tunnel, Tight squeeze, NA
Entrance Topo Position	Describes the topographic position of the cave entrance. Values = Sinkhole, Hillside, Topographic low, Hilltop, Quarry, Floodplain, etc.
Entrance Visibility	Indicates visibility of cave entrance. Values = Clearly visible, Obscured by vegetation, Obscured by rocks, etc.
Entrance Modification	Describes any modifications made to the cave entrance. Values = Widened, Artificial entrance, Gated, Road construction, Quarry, Blocked, Dug out/open
Entrance Min Size	Indicates the minimum size of cave entrance. Values = Squeeze, Crawl, Stoop, Walk, Vertical drop
Entrance Drop Depth	Depth of entrance drop if vertical (m)
Entrance Notes	Any notes relating to cave entrance
Passage Orientation	Passage orientations per survey station. Values = N-S, E-W, NE-SW, NW-SE, NE-SW & NW-SE, NE-SW & NW-SE & N-S & E-W
Passage Types	Passage type per survey station. Values = enlarged fissure, key hole, plus-sign, breakdown, phreatic, etc.
Passage Min Sizes	General size of passage per survey station. Values = squeeze, crawl, stoop, walk, etc.
Passage Hydrology	Hydrological resources per survey station. Values = seeps, drips, pool, aquifer, NA, etc.
Passage Floor	Floor type per survey station. Values = sediment, clay, breakdown, etc.
Passage Hazards	Possible hazards per survey station. Values = guano, unstable breakdown, steep drop, etc.

Table 1. Continued.

Attribute Name	Description
Passage Notes	Notes pertaining to passage characteristics
Tites/Mites/Columns/Condition	Stalactites, stalagmites, and/or columns and condition (depositing, dry, damaged, etc.) per survey station. NA = Not Applicable
Drapery Condition	Drapery and condition per survey station. NA = Not Applicable
Helictites Condition	Helictites and condition per survey station. NA = Not Applicable
Rimstone Condition	Rimstone and condition per survey station. NA = Not Applicable
Popcorn Condition	Popcorn and condition per survey station. NA = Not Applicable
Flowstone Condition	Flowstone and condition per survey station. NA = Not Applicable
Spar Condition	Spar and condition per survey station. NA = Not Applicable
Calcite Coating	Calcite coating and description per survey station. NA = Not Applicable
Calcite Rafts	Calcite rafts and description per survey station. NA = Not Applicable
Ripple Marks/Scallops	Ripple marks and/or scallops per survey station. NA = Not Applicable
Anastomoses	Anastomoses per survey station. NA = Not Applicable
Sediments	Describes sediment per survey station in cave. Values = sorted, unsorted, clay, fine lamination, organics present, etc.
Sediment Notes	Any notes relating to cave sediments
Fossils	Location and description of fossils per survey station. NA = Not Applicable
Bones	Location and description of bones per survey station. NA = Not Applicable
Geologic Strata	Geologic unit per survey station. Values = Ocala limestone (Eocene), Suwannee Limestone (Oligocene), Avon Park Formation (Middle Eocene), Tampa Member (Arcadia Formation)(Upper Oligocene-Lower Miocene)
Other Geologic Strata	Other geologic unit found per survey station. Same values as ''Geologic_Strata'' (in case of more than one strata per station)
Geologic Notes	Any notes for geology of cave
Biological Vertebrates	List and location of biological vertebrates per survey station. NA = Not Applicable
Biological Invertebrates	List and location of biological invertebrates per survey station. NA = Not Applicable
Mold/Bacteria	List and location of any mold or bacteria per survey station. NA = Not Applicable
Roots	Location of roots per survey station. NA = Not Applicable
Roost Stains	Location of roost stains per survey station. NA = Not Applicable
Guano Piles	Location of guano piles per survey station. NA = Not Applicable
Biological Notes	Any notes pertaining to cave biology.
Artifacts- Historical	List and location of possible historical artifacts per survey station. NA = Not Applicable
Cultural Notes	Any notes pertaining to possible cave artifacts. NA = Not Applicab
Scientific Potential Area Note	Notes for scientific potential areas (location and description) per survey station
Special Interest Areas Note	Notes for special interest, non-scientific areas (location and description) per survey station.

water-proof case was used to ensure the protection of the PDA device while conducting the inventory in wet and/or muddy cave environments (Fig. 5). Certain GIS data layers were loaded into ArcPad 7.1 for use in the field. These layers included: a polygon coverage of Florida counties and roads, a point coverage of WSF cave locations, and a polygon coverage of WSF. Both polygon coverage layers were acquired from the Florida Geographic Data Library and served as a spatial reference for the point coverage of WSF caves that was created during this study. All shapefile layers and the geodatabase were viewable on the PDA, which allowed for editing and updating in the field.

The cave inventory data for each cave was stored in a GIS geodatabase (Table 1). The cave inventory geodatabase was created in ArcCatalog and maintained in ArcMap 9.2, both of which are applications included in the ESRI ArcView 9.2 ArcGIS software package. ArcPad 7.1 and ArcView 9.2 are interchangeable GIS applications, making data transfer from the PDA to the geodatabase straightforward. When data were ready to be transferred to the geodatabase after applying the inventory, the PDA was synced to a personal computer via Microsoft Active Sync version 4.1.0. Once synchronized, the data were copied from the PDA directly to the geodatabase in ArcMap 9.2.

Figure 4. The tools used for inventory data collection in the field included ArcPad 7.1 displayed on a Dell Axim X51 device.

Additionally, each cave was documented with photographs using a digital camera. Documenting cave features with photographs produces a visual representation of those features during the time of inventory and is useful when comparing cave conditions through time (DuChene, 2006).

FIELD INVENTORY METHODS

Cave inventory teams consisted of an average of three people, depending upon the availability of an existing survey. If an accurate survey existed, two people were sufficient; while one read the map and identified resources at and between each survey station, the other input the data into the PDA. If no survey was available, then a three-person team simultaneously surveyed and inventoried the cave, as the additional person sketched and assisted with the survey/inventory. Every participant in this project was an experienced caver or karst scientist well-versed in the identification of features within the caves.

The inventory of each of the 19 caves in WSF began at the entrance, and included both vertical and horizontal openings. Data collection commenced at the entrance with one person using the PDA to input features found within the cave as identified by the second and/or third individual. Survey stations were used as markers to spatially identify features entered into the geodatabase. This method of data entry continued until the entire cave and its contents were surveyed (if needed) and inventoried.

DATABASE DESIGN

A comprehensive cave inventory geodatabase was created using the electronic PDA inventory method. The inventory database includes a point shapefile (each point represents a cave) and a database file (dbf). The dbf contains the descriptive data for each cave obtained during inventory in the field (Table 1). This database is easily queried to locate cave features and parameters by WSF personnel, which also allows future updates as cave inventories are added for newly discovered caves, or updates from future inventories of existing caves. By using an electronic cave inventory method, the functionality, comprehensiveness, and transferability of cave inventory data were improved,

Figure 5. The PDA device was protected in the field with an Aqua Quest, water-proof cover.

thereby providing WSF personnel with the necessary information to use in managing their caves. Additionally, the variety of fields (Table 1) in the geodatabase allowed for substantial data collection above and beyond that of standard inventories collected by other methods. Cave inventory data are secured via password-protected software used by WSF to guard the inventory information and allow access only by authorized users. Thus, WSF personnel are able to use additional data to manage caves by resources, location, size, features, etc. by querying the geodatabase and utilizing ArcGIS to determine which caves require special management and attention.

WSF personnel are now able to view the exact locations of caves and access the associated attribute table (dbf) to view the cave-specific resources, anthropogenic impacts, and other characteristics of each cave. Knowing the entrance location and attribute data for each cave are the initial steps needed for resource protection and proper management decisions, emergency response planning, prevention of unintentional impacts to cave systems from land management activities such as logging, road maintenance, construction of recreational facilities, prescribed forest burns, exotic plant control, and other activities. By having the ability to query and rank caves based on their features and resources, land managers are able to use the geodatabase to help prioritize cave management based on their needs.

With a comprehensive inventory system in place, WSF continues the inventory of each cave on a regular basis. The inventory system also provides them the basis needed to conduct visitor impact mapping, such as that described in Bodenhamer (1995, 2006), as well as implement a GIS-based management strategy that geospatially links cave inventory data with each geo-referenced survey station (Despain and Fryer, 2002). By using an easily adapted electronic method for inventory, data fields can be added in the field, and data transcription errors and time are reduced, which is a benefit for management entities such as WSF that have limited personnel and financial resources to address cave protection and management.

This GIS-based method of cave inventory is easily adaptable for use in caves in other karst areas, including water-filled cave systems. The limiting factors are the availability of the necessary computer hardware and software and the expertise to link all the components of the inventory together using GIS. However, these factors can be overcome with expanded funding and staffing. Additionally, those conducting the inventory need to adapt the comprehensive fields included in the geodatabase to include the parameters specific to their particular caves. For example, we tailored the original cave inventory parameters from O'Dowd and Broeker (1996) (which was created for use in Oregon caves) for applicability in caves of west-central Florida. Certain parameters were simply not applicable, as the caves and karst of Oregon differs from Florida.

Mobile GIS as an Inventory Tool

A new electronic method for cave inventory using ArcGIS and ArcPad allows for enhanced data collection and reduces the need for WSF personnel to conduct and transcribe data acquired during inventories. In this pilot study, the cave inventory geodatabase serves as the first step in developing a cave management strategy for each of the 19 caves in WSF. This first step of understanding cave contents is crucial in drafting, implementing, enforcing, and analyzing sound management policy for each cave. The completion of the inventory in each of the 19 WSF caves reveals several important findings:

1. Several species of invertebrates were discovered in six caves, which were previously unbeknownst to WSF biologists. This demonstrates the need for a biological, project-specific inventory of each cave containing these resources.
2. Pristine speleothems were found in several caves in need of immediate protection from vandals and souvenir-seekers.
3. The data reveal the need for gates on numerous caves, either for resource protection or liability issues brought on by day-use activities.
4. Several caves were found to be in areas of forest-personnel activity (logging, control burning, cattle grazing, etc.) and procedures can now be implemented to protect the resources found within these caves.

WSF is constantly performing prescribed control burns and granting agricultural lease permits in certain sections of the forest. Forest personnel can now reference the cave inventory geodatabase when making land use decisions. The inventory GIS data also enables WSF personnel to make conservation-wise decisions regarding the relative location of caves in relation to their daily activities which could result in the degradation of a cave environment. This decreases the human-environmental impact and ensures the conservation and protection of each cave in WSF.

Currently, the GIS-based inventory developed for WSF caves is easily applied by state forest personnel and is progressing the drafting of management plans for each cave. Furthermore, we believe this method of inventorying caves should be incorporated in other karst areas, as it can be more beneficial to cave managers than previous methods.

Acknowledgements

We thank the following people: Colleen Werner at Withlacoochee State Forest for supporting this project and providing access to WSF caves; Robert Brinkmann, along with others, for conceiving and promoting this project from its inception; Robert Brooks and Tom Turner for help with locating and inventorying caves; Lee Florea for contributing his cave maps and advice to the project, and

the Florida Center for Community Design and Research for use of their PDA and software.

REFERENCES

Bodenhamer, H., 1995, Monitoring human-caused changes with visitor impact mapping, *in* Proceedings, 10th National Cave Management Symposium, Indianapolis, October 1995, Indiana Karst Conservancy, p. 28–37.

Bodenhamer, H., 2006, Visitor Impact Mapping in Caves, *in* Hildreth-Werker, V., and Werker, J.C., eds., Cave Conservation and Restoration, Huntsville, Ala., National Speleological Society, p. 193–202.

Brantingham, P., and Brantingham, P., 1995, Location quotients and crime hotspots in the city, *in* Block, C., Dabdoub, M., and Fregly, S., eds., Crime analysis through computer mapping, Washington, D.C., Police Executive Research Forum, p. 129–149.

Brown, T., and Kirk, D., 1999, A Karst Resource Inventory of the George Washington and Jefferson National Forests, *in* Proceedings, 14th National Cave and Karst Management Symposium, October 1999: Chattanooga, Tenn., Southeastern Cave Conservancy, p. 12–18.

Carrara, A., Cardinali, M., Detti, R., Guzzetti, F., Pasqui, V., and Reichenbach, P., 1991, GIS techniques and statistical models in evaluating landslide hazard: Earth Surface Processes and Landforms, v. 16, p. 427–445.

Chainey, S., and Ratcliffe, J., 2005, GIS and Crime Mapping, Hoboken, N.J., John Wiley & Sons, 442 p.

Clarke, S., Greenwald, C., and Spalding, V., 2002, ArcPad 6, Using ArcPad, Redlands, Cal., ESRI, 6 p.

Dai, F.C., Lee, C.F., and Zhang, X.H., 2001, GIS-based geo-environmental evaluation for urban land-use planning: a case study: Engineering Geology, v. 61, no. 4, p. 257–271.

Dasher, G.R., 1994, On Station, Huntsville, Ala., National Speleological Society, 240 p.

Despain, J., and Fryer, S., 2002, Hurricane Crawl Cave: A GIS-based cave management plan analysis and review: Journal of Cave and Karst Studies, v. 64, no. 1, p. 71–76.

Douglas, J., 1999, Historic Preservation at Hubbards Cave: Inventory and Management of Cultural Resources, *in* Proceedings, 14th National Cave and Karst Management Symposium, October 1999: Chattanooga, Tenn., Southeastern Cave Conservancy, p. 46–50.

DuChene, H.R., 2006, Resource Inventory: A Tool for Cave Science, Management, and Restoration, *in* Hildreth-Werker, V., and Werker, J.C., eds., Cave Conservation and Restoration, Huntsville, Ala., National Speleological Society, p. 19–32.

Florea, L.J., 2006, Architecture of air-filled caves within the karst of the Brooksville Ridge, west-central Florida: Journal of Cave and Karst Studies, v. 68, no. 2, p. 64–75.

Florea, L.J., Hashimoto, T., Kelley, K.N., Miller, D., and Mrykalo, R., 2003, Karst Geomorphology and Relation to the Phreatic Surface, Briar Cave, Marion County, Florida, *in* Florea, L.J., Vacher, H.L., and Oches, E.A., eds., Karst Studies in West Central Florida, Brooksville, Fla., Southwest Florida Water Management District, p. 9–19.

Goodchild, M.F., 1993, The state of GIS for environmental problem solving, *in* Goodchild, M.F., Parks, B.O., and Steyaert, L.T., eds., Environmental Modeling with GIS, New York, Oxford University Press, p. 8–15.

Horrocks, R., and Szukalski, B.W., 2002, Using geographic information systems to develop a cave potential map for Wind Cave, South Dakota: Journal of Cave and Karst Studies, v. 64, no. 1, p. 63–70.

Hung, L.Q., Dinh, N.Q., Batelaan, O., Tam, V.T., and Lagrou, D., 2002, Remote sensing and GIS-based analysis of cave development in the Suoimuoi Catchment (Son La — NW Vietnam): Journal of Cave and Karst Studies, v. 64, no. 1, p. 23–33.

Jankowski, P., 1989, Mixed-data multicriteria evaluation for regional planning: a systematic approach to the decision-making process, Environment and Planning, v. 21, p. 349–362.

KWI, 2009, Karst Waters Institute, http://www.karstwaters.org/ [accessed October 10, 2008].

Knutson, S., 1997, Cave maps as geographical information systems: An example from Oregon Caves National Monument, *in* Proceedings, 13th National Cave and Karst Management Symposium, October 1997: Chattanooga, Tenn., Southeastern Cave Conservancy, p. 116.

McNeil, B.E., Jasper, J.D., Luchsinger, D.A., and Rainsmier, M.V., 2002, Implementation and application of GIS at Timpanogos Cave National Monument, Utah: Journal of Cave and Karst Studies, v. 64, no. 1, p. 34–37.

Moyes, H., 2002, The use of GIS in the spatial analysis of an archaeological cave site: Journal of Cave and Karst Studies, v. 64, no. 1, p. 9–16.

O'Dowd, J., and Broeker, L., 1996. Cave Management Handbook, http://www.fs.fed.us/r6/umpqua/publications/cave-mgt-handbook-12-02-04_files/cave-mgt-handbook-12-02-04htm#_Toc8724 5850 [accessed September 21, 2008].

Ohms, R., and Reece, M., 2002, Using GIS to manage two large cave systems, Wind and Jewel Caves, South Dakota: Journal of Cave and Karst Studies, v. 64, no. 1, p. 4–8.

Pfaff, R., Glennon, J., Groves, C., Meiman, J., and Fry, J., 2000, Geographic information systems as a tool for the protection of the Mammoth Cave karst aquifer, Kentucky, *in* Proceedings, 8th Mammoth Cave Science Conference: Mammoth Cave, Kentucky, National Park Service, p. 89–99.

Van Beynen, P., and Townsend, K., 2005, A Disturbance Index for Karst Environments: Environmental Management, v. 36, no. 1, p. 101–116.

Walz, J., and Spoelman, S., 2005, Integrating Cave and Karst Inventory Methods with GIS, 2003–2004 Cave and Karst Inventory Project, Wind Cave National Park, Inside Earth: Wind Cave National Park, National Park Service, v. 8, no. 1, p. 17–24.

White, W.A., 1970, The Geomorphology of the Florida Peninsula: State of Florida Department of Natural Resources Geological Bulletin 51, 164 p.

S. Galdenzi, F. Cocchioni, G. Filipponi, L. Morichetti, S. Scuri, R. Selvaggio, and M. Cocchioni – The sulfidic thermal caves of Acquasanta Terme (central Italy). *Journal of Cave and Karst Studies,* v. 72, no. 1, p. 43–58. DOI: 10.4311/jcks2008es0056

THE SULFIDIC THERMAL CAVES OF ACQUASANTA TERME (CENTRAL ITALY)

Sandro Galdenzi[1]*, Filippo Cocchioni[2], Giampaolo Filipponi[3], Luciana Morichetti[2], Stefania Scuri[2], Rosario Selvaggio[3], and Mario Cocchioni[2]

Abstract: The caves of Acquasanta Terme (central Italy) open at the core of a wide anticline, in the valley of the Tronto River. Cave development is due to the rise of sulfidic thermal water flowing through a thick marine limestone sequence, overlain by thick, low-permeability formations. Some minor caves are developed in the terraced travertines deposited by the thermal water, but the major caves are developed in marine limestone in the small gorge of the Rio Garrafo stream, a tributary of the Tronto River. These caves have a rising pattern, due to the past flow of thermal water toward the surface. The deepening of the Tronto River Valley lowered the regional water table, perching the Rio Garrafo stream ~50 m above the thermal groundwater. At present, surface water sinks through the pre-existing karst passages to reach the thermal water flowing in the lower parts of the caves. Where these waters mix, rapid corrosion of the walls through sulfuric acid speleogenesis occurs. Annual temperature and chemistry monitoring of the cave water showed that freshwater contributes up to 45% of the volume at the water table. Dilution events are associated with falling water temperature, which ranges between 44°C and 32°C. At the main spring, 2 km downstream, groundwater dilution was higher resulting in lower temperatures (32°C–21°C) and salinity. The periods of high freshwater dilution correspond with a lowering of pH in the phreatic water and with the release of H_2S and CO_2 to the cave atmosphere. In the thermal zones, the concentration of H_2S increased from 40 to over 240 ppm, while CO_2 increased from 0.44% to 2.7%. These data evidence the influence of sinking surface water on the cave environment and speleogenesis.

Introduction

The thermal caves of Acquasanta Terme represent a window on active sulfuric acid speleogenesis. Some caves in the area have been known since ancient times due to their large entrances and easy accessibility. A modern exploration, however, began only after World War II when the management of the thermal baths invited the speleologist of the Società Adriatica di Scienze Naturali (Trieste, Italy) to explore the area some tens of years later than in nearby zones. The speleologist of the Società Adriatica, helped by the Gruppo Speleologico Marchigiano from Ancona (G.S.M.), explored the siphon in the Acquasanta cave, which feeds the spring and some short caves in the narrow limestone outcrops of the nearby Rio Garrafo Valley. Based on these explorations, Maucci (1954) recognized the possibility of a hydraulic connection between the caves in the Rio Garrafo Valley and the thermal spring. He believed that the role of the thermal water was only secondary, because in his opinion, the rising thermal water used a pre-existing cave to reach the surface and caused only minor chemical alteration of the cave walls. Even if this interpretation is clearly related to the ideas of the period, Principi (1931) had already proposed, based on his study of the nearby thermal sulfidic Triponzo spring, that sulfidic water causes cave formation due to sulfuric acid production, followed by the replacement of limestone with gypsum that is easily removed by flowing water.

New explorations were carried out by speleologists of the G.S. CAI Teramo, who explored the Grotta Fredda during the 1970s, and by the members of the G.S.M. CAI di Ancona and the Associazione Speleologica Acquasantana, who explored the Grotta Lunga and the Grotta Nuova in the 1980s. Cave explorers in the Grotta Lunga and Grotta Nuova reached some active thermal zones below the valley of the Rio Garrafo. Since these explorations, the speleologists have continuously explored the area even though a complete survey of the explored passages is not still available. At present, the total extension of the cave passages exceeds 3000 m in length.

New ideas about the cave origins were discussed in 1994 at the XVII National Congress of Speleology, where Galdenzi described the general features and setting of the caves, attributing their development to the mixing of this rising sulfidic water with the descending freshwater infiltrating from the Rio Garrafo, mainly in phreatic conditions. These ideas, published in 1997, were then summarized in a paper on the sulfidic caves of central Italy (Galdenzi and Menichetti, 1995). In a subsequent paper,

* Corresponding author.

[1] Viale Verdi 10, 60035 Jesi, Italy. galdenzi.sandro@tiscali.it

[2] Dipartimento di Medicina Sperimentale e Sanità Pubblica, Università di Camerino, Italy. filippo.cocchioni@unicam.it, luciana.morichetti@unicam.it, stefania.scuri@unicam.it, mario.cocchioni@unicam.it

[3] Associazione Speleologica Acquasantana, Frazione Santa Maria, 63041 Acquasanta Terme, Italy. geotritone1@libero.it

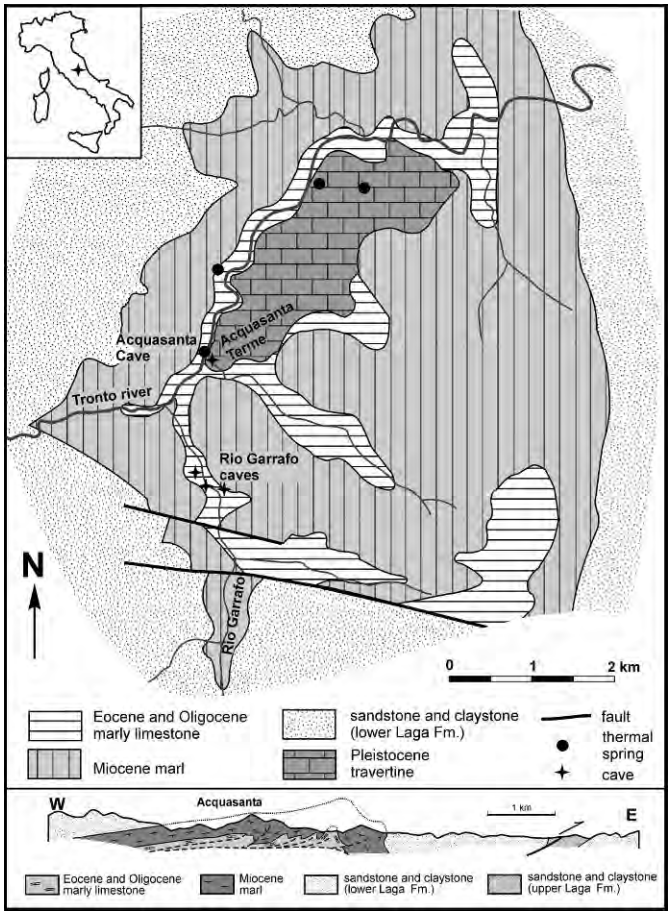

Figure 1. Geologic map of the study area. Geologic section after Scisciani and Montefalcone (2005), simplified.

Galdenzi (2001) compared geomorphic characteristics and environmental conditions of the Acquasanta caves with those of the Frasassi caves and Movile Cave (Romania). More recently, research on the microbiota of the thermal zone of the cave has begun (Jones et al., 2006). In this paper, we present new data on the air and water characteristics and discuss the present and past conditions of the cave development.

GEOLOGIC SETTING

LOCATION AND CLIMATE

The karst area of Acquasanta Terme is on the eastern side of the Apennine Mountains, 40 km from the Adriatic Sea, in the southern Marche region (central Italy). The caves open in the deep transverse valley that Tronto River cuts in the northern termination of the Laga Mountains (Fig. 1). A mountainous landscape prevails, with altitudes ranging between 300 m at the bottom of the valley to about 1100 m in the surrounding mountains. The climate is Apenninic sub-continental, with an annual average temperature of about 12°C and an average rainfall of about 950 mm yr^{-1} in the valley (Nanni, 1991). Precipitation generally reaches a maximum in autumn and spring and thunderstorms are frequent at the end of summer. In the winter, snowfall is common in the mountains where the thawing occurs at the beginning of the spring.

REGIONAL GEOLOGY

The Appennines consist of a sequence of anticlines overthrust to the east. The folds originated during the late Miocene and the Pliocene during a tectonic compressive phase that caused the uplift and emersion (for details on the regional geology, see Regione Marche, 1991, and Crescenti et al., 2004, with references).

The lower part of the stratigraphic sequence includes a 2000-m-thick Late Triassic evaporitic sequence. Jurassic, Cretaceous, and Paleogene deposits are 2000-m-thick and mainly carbonates. In the Oligocene and Miocene, marl deposition prevailed in the whole area. Messinian (Late Miocene) deposits consist of a foredeep turbiditic siliciclastic sequence (Laga Formation, over 3000-m-thick), where thick beds of sandstone alternate with thinner mudstone. The very fast sedimentation rate overprinted the effects of the Messinian salinity crisis that occurred in the Mediterranean Basin, and as a result, only a few gypsum-arenitic turbidites record evaporitic conditions in the source area. The area emerged over sea level during the Pliocene; after this event, a low relief energy paleosurface developed. At the end of early Pleistocene, the river entrenched the present valleys into the old erosional surface.

SITE GEOLOGY

The karst area is located in the core of the wide anticline of Acquasanta Terme, constituted by Miocene marl, sandstone, and mudstone (Fig. 1). The thick marly and terrigenous Oligocene and Miocene sequence outcrops everywhere and only in the core of the anticline the top of the underlying limestone sequence is exposed in the valley of the Rio Garrafo, a tributary of the Tronto River.

A gently dipping bedding prevails in the core of the anticline even if some detachment levels occur (Marsili and Tozzi, 1995). On the eastern limb, the bedding inclination increases rapidly and the Acquasanta Anticline overthrusts the Miocene sandstone of the Laga Formation (Fig. 1) with a throw of up to 2 km (Scisciani and Montefalcone, 2005). The Acquasanta anticline, 10 km to the west, lies on the footwall of the Sibillini Mountain Thrust, a regional structure that carries the Mesozoic limestone above the Messinian sequence.

Continental deposits in the Acquasanta zone form a diffuse, thin cover of colluvial and detrital slope deposits and, in the main valleys, some terraced sand and gravel deposits. The most significant terrestrial unit, however, is the large plate of travertine along the right bank of the Tronto River, whose deposition was related to the rise of sulfidic water from a confined aquifer (Boni and Colacicchi, 1966). Both alluvium and travertine deposition were influenced by climate changes between glacial and interglacial periods that caused alternating depositional and

erosional periods in the river valley. More recently, Farabollini et al. (2001) related the travertine deposition to revegetation in the mountains at the beginning of interglacials. The increase of CO_2 content in the seepage water that reaches the confined aquifer should have favored the travertine deposition. Madonna et al. (2005) described the physical and petrographic characteristics of travertine, linking their depositional setting to the rise of thermal water.

Lithology

The lowest stratigraphic unit that outcrops locally is the Scaglia Rossa Formation (Cenomanian – Middle Eocene). This unit has variable regional characteristics and its thickness can vary between 200 and 500 m. In the area, only the upper part of the Scaglia Rossa outcrops, and consists of reddish limestone and marly limestone that is well stratified in layers of ~20 cm. The top of this unit also contains cherty beds, while in its lower levels (not outcropping in the area), a gradual decrease of the marly content occurs. At depth, below the Scaglia Rossa Formation, the carbonate sequence continues with other limestone and cherty limestone formations that are interbedded with two main marl levels (up to 50 m thick). This mainly permeable sequence reaches 1500–2000 m in thickness and outcrops widely in the Umbria-Marche Apennines where it hosts the most important aquifers.

The overlying Scaglia Variegata (Middle Eocene – Upper Eocene) is a 50 m thick unit, which represents the transition between the Scaglia Rossa and the Oligocene marls. It is a cherty and marly limestone with alternating whitish and reddish color. In the Acquasanta area, this unit has been karstified.

The carbonate content further decreases in the Oligocene Scaglia Cinerea, a marl unit up to 200-m-thick. This Formation and the overlying Miocene marly units (Bisciaro, Marne con Cerrogna, Marne a Pteropodi) constitute the most important regional aquiclude, with a total thickness that exceeds 500 m.

The Messinian Laga Formation outcrops everywhere in the surrounding mountains. This unit alternates thick turbiditic sandstone and clay and silt beds to create characteristic steps in the mountainsides. Groundwater flow is possible in the permeable sandy zones where small springs can occur.

The pure, porous limestone of the Pleistocene travertine represents a further karstified unit. These deposits reach a thickness of tens of meters and extend for several km^2 at three different elevations located along the right bank of the Tronto River (Fig. 2; Boni and Colacicchi, 1966).

Hydrogeology

The Tronto River and its tributaries have an irregular discharge due to the low permeability of their basins and to the contribution of snow thawing from the mountains. The groundwater in the area consists mainly of the thermal sulfidic water that rises from the capped aquifer hosted in the carbonate sequence. The most important spring in the area is in the village of Acquasanta Terme at the outflow of the Acquasanta Cave. This spring has a discharge that seasonally varies between 60 and 220 L s^{-1} (Perrone, 1911) and is located in the right bank of the Fiume Tronto stream (Fig. 3), near the core of the anticline in the Scaglia Cinerea formation.

Some further minor thermal springs are downstream near the river bed and also at higher altitude in the right side of the valley. One spring is located at the bottom of a large shaft in the terraced travertine deposits, ~100 m above the river bed. The thermal groundwater can be reached also in the lower sections of the caves in the Rio Garrafo Valley.

The groundwater flowpath in the area is heavily influenced by the geologic setting. The prevailing low-permeability formations that cap the thermal aquifer reduce the local recharge of the aquifer. Only in the Rio Garrafo Gorge, sinking stream water directly reaches the thermal water inside caves.

The chemistry of the spring water, enriched in Cl^- and Na^+, and the isotopic data (Zuppi et al., 1974) indicate the co-existence of a deep circuit involving water with a probable meteoric origin that rises and dilutes with a variable amount of cold water coming from fast surface circuits. The high salt content could be acquired flowing through the underlying Triassic evaporitic sequence at the core of the anticline or through Messinian gypsum in the footwall of the Acquasanta thrust (Nanni and Vivalda, 2005). Madonna et al. (2005), however, hypothesize a contribution of volcanic fluids to explain the water chemistry. The high temperature of the geothermal field of Acquasanta could also be due to a magmatic intrusion at the core of the anticline (Madonna et al., 2005), that, however, is not reported by most authors who have analyzed the deep structure of the anticline (Scisciani and Montefalcone 2005, with references).

The Karst Area of Acquasanta Terme

Surface karst phenomena are not well developed in the area where mainly siliciclastic or marly formations prevail. The widest limestone outcrop, the large travertine plate, is generally covered by colluvial deposits or soils and only small scale corrosion features develop in narrow zones where the limestone surface is directly exposed to meteoric water. Deep karst, however, has a greater development in a hypogenic setting and thirteen caves are known with a total length that exceeds 3 km. Only a few caves are known in the large travertine deposits, and the major caves (Grotta Fredda, Grotta Nuova, and Grotta Lunga) developed in the small limestone outcrop of the Meso-Cenozoic marine sequence in the Rio Garrafo Valley.

The Travertine Caves

Grotta di Acquasanta

The Grotta di Acquasanta (length: ~300 m) is the main cave in the travertine. It is a wide chamber flooded by sulfidic water that directly feeds the main thermal spring

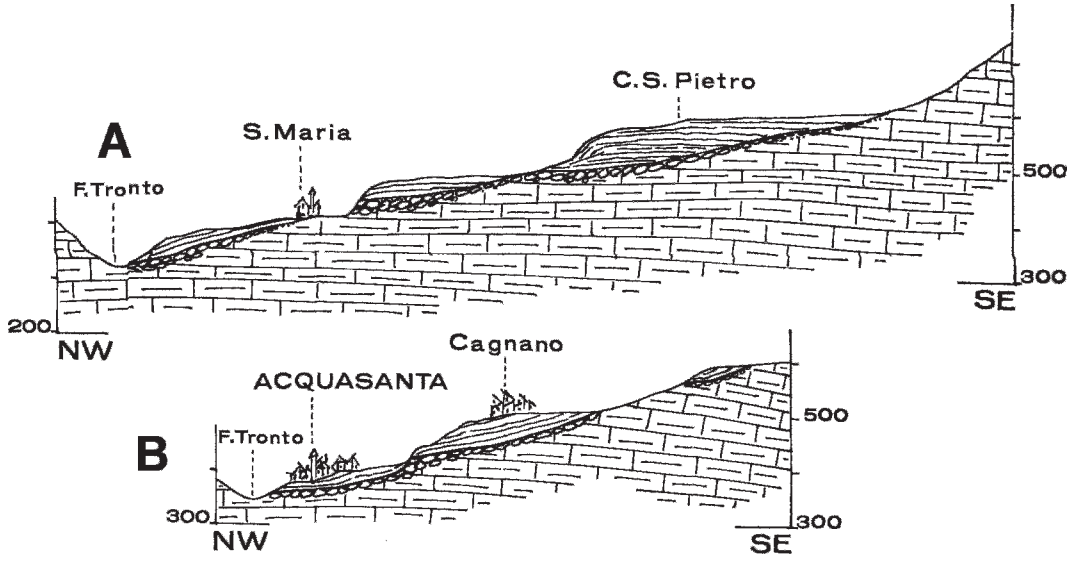

Figure 2. Geologic sections in the central (A) and south (B) part of the travertine deposit (after Boni and Colacicchi, 1966).

through a brief active passage. This cave developed at the base of the travertine body where it overlies the Oligocene marl formation of Scaglia Cinerea (Fig. 2). The bottom of the lake in the cave is covered by soft organic mud and water rises to the lake through a highly inclined passage explored up to 12-m-deep (Maucci, 1954). Gas release causes the corrosion of walls and roofs in the whole cave. The thermal stream water is causing carbonate deposition near the spring. At present, the cave is not directly utilized for thermal baths and water in the nearby commercial bath is derived from a drilled well.

THE RIO GARRAFO CAVES

The most important caves are located in a small area in the lower part of the Rio Garrafo Valley, where the stream entrenches in a narrow canyon inside the limestone sequence (Fig. 4). Rio Garrafo is a small tributary of the Tronto River with a recharge basin almost entirely in the Laga Formation at altitudes ranging from 300 m to 2050 m. Gravel deposits, coming from the upper part of the basin, fill the bottom of the gorge near the caves entrances, while in the lower part of the canyon, the stream is still eroding the bedrock.

Figure 3. The thermal spring of Acquasanta Terme.

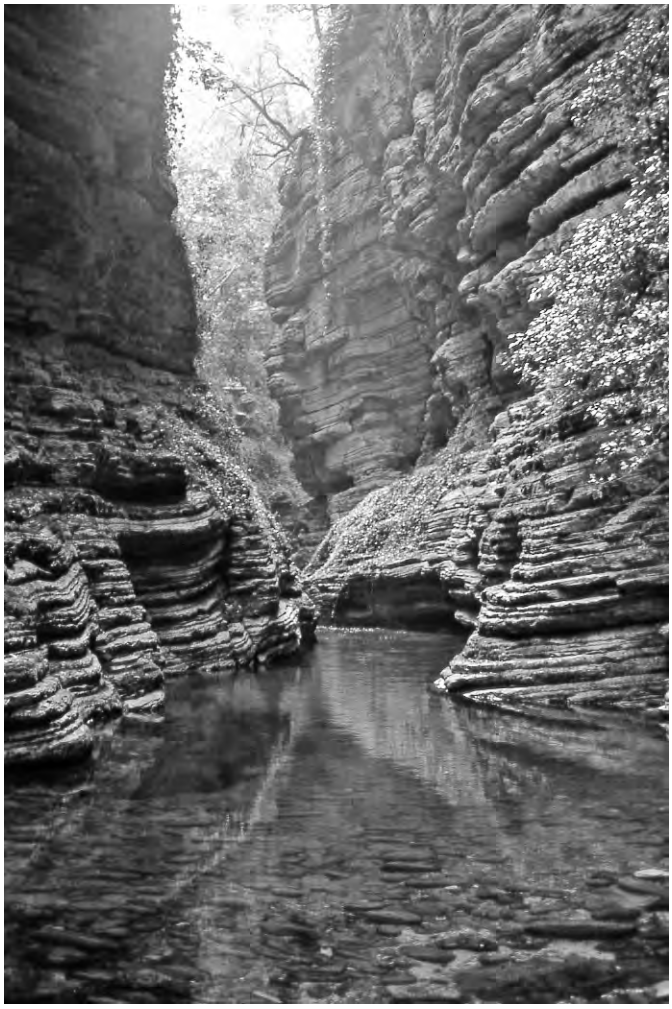

Figure 4. The Rio Garrafo gorge, at the Grotta Fredda entrance.

The main caves open at different altitudes in the vertical sides of the canyon and extend beneath the marly cover that outcrops above the canyon (Fig. 5); many passages in the caves develop below the present level of the stream. Other caves in the gorge are short fissure passages or rooms opened near the surface. These minor caves are often located in the same fracture in both the sides of the canyon. Some of these fissures near the river bed were artificially sealed in a rough attempt to prevent the loss of water in the stream (Fig. 6). Historically, the water sinking from the stream was identified as the cause of the cooling of the thermal spring.

Small travertine deposits overlying coarse fluvial gravel are on the canyon walls about 100 m downstream from the main cave entrances (Fig. 7). The presence of the travertine demonstrates that in the past the thermal water fed springs directly in the canyon. At present, the sulfidic water flows ~50 m below the Rio Garrafo bed in the lower levels of the caves.

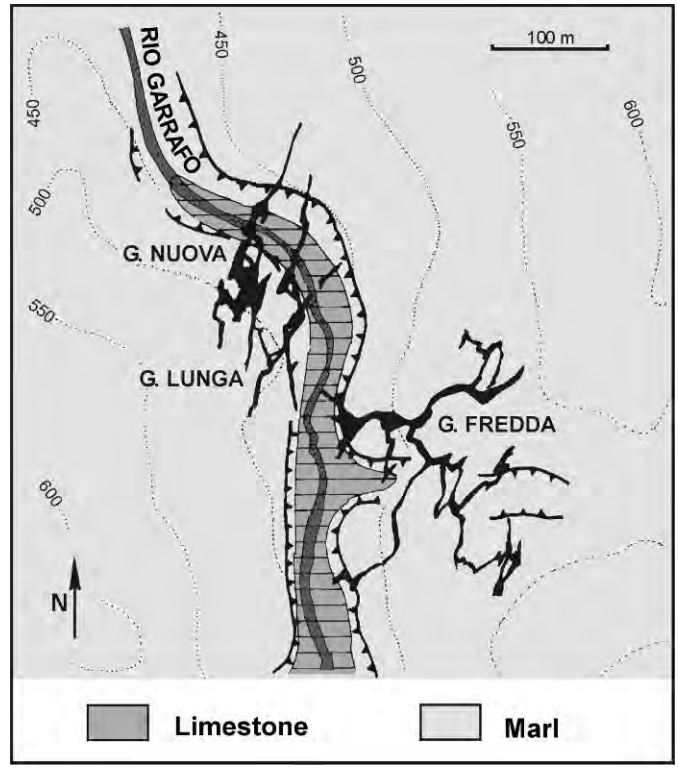

Figure 5. Plan view of the caves in the Rio Garrafo gorge. Note that caves develop below the marly cover. Cave maps based on survey by G.S.M.

Grotta Fredda

This cave has two nearby cave entrances, which open on the right side of the valley a few meters above the stream. The cave is sub-horizontal, with a ramified pattern, and consists mainly of bedding-plane passages developed at ~1500 m (Fig. 8). The main passage has an ascending profile from the east towards the canyon and clearly following the limestone bedding. Fractures and faults

Figure 6. Old dry walls, built to waterproof the Rio Garrafo stream bed.

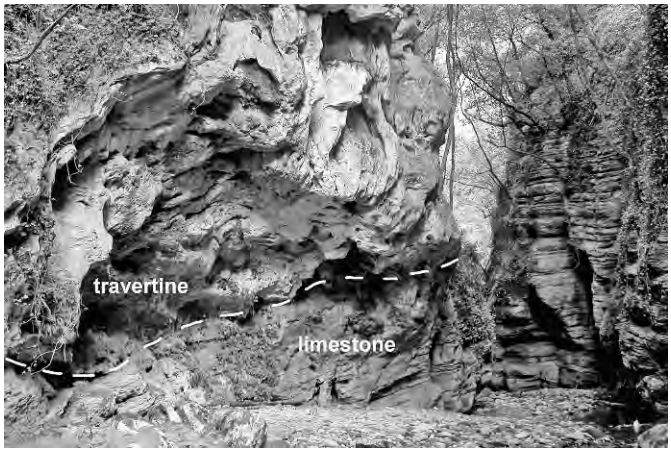

Figure 7. The small travertine deposit inside the Rio Garrafo gorge.

Figure 8. A typical passage in the Grotta Fredda. Sand deposits constitute the floor.

influence the cave development causing local changes in the direction of the main passages and in originating small lateral branches. Some fracture passages developed below the main passage and originated as crevasses that continue downward. In some crevasses, elevated rock and air temperature indicate the presence of unexplored thermal zones beneath. The low permeability of the overlying formation reduces the recharge of seepage water; therefore, flowstones develop mainly below the main fractures in the limestone.

The passage morphology is influenced by the lithology and breakdown deposits and unsteady blocks in the ceilings are common in the cave. Phreatic features prevail in the main passages with some wide cupolas on the roofs. On the floor, widespread deposits of sand partly covered by calcite deposition, might be due to past direct flooding of the cave. Furthermore, in some internal rooms, wood and shells on the walls clearly indicate the level reached by water inside the cave after recent flooding events.

White and microcrystalline gypsum occurs mainly as replacement crusts on the walls and generally it is recrystallized at the surface. The most important floor deposits can be 1–2 m thick and are clearly associated with replacement crusts and wide cupolas on the roofs (Fig. 9). These deposits often overly a silica silt that contains chert or limestone clasts. Together, the gypsum and the silt can constitute pebbly mud due to flow and redeposition.

Grotta Lunga and Grotta Nuova

These caves provide access to the groundwater in a thermal active zone ~50 m below the Rio Garrafo bed. They were explored through two different natural entrances, but a small passage partly filled by sand was later opened by speleologists to join the caves.

These caves extend ~1200 m and have a mainly vertical development in a fault zone with some horizontal or inclined passages at different altitudes. The upper horizontal passages open near the entrance zones at the same altitude of Grotta Fredda. In this zone, sand deposits can be related to the past direct influence of stream water as in the Grotta Fredda. In the inclined and vertical passages, roof features show the original ascending flow of the thermal water in the phreatic zone. These passages remained in the vadose zone after the lowering of the groundwater level and a few of them are permanently utilized by sinking water directly absorbed from the Rio Garrafo stream to the thermal aquifer.

The thermal water flows in the lower part of the cave and can be reached in four different areas with different environmental conditions (Fig. 10). Upstream a pool of thermal water (named lago arsenicale, for a suspected presence of arsenic, and identified herein as anoxic lake) can be reached in the Grotta Lunga beyond a siphon, at the end of a descending passage. Here, the rise of water from the depth feeds the pool, but the low air exchange makes this place extremely dangerous because of the high temperatures and unbreathable atmosphere.

The most well-known pool (lago dei bagni, i.e., baths lake) is in the Grotta Nuova at the bottom of the main shaft. Thermal water flows in some interconnected pools and small streams coming from the anoxic lake of Grotta Lunga through flooded passages. Warm vapor clouds rise from the stream toward the shaft and the free air exchanges permits speleologists to enter the rooms for a short time.

Downstream, other pools can be reached, including a small one in a different area of the main shaft. In this pool, the descending freshwater infiltrating from the surface directly mixes with the thermal water. This mixed water, after a narrow sandy passage, joins with thermal water in the last pool (Lago della Miscela, i.e., mixture lake) where it disappears into underwater passages.

Gypsum deposits are diffuse in these caves mainly as replacement crusts on the cave walls. They can encrust the whole passage section originating as a continuous rim few cm thick.

Figure 9. Cupola with gypsum deposits, in the Grotta Fredda.

Large floor deposits are rare but one is presently forming at the end of a passage in the thermal zone where active gypsum formation occurs on the cave walls. Here, the gypsum falls from the walls and is re-deposited as soft mud by the stream, occluding the passage itself. A further deposit, a few meters thick, is located on the rock bridge that divides the wide shaft over the thermal zone. This deposit, clino-stratified, originated from the detachment of replacement gypsum from the overlying wall.

Labirinto Rosso

Labirinto Rosso is a small cave (~170-m-long) with mainly small passages and a ramified, three-dimensional labyrinthic pattern. The cave opens near the Rio Garrafo bed in the left bank, upstream with respect to the other caves. The cave develops mainly below the present altitude of the stream and the high temperature of the limestone in some passages testifies to the presence of thermal active zones nearby. Gypsum replacement crusts also characterize many passages in this cave.

The Cave Environment

Methods

The study was based on field measurements of environmental parameters and on chemical analyses of water samples in the laboratory. Throughout the year, the water temperature was monitored every hour using four temperature loggers (Escort, New Zealand) with a resolution (0.3°C) that was considered sufficient for the large range of the temperature variations. The challenging environmental conditions and possible sabotage of the instruments required thick stainless steel boxes to contain the data loggers. Preliminary measurements verified that the thermometers inside the box equilibrates with the external water temperature after ~15 minutes. After more than a year of immersion in the sulfidic groundwater, the boxes were heavily corroded, with up to 3-mm-deep-cavities in the steel.

The water characteristics were analyzed at three localities: Acquasanta Terme spring, in the baths lake of Grotta Nuova (Fig. 10), and in the Rio Garrafo. Field measurements and water sampling were repeated for different hydrologic conditions and completed over a few hours. The water temperature, pH, and conductivity were measured in situ using probes (WTW, Germany). The sulfide and the dissolved oxygen were precipitated in situ

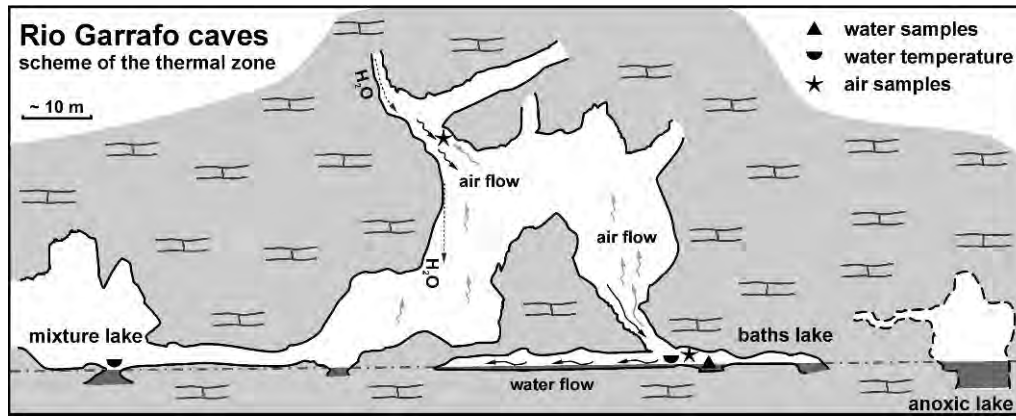

Figure 10. Map of thermal section of the cave, with sampling point locations.

Table 1. Chemical and physiochemical parameters of water samples and measurement methods.

Parameter	Method	Range	Analytical Error
Temperature	Digital thermometer, Hanna Instruments HI805	−50 to +150°C	±0.4°C
Conductivity	Conductivity meter, Crison mod. 524	0.0–199.9 mS cm^{-1}	≤0.5%
pH	Digital pH-meter, Hanna Instruments HI 824	0.0–14.0	±0.01
Hardness	Titrimetric Method, Standard Methods[a] 2340 C	0–50 mg L^{-1}	0.8%
Calcium	Titrimetric Method, Standard Methods[a] 3500 B	0–200 mg L^{-1}	1.9%
Magnesium	Calculation Method, Standard Methods[a] 3500 B	0–120 mg L^{-1}	2.1%
Sodium, Potassium	Flame Photometric Method, Standard Methods[a] 3500 B	0–50 mg L^{-1}	0.5 mg L^{-1}
Chloride, Sulfate	Ion Chromatography Method, Standard Methods[a] 4110 B	0–100 mg L^{-1}	0.26, 2.7 mg L^{-1}
Carbon dioxide	Titrimetric method, Standard Methods[a] 4500 C/D	10–2000 mg L^{-1}	±10%
Bicarbonate	Titrimetric method, Standard Methods[a] 2320 B	10–500 mg L^{-1}	1 mg L^{-1}
Sulfide	Iodometric method, Standard Method[a] 4500 F	0–50 mg L^{-1}	0.1 mg L^{-1}
Dissolved Oxygen	Iodometric method, Standard Methods[a] 4500 C	0–15 mg L^{-1}	<5%
Oxygen Saturation %	Calculation method	0–100%	<5%
Ionic balance	Δ% = [(meq. Cations – meq. Anions)/meq. Cations] ×100		

[a] Standard Methods for the Examination of Water and Wastewater 20th Edition.

for laboratory analysis. In the laboratory, the water samples were diluted, if necessary, and their physicochemical parameters were measured using the methods shown in Table 1.

The cave air was analyzed at the same time as water sampling at two localities and at different distances from the thermal water. We used a hand pump and short-term detector tubes (Gastec Corporation, Japan) for O_2 (measurement range: 3–24%), H_2S (0.1–4, 0.25–120 and 1–240 ppm), CO_2 (300–5,000 ppm and 0.13–6%), SO_2 (0.05–10 and 0.5–60 ppm). On two different occasions, unexpectedly high H_2S and CO_2 concentration exceeded the ranges of the available tubes.

WATER CHEMISTRY

Groundwater comprises two main types, bicarbonate and sulfidic. Bicarbonate water in the vadose zone consists of dripping water derived from the infiltration of meteoric water through fissures in the low permeable marly limestone, or which sinks directly through the bed of the Rio Garrafo stream.

The Rio Garrafo water, that in part feeds the thermal aquifer, was analyzed together with sulfidic water (Table 2). The stream water has a low salinity (about 250–300 mg L^{-1}) and a prevailing bicarbonate composition. The temperature fluctuates with seasonal cycles, while the chemical characteristics have shown only minor changes during the period. Once inside the cave, the stream water flows in wide inclined channels and quickly joins the thermal water in the deep zones of the cave.

The sulfidic thermal water has a higher salinity than the bicarbonate water, up to 7 g L^{-1}, has a high content of chloride, sodium, calcium, bicarbonate, sulfate, and contains hydrogen sulfide. These dissolved components are acquired before the water rises upward. The thermal water was sampled in the small stream at the entrance of the baths lake zone of Grotta Nuova before the junction with a descending stream of infiltrating freshwater (Fig. 10) and at the outflow of the Acquasanta Cave, the main sulfidic spring for the whole area. Water levels in the Grotta Nuova can increase up to 2.5 m during flooding events even though changes in the water levels were not observed on the sampling dates described here. From Grotta Nuova, the spring is almost 2 km distant and ~20 m deep; therefore, the hydraulic gradient should be ~1%.

The sulfidic water in the Acquasanta spring is more diluted than in the Grotta Nuova, but the seasonal trend of conductivity, salinity, and temperature is very similar (Fig. 11). The lowest values for these parameters occurred in April when rains and snow melt cause an increase in the surface discharge. In the Grotta Nuova, salinity ranged between 7.2 g L^{-1} (October 16, 2004, water temperature: 42.2°C) and 4.4 g L^{-1} (April 26, 2004, water temperature: 33.1°C). In the Acquasanta spring, salinity values were lower with the same seasonal variations; the highest values were on December 1, 2003 (4.6 g L^{-1}; temperature 31.4°C), and the lowest occurred on April 26, 2004 (1.9 g L^{-1}; temperature 21.9°C). Cation and anion compositions confirm the differences between these two types of water (Table 2). The concentration of ions is higher in the Grotta Nuova and follows the same annual trend, even if the seasonal dilution is less important than in the Acquasanta spring. In the baths lake of Grotta Nuova, the pH values are lower than in Acquasanta spring where the deposition of small amounts of carbonate occurs. During flood events, the pH values decreases at both locations.

To estimate the importance of the seasonal dilution, we assumed that the dilution is mainly due to the mixture of bicarbonate water that has low chloride content (~0.3 mmol L^{-1}) with the rising thermal water. Therefore, we compared chloride concentration in each sample with

Table 2. Data on water chemistry.

Date	Temperature (°C)	EC (mS cm^{-1})	pH	Calcium (mmol L^{-1})	Magnesium (mmol L^{-1})	Sodium (mmol L^{-1})	Potassium (mmol L^{-1})	Chloride (mmol L^{-1})	Sulfate (mmol L^{-1})	Bicarbonate (mmol L^{-1})	Hydrogen Sulfide (mmol L^{-1})	Oxygen (mmol L^{-1})	Δ% (mmol L^{-1})
						Acquasanta Terme spring							
Dec. 2, 2003	31.4	7.18	7.65	7.81	3.43	49.89	1.53	50.84	7.10	8.60	0.19	0.14	+0.10
Feb. 10, 2004	25.2	4.21	7.44	5.40	1.84	26.36	0.80	27.24	3.91	6.50	0.04	0.15	+0.10
Apr. 27, 2004	21.9	2.89	7.38	4.78	1.33	16.53	0.64	17.38	2.99	6.00	0.04	0.25	−0.03
Jun. 25, 2004	27.2	5.16	7.48	6.71	2.75	36.97	0.90	39.86	5.57	5.50	0.27	0.14	+0.04
Oct. 10, 2004	29.6	6.23	7.64	7.68	2.45	47.76	1.48	49.81	5.98	7.50	0.31	0.13	−0.12
						Grotta Nuova (baths lake)							
Dec. 1, 2003	43.4	10.42	6.75	10.38	4.22	79.56	2.05	80.57	9.90	9.80	0.54	NM	+0.10
Feb. 10, 2004	36.4	8.04	6.63	6.41	5.00	60.81	1.55	61.36	7.55	8.60	0.40	NM	−0.33
Apr. 26, 2004	33.1	6.76	6.58	8.14	2.20	48.46	1.07	47.86	6.96	7.60	0.38	NM	−0.64
Jun. 24, 2004	38.4	9.03	6.72	9.78	2.75	69.20	1.79	69.05	8.47	9.00	0.45	NM	+0.64
Oct. 10, 2004	42.2	10.18	6.75	10.58	3.85	84.95	2.63	87.44	9.96	9.40	0.66	NM	−0.84
						Rio Garrafo stream							
Dec. 1, 2003	5.8	0.34	8.54	1.20	0.57	0.26	0.03	0.22	0.16	3.29	NM	NM	0.00
Feb. 9, 2004	4.1	0.34	8.63	1.20	0.60	0.25	0.03	0.40	0.15	3.29	NM	NM	−2.84
Apr. 26, 2004	8.2	0.32	8.62	1.12	0.45	0.22	0.03	0.28	0.10	2.96	NM	NM	−1.47
Jun. 24, 2004	15.4	0.34	8.62	1.22	0.62	0.25	0.03	0.24	0.21	3.29	NM	NM	0.25
Oct. 10, 2004	11.2	0.30	8.48	1.06	0.51	0.21	0.03	0.23	0.13	2.88	NM	NM	0.30

NM = not measured

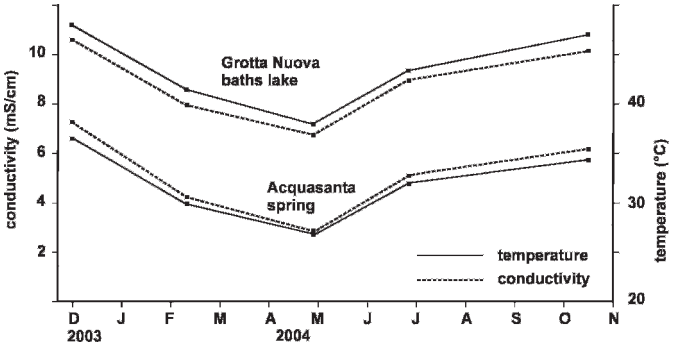

Figure 11. Correlation between temperature and conductivity in the Acquasanta spring and in the baths lake of Grotta Nuova on the sampling dates.

the values measured in the Grotta Nuova in October after a long dry period. Simple analytic calculations show that in the same lake the October water was diluted with ~45% of freshwater during flood events. In the Acquasanta spring, the dilution calculation for the Grotta Nuova water varied between ~40% in the autumn and 80% during floods. Seasonal changes in sodium and potassium content have the same seasonal trend as chloride, while the other major ions have a slightly different seasonal trend influenced by interaction with the bedrock and oxidation-reduction reactions.

Dissolved H_2S has higher concentration values in the Grotta Nuova (up to 0.66 mmol L^{-1}) when compared to Acquasanta spring where values were as high as 0.31 mmol L^{-1}. The sulfide, however, represents a small percentage (not exceeding 6%) of the total sulfur species dissolved in the water. The concentration of dissolved H_2S follows the general dilution of the thermal groundwater in the baths lake of Grotta Nuova, while during floods in the Acquasanta spring, it decreases to 0.04 mmol L^{-1}. These low values cannot be due only to dilution by nonsulfidic water, but are also accompanied by an increase in the dissolved O_2 concentration, suggesting that oxidation due to oxygenated freshwater from the surface contributes to H_2S decrease in the water.

WATER TEMPERATURE

The temperature of the water was monitored with data loggers placed at the same points where water samples were collected (i.e., Rio Garrafo Gorge, baths lake of Grotta Nuova and Acquasanta Spring, the outflow of Acquasanta Cave) and in the mixture lake of Grotta Nuova, where a stream of vadose water infiltrated from the Rio Garrafo directly mixes with the thermal sulfidic groundwater.

The thermograms confirm the seasonal variations suggested by the water chemistry and indicate that the water temperature was influenced by rain and flood events (Fig. 12). After a flood event, the temperature dropped quickly and the return to the pre-existing temperatures required a longer time. The maximum water temperature

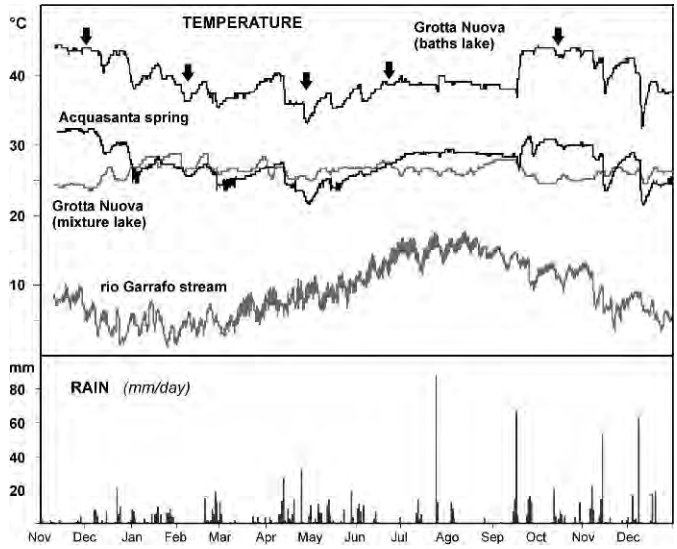

Figure 12. Temperature in the groundwater related to rain during the monitoring period. The arrows indicate the sampling days.

was ~44°C in baths lake of Grotta Nuova and ~32°C in the Acquasanta spring. Therefore, water samples collected December 1, and October 16, 2004, are representative of low-dilution periods. The lowest temperature values occurred on April 26, 2004 and December 10 and 11, 2003 (baths lake of Grotta Nuova, ~33°C; Acquasanta spring, ~21°C). The April 26 samples represent the composition of water during one of the main floods in the cave, corresponding to the most diluted water that occurred over the whole year. In the mixture lake of Grotta Nuova, the water temperature remained lower than in the baths lake throughout the year.

The thermograms of Grotta Nuova baths lake and Acquasanta spring have the same trends and changes in temperature are clearly related in timing and duration (Fig. 12). The temperature decrease in Grotta Nuova is very rapid following flooding events in the Rio Garrafo. The same occurs in the Acquasanta spring, showing that the spring is directly influenced by the same flooding events, but here the lowest temperature values are reached later, by a few days, and maintained for a longer time compared to baths lake (Fig. 13).

Thermograms for the two lakes of Grotta Nuova during the flooding events may have different trends. In most periods, flood events cause temperature decreases in both lakes (Fig. 13A, B). Sometimes, however, the two lakes show opposite variations during the same flood (Fig. 13C). While the baths lake is directly influenced by surface meteoric events, the mixture lake floods may produce a temperature increase. This is due to changes in the discharge of the karst channels that feed the lake with vadose and thermal water, which can cause a more direct contact between the warm water and the thermometer, with a consequent increase in the measured temperature.

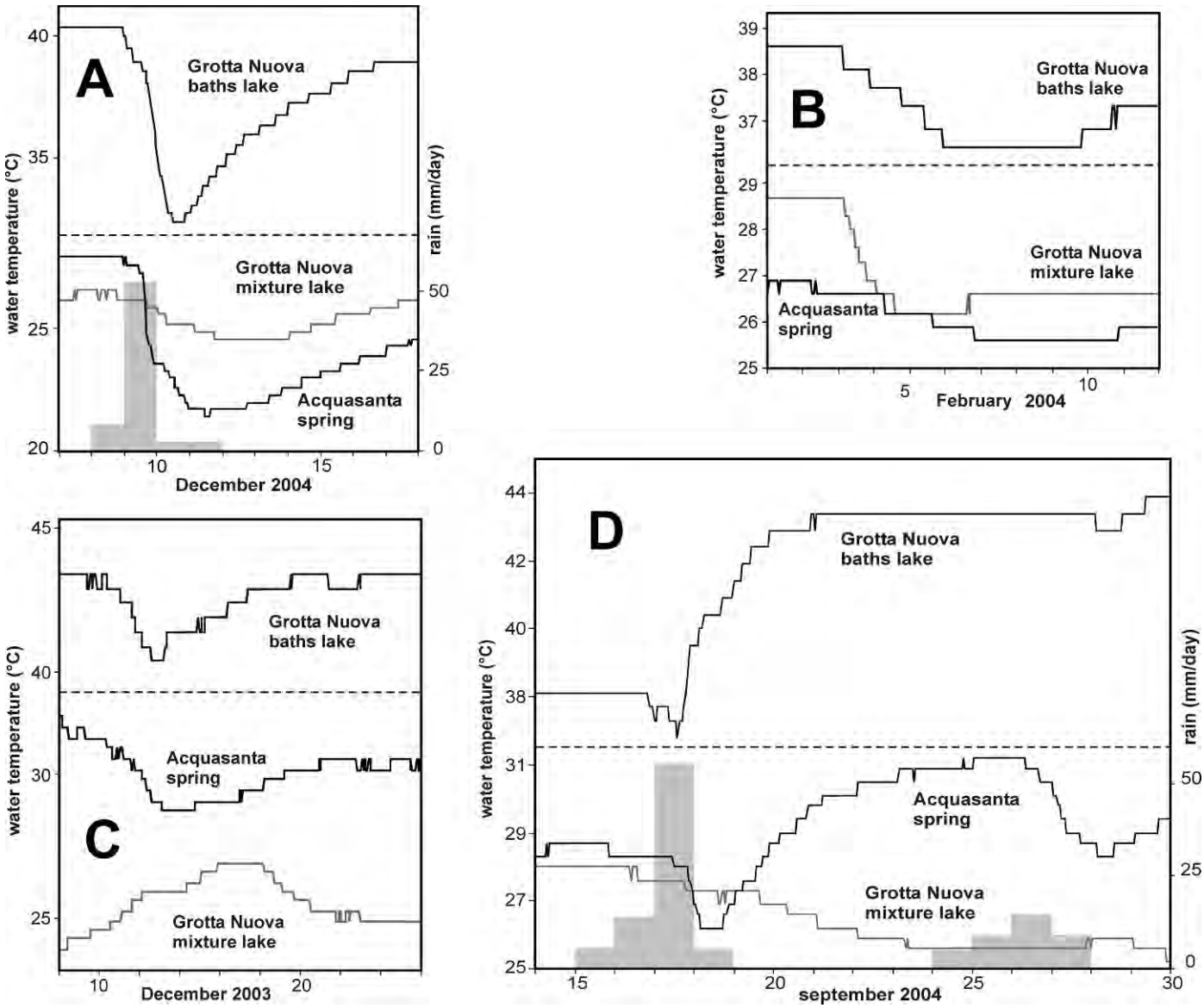

Figure 13. Temperature changes during flooding events. (A) The groundwater temperature after the rain of December 9, 2004. (B) February, 2004 – the arrival of freshwater was due to snow melt in the surrounding mountains. (C) December 11, 2003, temperature changes after an isolated snowfall in the mountains. (D) Groundwater temperature at the end of summer, after the rain of September 17, 2004.

Changes in water temperature during the summer are further indications of the complex pattern of karst water flow. In dry periods, corresponding to the lowest recharge of cold freshwater, the increase of water temperature ceased at all the monitoring locations. In the baths lake, the temperature remained even lower than the average annual temperature, probably due to slow water flow and heat exchange with the rock. A major rain event at the end of the summer (September 17) caused a small, but rapid decrease in water temperature in the baths lake and in the Acquasanta spring (Fig. 13D). In the following days, water temperature increased in the baths lake ($\Delta T \sim +6^{\circ}C$) and in the spring ($\Delta T \sim +3^{\circ}C$), while temperature decreased in the mixture lake ($\Delta T \sim -2^{\circ}C$). Similar changes, with a lesser range, also occurred after an important isolated rain event, on July 25 (Fig. 12). These data suggest that after these rains, the infiltration of surface water produced an increase in hydraulic pressure and a faster water flow, which restored normal conditions at the end of the dry season with an increase in water temperature at the spring and at the baths lake.

The thermograms and water chemistry of Grotta Nuova and Acquasanta spring suggest a different importance at the input of freshwater in the different sites. The mixture lake water has a generally lower temperature due to the direct arrival of freshwater and is also affected by

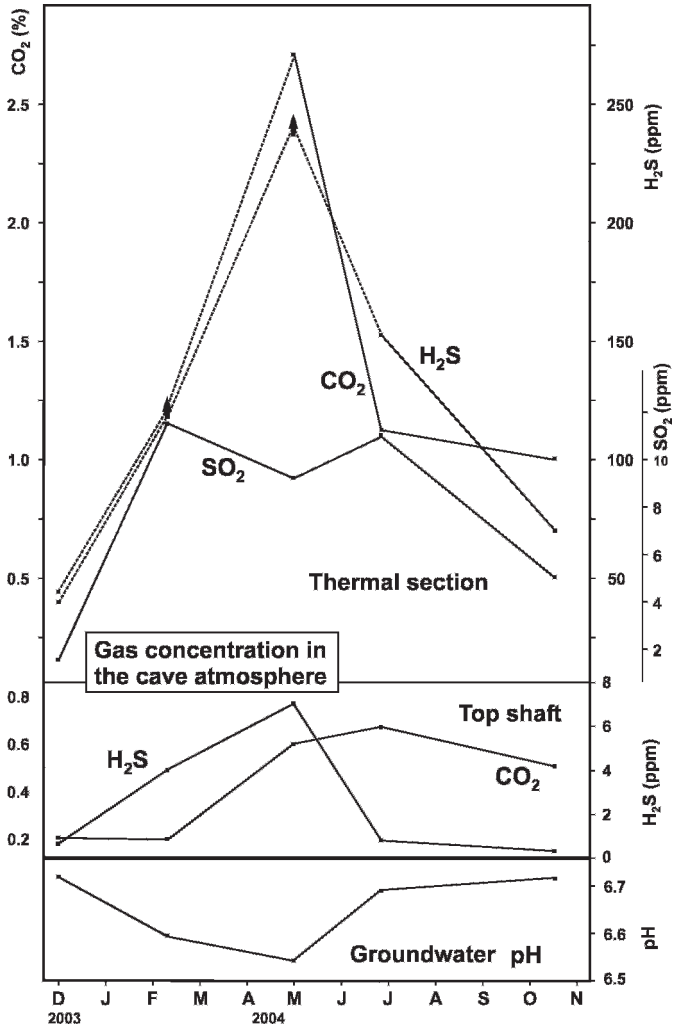

Figure 14. Relationships between gas concentration in the cave atmosphere and pH in the groundwater. The arrows indicate values outside the range of the available detector tubes. Therefore the reported values are minimum estimates.

changes resulting from flow of thermal and vadose water. The baths lake is directly influenced by the flood events that cause dilution immediately after the meteoric events. Acquasanta spring is also directly influenced by a rapid recharge of freshwater through karst passages, but it is probable that the average temperature and salinity remain lower than in the Grotta Nuova partly because of the contribution of water infiltrating from Rio Garrafo. Thermal water dilution at the spring might also depend on the contribution of different sources of water infiltration in the Tronto Valley, including the large travertine plate where the Acquasanta Cave and spring develop.

AIR COMPOSITION

The air composition changes in the different cave branches, depending on the connection with the sulfidic lakes or streams and with the surface. Extremely dangerous conditions for humans are present in isolated rooms, such as the anoxic lake in the Grotta Lunga where the small water-filled entrance reduces air exchange with the non-sulfidic upper cave levels.

After considering the features of the rooms and the difficulties of accessing them with appropriate safety equipment, we decided to analyze the air composition in the main room of Grotta Nuova where water samples were also collected. This room has a complex structure (Fig. 10). It is developed along a fault and is divided by a rock bridge into two different shafts. Sub-horizontal or inclined passages intersect the room in its upper and lower parts and active flow of sulfidic thermal water occurs in the lowest zones. Two room entrances are known, constituted by an inclined passage and by a narrow shaft, that isolate the room from the upper zones of the cave. A small waterfall of freshwater, infiltrated from the Rio Garrafo stream, permanently runs along the shaft wall coming from a narrow vertical passage.

The cave atmosphere is influenced by the gas released from the thermal water. The presence of sulfur gases is clearly detectable by smell at the top of the room near the entrances. A first sampling point was located at the top of the shaft, where the rising sulfur-rich air mixes with air coming from the surface (Fig. 10). The second sampling point was at the bottom of the shaft, inside the warm zone of the baths lake at the same location where water samples were collected. The high temperature, humidity, and dangerous air composition, allow only a few minutes for sample collection. This thermal part of the cave is well-divided from the remaining part of the room by a small descending passage where a steam cloud continuously rises and mixes with the cave air.

The air composition at both sampling sites was significantly influenced by gases released from the sulfidic water (Fig. 14). The O_2 concentration remained high (~20%), thanks to rapid air exchange with the nonsulfidic sections of the cave. The amount of CO_2, SO_2, and H_2S was significantly higher in the thermal section than at the top of the shaft. In the thermal zone, the CO_2 varied between 0.44% to 2.7%, H_2S between 40 to over 240 ppm[1], and SO_2 between 1.1 to 9.2 ppm. At the top of the shaft, the CO_2 ranged between 0.20% and 0.64%, H_2S between 3 and 8 ppm, while SO_2 had lower concentrations, not exceeding 0.2 ppm.

The most extreme conditions were measured on April 26, after a strong rain event when CO_2, SO_2, and H_2S reached maximum percentages in the air. This unexpected high concentration of gases in the air made measurement

[1] Editors Note: The atmospheric concentrations of H_2S reported here are hazardous to human health. The United States Occupational Safety and Health Adminstration (OSHA) has specified a Permissible Exposure Limit (PEL) of 10 ppm and an Immediately Dangerous to Life and Health (IDLH) limit of 100 ppm. Atmospheres with H_2S at the concentrations reported here should not be entered without proper monitoring and protective equipment.

and sampling operations very difficult. Similar flooding incidents have also put cavers in danger in the past.

Seasonal variations in the cave atmosphere composition have similar trends at both sampling locations (Fig. 14). Minor differences may be attributable to differences in the air flow patterns in the cave during the cold and warm seasons. Gas concentration is clearly related to the hydrologic cycle and increases for the dilution of thermal water by the freshwater. The highest values occurred during important flooding events, confirming cavers' observations about unbreathable air in the days following large rain events.

The gas concentrations have an opposite trend to water temperature, conductivity, and dissolved gases or their ionic equivalents. H_2S in the air has higher values when total sulfide concentration in the water is lower. A similar trend also occurs for CO_2 in the air and HCO_3^- in the water. The increase in gas released to the cave atmosphere is correlated with pH (Fig. 14). At values close to the pK of H_2S and H_2CO_3, pH influences the following equilibria:

$$H^+ + HS^- \leftrightarrow H_2S \quad (1)$$

$$H^+ + HCO_3^- \leftrightarrow H_2CO_3 \quad (2)$$

$$H_2CO_3 \leftrightarrow H_2O + CO_2 \quad (3)$$

For this reason, the lowering of pH favors the release of H_2S and CO_2 into the cave atmosphere.

Discussion

The development of the Acquasanta caves is related to the rise of thermal water at the core of the anticline and the oxidation of H_2S enhanced by the recharge of freshwater is probably the main cave forming process (Galdenzi, 1997). The characteristics of each cave are influenced by the hydrologic and geomorphologic settings and by their evolution through time.

The Acquasanta Cave is a young cave, formed after the deposition of the lowest travertine plate in the Tronto Valley. The explored part of the cave represents the outflow of sulfidic water rising from the thermal aquifer and flowing at the bottom of the travertine plate, influenced by the difference of permeability with the underlying marl. The cave has evolved near the water table, and easy gas changes with the atmosphere produce condensation corrosion on the walls in the whole cave.

The Rio Garrafo caves have had a more complex history. Their general features are due to their development as phreatic passages, but each zone of the cave has been influenced by different processes after the water table lowered to its present level. Their evolution will be discussed in detail in the following sections, considering both active processes and old morphologies and deposits. They also provide a useful example of the evolution of speleogenetic conditions in hypogenic caves as a consequence of the increase of direct connections with the surface.

Active Processes

Large parts of the old phreatic passages in the Rio Garrafo caves emptied after the lowering of the groundwater level, and thermal water flow continued down into the lowest sections of the caves where sulfidic water is in contact with the cave atmosphere in a few rooms. The analytic measures demonstrate that the thermal water chemistry undergoes seasonal changes because of the variable recharge of cold meteoric water. This recharge of O_2-rich water can contribute to maintain active solutional processes in the thermal groundwater because it can cause the oxidation of H_2S to sulphuric acid and the consequent dissolution of limestone where the mixture of waters occurs.

Above the water table, the cave evolution is mainly due to dripping water, sinking stream water, and gases released from the thermal zones, which have a different importance in each part of the caves.

The flow of dripping water has produced flowstone in some parts of the cave, but this process is significant only in some rooms and passages. The thick marly cover, in fact, prevents infiltration, which is possible only through important fractures or faults, or in the zones nearest to the gorge where the limestone outcrops. Also, the water directly infiltrated from Rio Garrafo does not play a significant morphogenetic role and causes only minor changes in the old phreatic passages utilized by water to descend.

In the zones directly exposed to the flow of thermal water, the release of gas has important influences on the cave evolution. The high bicarbonate content of thermal water causes the release of CO_2 when the water reaches the cave atmosphere; this phenomenon, however, produces deposition of carbonates only at the outflow of the Acquasanta Cave, where gours are forming in the stream before it reaches the surface.

Inside the caves, corrosion due to condensing water is the dominant process. Steep air temperature gradients favor air convection, and gases released from the groundwater consequently rise toward the upper levels. Low pH values were measured in all the rooms sampled for gas composition, including at the top of the shaft (Fig. 10). These data are consistent with the presence of H_2S and SO_2 detected in the air. The oxidation of H_2S leads to an active replacement of the limestone with gypsum in all zones, even where the walls are not directly exposed to the thermal water flow. The gypsum can be white or weakly colored due to impurities in the marly limestone and is generally found as thin crusts that are re-crystallized at the surface. The intensity of the corrosion strongly increases in the thermal section where the walls are more directly exposed to the degassing phenomena. A continuous crust of gypsum covers the walls and ceilings; the crust can be

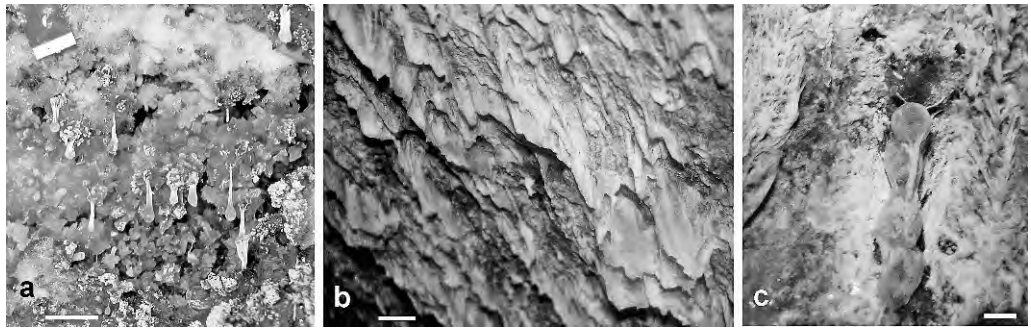

Figure 15. Organic formations at the entrance of the thermal zone (Scale bar: ~1 cm). (a) stalactites with acidic droplets; (b) curtains; (c) sequence of gas-filled and empty balloons.

dry, and often it is detaching from the limestone. In the places most directly exposed to degassing, elemental sulphur deposits are found on the walls and the gypsum.

Gypsum replacement crusts, however, are also in zones of the cave that, at present, are not influenced by the flow of thermal water. These deposits testify to the past influence of gas released by thermal water in a different hydrologic or morphologic setting.

GYPSUM FORMATION AND BIOLOGIC ASPECTS

Actively forming gypsum crust at Acquasanta has different features when compared with gypsum crusts observed in Frasassi sulfidic zones. At Frasassi, the gypsum is a moonmilk-like rim growing in a well-defined surface crust or in limestone pockets. In contrast, in the Acquasanta caves, the replacement gypsum has a gradational relationship to the underlying limestone. This is probably due to the higher silt and clay content of the limestone, which favors alteration without a well-defined separation surface. To clarify this aspect, limestone tablets composed of Acquasanta marly limestone were exposed for three years in the Frasassi caves, repeating an experiment previously conducted using pure limestone tablets (Galdenzi et al., 1997). The pure limestone tablets in the first experiment were covered by a thin layer of gypsum, whose removal revealed a hard, irregularly corroded limestone surface with incipient pockets a few millimeters deep. In contrast, the marly limestone tablets were covered by a layer of gypsum grading through a nondefinite surface into a soft, friable layer of limestone which crumbled as the gypsum was removed. Compared to other caves known to have active gypsum formations, such as Frasassi (Sarbu et al., 2000) and Cueva de Villa Luz (Hose et al., 2000), the growth of gypsum replacement crusts at Acquasanta is rarely associated with evident biofilms.

Inside the thermal zone, bacterial mats colonize the running sulfidic water, but no macroscopic evidence of life was found on the walls above the water table. On the contrary, thin, extremely acidic (pH 0–1) organic formations are present at the entrance to the thermal zone where curtains, stalactites, and balloons (Fig. 15) are forming in a zone with active condensation phenomena, due to the rapid rise of warm air. These thin, weak structures, swinging in the air currents, disappear in the intensely thermal zone below and are also absent on nearby walls not directly influenced by the warm air currents and condensation. Their development is likely related to sulfur oxidizing bacteria or archaea (Jones et al., 2006). Sulfur bacteria living at extremely low pH have been described at Frasassi and Cueva de Villa Luz (Vlasceanu et al., 2000; Hose et al., 2000; Macalady et al., 2007).

In the same room, in the zones not directly exposed to intense warm air flow, small zones of the walls with active gypsum growth are covered by a thin organic layer that can give rise to small gelatinous stalactites. These formations are similar to widespread features described in the Frasassi caves (Vlasceanu et al., 2000; Macalady et al., 2007), where the active gypsum replacement crust is often covered by an organic layer involved in the oxido-reduction of sulphur species.

In the Frasassi caves, bacterially-produced organic matter on the cave walls represents the main food source for the cave fauna (Sarbu et al., 2000), as shown earlier in Movile Cave (Sarbu and Kane, 1995; Sarbu et al, 1996). Preliminary research carried out in Acquasanta in 1997 revealed a non specialized fauna, with surface sources of organic matter (bat guano) as the main food source (Sarbu, unpublished data). At present, however, the importance of life, its adaptation to the cave environment, and the possible role in speleogenesis are interesting subjects that remain to be explored and discussed.

ORIGIN AND EVOLUTION OF THE CAVES

The general development of the Rio Garrafo caves can be related to the same speleogenetic processes that are still active, although changes in the geomorphic and hydrogeologic setting in the area through time also have influenced speleogenesis and cave characteristics. The cave development began under phreatic conditions because of the rise of thermal water to the surface through vertical fissures in the marl units. These first phases that were partly concealed by the subsequent evolution probably

occurred before the stream valley had cut down to the top of the limestone sequence.

The progressive deepening of the valley, however, permitted the stream to reach the top of the limestone sequence, where erosion of the gorge began. The pre-existing small passages remained perched above the water table, where they had evolved only because of the flow of vadose water. The thermal water flow continued into the upper part of the limestone sequence. In this phase, the mainly horizontal passages of Grotta Fredda and the upper levels of Grotta Nuova and Grotta dei Pipistrelli evolved, at the same altitude as the small travertine deposits produced by thermal springs in the Rio Garrafo gorge (Fig. 16A). Because the stream bed was close to the water table, small changes in the stream bed elevation could have emptied the cave passages or caused a return to phreatic conditions, also favoring the deposition of sand in the caves.

An important change in the evolution of these upper cave levels was due to the deepening of the Tronto Valley, which also caused the deepening of the tributary valleys and the generalized lowering of the regional base level. The most important consequence of this event was the lowering of the water table in the Rio Garrafo Valley where it became significantly lower than the canyon bottom (Fig. 16B). Therefore, after this event, direct input of thermal water at the surface in the canyon was no longer possible and the cave water emerged at the main spring farther downstream in the Tronto Valley. Moreover, the stream remained perched above the already karstified limestone and rapid recharge of surface water to the aquifer through the pre-existing phreatic karst passages became very easy. The deepening of the canyon bottom also prevented any direct flooding of stream water in the upper level of Grotta Fredda and Grotta Lunga where dripstones covered the old sand deposits.

These old cave levels, however, were newly influenced by the stream because the recent deposition of gravel in this part of the gorge caused a small increase in the elevation of the stream bed. Subsequently, stream water could flood the Grotta Fredda in rare occasions as evidenced by the recent wall deposits of organic material floated into the cave.

The changes in the geomorphic and hydrologic setting significantly modified the speleogenetic conditions for the cave development over time. In the beginning, the surface recharge of freshwater was probably low and the cave evolved mainly under phreatic conditions even if the progressive deepening of the Rio Garrafo Valley facilitated exchanges between thermal and surface stream water in the caves (Fig. 16A). After the deepening of the main surface stream (Tronto River) and resulting lowering of the water table, the amount of water infiltrating from the Rio Garrafo strongly increased, while interfaces between the cave atmosphere and the thermal water became more common inside the pre-existing cave passages (Fig. 16B). Rapid air exchange with the surface also favored condensation corrosion and gypsum formation on the cave walls.

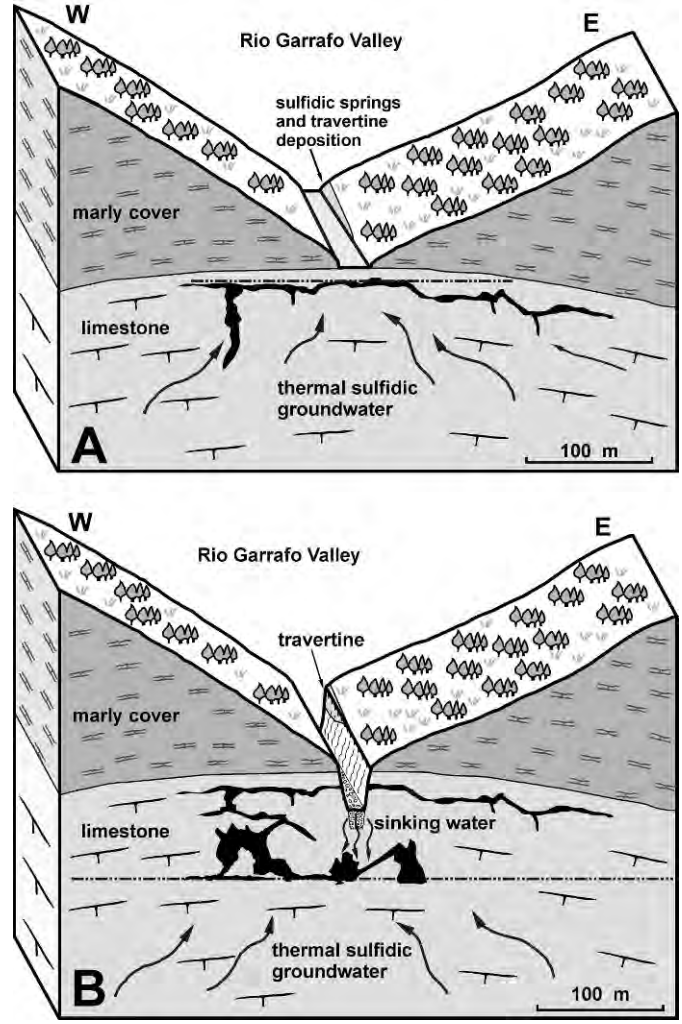

Figure 16. Sketch of the Rio Garrafo karst area. (A) The gorge in the past, with sulfidic spring located in the valley. (B) The gorge in the present, after the lowering of the water table. The water loss from the stream can easily reach the thermal groundwater.

Conclusions

The Acquasanta hypogenic caves formed at the core of an anticline because of the rise of thermal water in a capped aquifer hosted in the carbonate sequence. Cave development, however, was influenced by changes in the surface geomorphic and hydrologic setting, which have modified the morphogenetic processes and the general features of the caves over the course of their history.

The present morphogenetic conditions in the caves are strongly influenced by freshwater infiltrating from the Rio Garrafo canyon, perched ~50 m above the water table. The descending oxygen-rich freshwater has only minor influences on cave features in the vadose zone, but enhances limestone corrosion when it mixes with the thermal groundwater by the H_2S oxidation.

The data on water chemistry show that the increased freshwater recharge during floods causes the lowering of

pH of the groundwater and the release of significant amount of H_2S, S_2O, and CO_2 to the cave atmosphere. Due to strong air convection related to high air-water temperature differences, these gases can reach upper cave levels where they cause corrosion of the limestone or its replacement with gypsum.

The current conditions, however, originated only after the deepening of the regional base level lowered the thermal water level. In the beginning, the direct sinking of stream water was more difficult and had minor importance for the cave development. It is probable that cave development began before the Rio Garrafo reached the top of the limestone sequence, in a wholly phreatic setting, but an important step in the cave development occurred after the incision of the river canyon at the top of the limestone sequence. During this phase, some well-developed ascending passages testify to the flow of sulfidic water towards springs inside the canyon where travertine deposition occurred. These conditions were maintained until the present hydrogeologic setting originated.

ACKNOWLEDGMENTS

This research was partly funded by a grant from the Marche Region for the project "Speleogenetic evolution in the underground karst system of Acquasanta Terme" to the FSM (Federation of Speleological Groups of Marche Region), Istituto Italiano di Speleologia – Frasassi section, and Associazione Speleologica Acquasantana. We wish to thank Rossano Morici and the staff of the Osservatorio Geofisico di Macerata, who provided data on surface meteoric events in the study area. We also thank Jennifer Macalady for the photo in Figure 15(A) and for the useful suggestions and the help in the review of the text and we thank Fabio Baldoni for the photo in Figure 15(B).

REFERENCES

Boni, C., and Colacicchi, R., 1966, I travertini della valle del Tronto [The travertines of the Tronto Valley]: Memorie Società Geologica Italiana, v. 5, p. 315–339.

Crescenti, U., D'Offizzi, S., Merlino, S., and Sacchi, L., eds., 2004, Geology of Italy: Special Volume of Italian Geologic Society for the 32th International Geologic Congress, Florence 2004, 234 p.

Farabollini, P., Gentili, B., and Materazzi, M., 2001, Freshwater travertines in the Central Apennine (Italy): Genesis and climatic and neotectonic significance, *in* Proceedings, International Conference on Geomorphology 5th, Tokyo, p. 8–10.

Galdenzi, S., 1997, Le grotte termali di rio Garrafo (Marche) [The thermal caves of Rio Garrafo (Marche Region, Italy], *in* Proceedings, Congresso Nazionale di Speleologia, 17th, 1994, Castelnuovo Garfagnana, Italy, p. 235–238.

Galdenzi, S., 2001, L'azione morfogenetica delle acque sulfuree nelle Grotte di Frasassi, Acquasanta Terme (Appennino marchigiano – Italia) e di Movile (Dobrogea – Romania) [Morphogenetic action of the sulphidic waters in the caves of Frasassi and Acquasanta Terme (Marche Apennines — Italy) and Movile (Dobrogea – Romania)]: Le Grotte d'Italia, s. V, v. 2, p. 49–61.

Galdenzi, S., and Menichetti, M., 1995, Occurrence of hypogenic caves in a karst region: Examples from central Italy: Environmental Geology, v. 26, p. 39–47.

Galdenzi, S., Menichetti, M., and Forti, P., 1997, La corrosione di placchette calcaree ad opera di acque sulfuree: dati sperimentali in ambiente ipogeo [Limestone tablets corrosion due to sulphidic water: experimental measurements in cave environment], *in* Proceedings, International Congress of Speleology, 12th, Le Chaux-de-Fonds, Switzerland, v. 1, p. 187–190.

Hose, L.D., Palmer, A.N., Palmer, M.V., Northup, D.E., Boston, P.J., and DuChene, H.R., 2000, Microbiology and geochemistry in a hydrogen-sulphide-rich karst environment: Chemical Geology, v. 169, p. 399–423.

Jones, D.S., Stoffer, T.L., Lyon, E.H., and Macalady, J.L., 2006, Biogeochemistry and genomics of extremely acidic limestone-corroding cave wall biofilms: Geological Society of America Abstracts with Programs, v. 38, p. 138, A51–3.

Macalady, J.L., Jones, D.S., and Lyon, E.H., 2007, Extremely acidic, pendulous microbial biofilms from the Frasassi cave system, Italy: Environmental Microbiology, v. 9, no. 6, p. 1402–1414.

Marsili, P., and Tozzi, M., 1995, Un livello di scollamento nella dorsale di Acquasanta (AP) [A detachment level in the Acquasanta ridge (central Italy)]: Bollettino della Società Geologica Italiana, v. 114, p. 177–194.

Madonna, R., Signanini, P., Crema, G., Di Sabatino, B., Rainone, M.L., and Di Nunzio, A., 2005, The geothermal area of Acquasanta Terme (Central Italy): Main characteristics and an attempt of field evaluation, *in* Proceedings, World Geothermal Congress Antalya, Turkey, p. 1–8.

Maucci, W., 1954, La Grotta termale di Acquasanta [The thermal Cave of Acquasanta], *in* Proceedings, Congresso Nazionale di Speleologia, 6th, p. 1–12.

Nanni, T., 1991, Caratteri idrogeologici delle Marche [Hydrogeologic character in the Marche Region], *in* Regione, Marche, ed., L'ambiente fisico delle Marche [Physical environment of the Marche Region], S.E.L.C.A., Firenze, p. 115–209.

Nanni, T., and Vivalda, P., 2005, The aquifers of the Umbria-Marche Adriatic region: relationships between structural setting and groundwater chemistry: Bollettino della Società Geologica Italiana, v. 124, p. 523–542.

Nanni, T., and Zuppi, G.M., 1986, Acque salate e circolazione profonda in relazione all'assetto strutturale del fronte adriatico e padano dell'Appennino [Salt water and deep flowpath related to structural setting of the Adriatic and Po Valley front of the Apennines]: Memorie Società Geologica Italiana, v. 35, p. 979–986.

Perrone, E., 1911, Carta idrografica d'Italia. [Hydrographic map of Italy], Ministero Industria e Commercio, Roma, 436 p.

Principi, P., 1931, Fenomeni di idrologia sotterranea nei dintorni di Triponzo (Umbria) [Subterranean hydrologic phenomena near Triponzo (central Italy)]: Le Grotte d'Italia, v. 5, p. 1–4.

Regione, Marche, ed., 1991, L'ambiente fisico delle Marche [Physical environment of the Marche Region], S.E.L.C.A., Firenze, 256 p.

Sarbu, S.M., Galdenzi, S., Menichetti, M., and Gentile, G., 2000, Geology and Biology of the Frasassi Caves in Central Italy, an ecological multidisciplinary study of a hypogenic underground ecosystem, *in* Wilkens, H., Culver, D.C., and Humphreys, W.F., eds., Ecosystems of the World, Subterranean Ecosystems, New York, Elsevier, p. 359–378.

Sarbu, S.M., and Kane, T.C., 1995, A subterranean chemoautotrophically based ecosystem: The National Speleological Society Bulletin, v. 57, p. 91–98.

Sarbu, S.M., Kane, T.C., and Kinkle, B.K., 1996, A chemoautotrophically based groundwater ecosystem: Science, v. 272, p. 1953–1955.

Scisciani, V., and Montefalcone, R., 2005, Evoluzione neogenico-quaternaria del fronte della catena centro-appenninica: vincoli del bilanciamento sequenziale di una sezione geologica regionale [Neogene–Quaternary evolution of the Central Apennine thrust front: constraints from sequence and forward balancing of a regional cross-section]: Bollettino della Società Geologica Italiana, v. 124, p. 579–599.

Vlasceanu, L., Sarbu, S.M., Engel, A.S., and Kinkle, B.K., 2000, Acidic, cave-wall biofilms located in the Frasassi Gorge, Italy: Geomicrobiology Journal, v. 17, p. 125–139.

Zuppi, G.M., Fontes, J.Ch., and Letolle, R., 1974, Isotopes du milieu et circulation d'eaux sulfurées dans le Latium [Environmental isotopes and sulfureos water flow in the Latium], *in* Proceedings, Isotope techniques in ground water hydrology Congress, International Atomic Energy Agency, Vienna, v. 1, p. 341–361.

BOOK REVIEW

Subterranean Twin Cities

Greg Brick, 2009. Minneapolis, MN, University of Minnesota Press, 227 p., ISBN 978-0-8166-4597-8, 6 × 9 inches, softbound, $18.95.

Geologist and long-time NSS member Greg Brick has written a delightful and witty book on the underground spaces found in the Twin Cities of St. Paul and Minneapolis, Minnesota, which include both man-made and natural caves. Part adventure memoir, part geology text, and part local history, this book is a valuable account of how caves in this predominantly sandstone area were formed (and made), how they were utilized for industries such as tourism, brewing, mushroom growing, cheese production, and sand mining, and how these spaces became important parts of the urban infrastructure, serving as conduits for water, sewerage, and other utility systems. It is an important, though often neglected topic, as caves have increasingly been integrated into the built environment. The author gives the readers pause as he challenges them to think more broadly about caves and their role in contemporary America. After reading this book, no one will hold onto the false idea that caves are only to be found in rural or wilderness areas.

It is also a darn good tale. Brick relates harrowing stories of urban exploration under the city streets that both fascinate and revolt the reader. It is a form of caving that few people have undertaken. Brick's rich descriptions of his often surreptitious experiences, especially in the sewers of St. Paul, will leave most readers willing to contemplate urban underground spaces only from afar. Well written, and well produced, this book contains many archival photographs that add visual depth to the text. The addition of a few contemporary photographs, especially of some of the nightmarish spaces Brick describes, would have further enhanced the work, as would a map of the Twin Cities showing some of the subterranean spaces featured in the text. The exclusion of the latter is understandable, though, as Brick notes that exploration of some of the spaces is quite dangerous. It is illegal to enter some, and many others are now closed. This is not intended as a guidebook.

Nor is it a scholarly work in the ordinary sense. Although deeply grounded in geological and historical research, it is episodic in organization and has no central thesis. Scholarly notation (e.g., footnotes or endnotes) is lacking, though some sources are identified in the text. The book does include a bibliography. The author references other works on urban underground spaces in his introduction but seldom returns to that literature or attempts to place his work in the field. In general, the book focuses on the local. Thus, the larger context is absent; and how this study relates to the larger history of American caves or urban history is not explored. But this is small criticism, because as the Press description notes, this is a work of regional and local interest, not a scholarly monograph. As such, it works very well and deserves wide readership.

One of Brick's major innovations is his attention to the similarities and differences between caves intentionally made by humans, and those whose creation was inadvertent, formed for example through piping related to leaks in wells and sewers, which he calls anthropogenic. Many scholars already use anthropogenic to refer to artificial caves, but highlighting these differences and the key question of intent is a valuable insight. Other important topics in the book include the impact of railways on urban topography, especially the ravines and streams of St. Paul, and the re-engineering of natural streams below ground as a solution to competing land uses. Future scholars will use

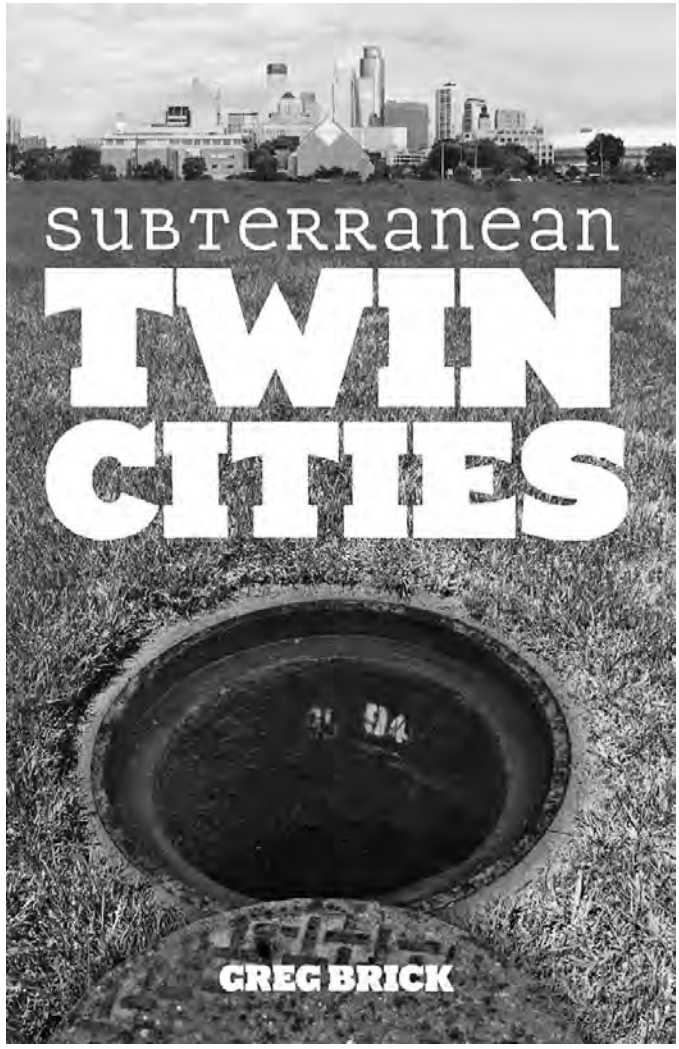

DOI: 10.4311/jcks2009br0111

this work for case studies to help build larger interpretive models of the history of the urban environment.

The book has much to recommend it. Merely relating what the author knows of the history, geology, and caves of the area would have been an important achievement, while a memoir only relating his personal experiences exploring the urban underground would have been an exciting adventure tale. Here, we have it all in a single work.

Reviewed by Joseph C. Douglas, Department of History, Volunteer State Community College, 1480 Nashville Pike, Gallatin, TN 37066 (joe.douglas@volstate.edu).

GUIDE TO AUTHORS

The *Journal of Cave and Karst Studies* is a multidisciplinary journal devoted to cave and karst research. The *Journal* is seeking original, unpublished manuscripts concerning the scientific study of caves or other karst features. Authors do not need to be members of the National Speleological Society, but preference is given to manuscripts of importance to North American speleology.

LANGUAGES: The *Journal of Cave and Karst Studies* uses American-style English as its standard language and spelling style, with the exception of allowing a second abstract in another language when room allows. In the case of proper names, the *Journal* tries to accommodate other spellings and punctuation styles. In cases where the Editor-in-Chief finds it appropriate to use non-English words outside of proper names (generally where no equivalent English word exists), the *Journal* italicizes them. However, the common abbreviations i.e., e.g., et al., and etc. should appear in roman text. Authors are encouraged to write for our combined professional and amateur readerships.

CONTENT: Each paper will contain a title with the authors' names and addresses, an abstract, and the text of the paper, including a summary or conclusions section. Acknowledgments and references follow the text.

ABSTRACTS: An abstract stating the essential points and results must accompany all articles. An abstract is a summary, not a promise of what topics are covered in the paper.

STYLE: The *Journal* consults The Chicago Manual of Style on most general style issues.

REFERENCES: In the text, references to previously published work should be followed by the relevant author's name and date (and page number, when appropriate) in parentheses. All cited references are alphabetical at the end of the manuscript with senior author's last name first, followed by date of publication, title, publisher, volume, and page numbers. Geological Society of America format should be used (see http://www.geosociety.org/pubs/geoguid5.htm). Please do not abbreviate periodical titles. Web references are acceptable when deemed appropriate. The references should follow the style of: Author (or publisher), year, Webpage title: Publisher (if a specific author is available), full URL (e.g., http://www.usgs.gov/citguide.html) and date when the web site was accessed in brackets; for example [accessed July 16, 2002]. If there are specific authors given, use their name and list the responsible organization as publisher. Because of the ephemeral nature of websites, please provide the specific date. Citations within the text should read: (Author, Year).

SUBMISSION: Effective July 2007, all manuscripts are to be submitted via AllenTrack, a web-based system for online submission. The web address is http://jcks.allentrack2.net. Instructions are provided at that address. At your first visit, you will be prompted to establish a login and password, after which you will enter information about your manuscript (e.g., authors and addresses, manuscript title, abstract, etc.). You will then enter your manuscript, tables, and figure files separately or all together as part of the manuscript. Manuscript files can be uploaded as DOC, WPD, RTF, TXT, or LaTeX. A DOC template with additional manuscript specifications may be downloaded. (Note: LaTeX files should not use any unusual style files; a LaTeX template and BiBTeX file for the *Journal* may be downloaded or obtained from the Editor-in-Chief.) Table files can be uploaded as DOC, WPD, RTF, TXT, or LaTeX files, and figure files can be uploaded as TIFF, EPS, AI, or CDR files. Alternatively, authors may submit manuscripts as PDF or HTML files, but if the manuscript is accepted for publication, the manuscript will need to be submitted as one of the accepted file types listed above. Manuscripts must be typed, double spaced, and single-sided. Manuscripts should be no longer than 6,000 words plus tables and figures, but exceptions are permitted on a case-by-case basis. Authors of accepted papers exceeding this limit may have to pay a current page charge for the extra pages unless decided otherwise by the Editor-in-Chief. Extensive supporting data will be placed on the *Journal*'s website with a paper copy placed in the NSS archives and library. The data that are used within a paper must be made available. Authors may be required to provide supporting data in a fundamental format, such as ASCII for text data or comma-delimited ASCII for tabular data.

DISCUSSIONS: Critical discussions of papers previously published in the *Journal* are welcome. Authors will be given an opportunity to reply. Discussions and replies must be limited to a maximum of 1000 words and discussions will be subject to review before publication. Discussions must be within 6 months after the original article appears.

MEASUREMENTS: All measurements will be in Systeme Internationale (metric) except when quoting historical references. Other units will be allowed where necessary if placed in parentheses and following the SI units.

FIGURES: Figures and lettering must be neat and legible. Figure captions should be on a separate sheet of paper and not within the figure. Figures should be numbered in sequence and referred to in the text by inserting (Fig. x). Most figures will be reduced, hence the lettering should be large. Photographs must be sharp and high contrast. Color will generally only be printed at author's expense.

TABLES: See http://www.caves.org/pub/journal/PDF/Tables.pdf to get guidelines for table layout.

COPYRIGHT AND AUTHOR'S RESPONSIBILITIES: It is the author's responsibility to clear any copyright or acknowledgement matters concerning text, tables, or figures used. Authors should also ensure adequate attention to sensitive or legal issues such as land owner and land manager concerns or policies.

PROCESS: All submitted manuscripts are sent out to at least two experts in the field. Reviewed manuscripts are then returned to the author for consideration of the referees' remarks and revision, where appropriate. Revised manuscripts are returned to the appropriate Associate Editor who then recommends acceptance or rejection. The Editor-in-Chief makes final decisions regarding publication. Upon acceptance, the senior author will be sent one set of PDF proofs for review. Examine the current issue for more information about the format used.

ELECTRONIC FILES: The *Journal* is printed at high resolution. Illustrations must be a minimum of 300 dpi for acceptance.

Journal of Cave and Karst Studies

Volume 72 Number 1 April 2010